1949

APPLICATION OF CHLOROPHYLL FLUORESCENCE IMAGING IN DUCKWEED ECOTOXICOLOGICAL TESTING

Thesis for the Degree of Doctor of Philosophy (PhD)

by Muhammad Irfan

Supervisor:

Dr. Viktor Oláh
Associate Professor

UNIVERSITY OF DEBRECEN
Doctoral Council of Natural Sciences and Information Technology
Juhász-Nagy Pál Doctoral School

Debrecen, 2024

Hereby I declare that I prepared this thesis within the Doctoral Council of Natural Sciences and Information Technology, ***Juhász-Nagy Pál Doctoral School****, University of Debrecen in order to obtain a PhD Degree in Natural Sciences at Debrecen University. The results published in the thesis are not reported in any other PhD theses.*

Debrecen, 2024. ……

Muhammad Irfan
PhD candidate

Hereby I confirm that ***Muhammad Irfan*** *conducted his studies with my supervision within the* ***Hydrobiology*** *Doctoral Program of* ***Juhász-Nagy Pál Doctoral School*** *between 2020 and 2024. The independent studies and research work of the candidate significantly contributed to the results published in the thesis.*

I also declare that the results published in the thesis are not reported in any other theses.

I support the acceptance of the thesis.

Debrecen, 2024. ……

Dr. Viktor Oláh
Dissertation supervisor

APPLICATION OF CHLOROPHYLL FLUORESCENCE IMAGING IN DUCKWEED ECOTOXICOLOGICAL TESTING

Dissertation submitted in partial fulfilment of the requirements for the doctoral (PhD) degree in Environmental Sciences

Written by
Muhammad Irfan

Prepared in the framework of Juhász-Nagy Pál Doctoral School of the University of Debrecen
(**Hydrobiology** program)

Dissertation supervisor:
Dr. Viktor Oláh

The official opponents of the dissertation:

…..... …..

…..... …..

The evaluation board:

Chairperson: …..... …..

members: …..... …..

…..... …..

…..... …..

…..... …..

The date of the dissertation defense: ……..2024

Table of contents

List of Abbreviations

α	Maximal photon-use efficiency
AIC	Akaike information criterion
ChlF	Chlorophyll Fluorescence
EC	Effective Concentration
EC_{max}	Effective Concentration associated with maximum stimulatory response
ETR	Electron Transport Rate
ETR_{max}	Maximum value of Electron Transport Rate
F_m	Maximum fluorescence level under the dark-adapted photochemistry
F'_m	Maximum fluorescence level under the stable photochemistry
F_o	Ground state fluorescence under the dark-adapted photochemistry
F'_o	Ground state fluorescence under the light-adapted photochemistry
F_s	Steady state fluorescence
F_v	Variable fluorescence under the dark-adapted photochemistry
F_v/F_m	Maximum quantum yield of PSII photochemistry
F_v/F_o	Maximum ratio of quantum yields of photochemical and concurrent non-photochemical processes in PSII in dark-adapted state
ISO	International Standard Organization
MAX	Maximum stimulatory response
NOAEC	No Observed Adverse Effect Concentration
NOAEL	No Observed Adverse Effect Level
OECD	Organization for Economic Cooperation and Development
PAM	Pulse Amplitude Modulated fluorometer
PSII	Photosystem complex II
qN	Non-photochemical quenching
qP	Photochemical quenching
Rfd	Relative fluorescence decrease
RGR	Relative Growth Rate
RLC	Rapid Light Curve
Y(II)	The effective quantum yield of photochemical energy conversion in PSII; a.k.a. Genty parameter
Y(NPQ)	Quantum yield of regulated non-photochemical energy loss in PSII
Y(NO)	Quantum yield of non-regulated heat dissipation and fluorescence emission

1. Introduction

An ever-increasing human development and unsustainable population growth has led to industrialization, modern agriculture and pharmaceutical advancements. The industrial processes release a variety of pollutants including heavy metals, persistent organic pollutants (POPs), and emerging pollutants such as micro(nano)plastics and polyfluoroalkyl substances (PFAs) into the environment (Jafarzadeh et al., 2022; Eid et al., 2024). Industrial wastewater contains a substantial load of heavy metals causing pollution (Amal Raj et al., 2024). Freshwater bodies, being in the closest vicinity of industrial and municipal sources, are at the highest risk of getting contaminated (Reid et al., 2019; Ceschin et al., 2021). The increasing levels of heavy metals and their subsequent exposures are associated with many health issues in humans including carcinogenesis, kidney damage, liver problems, hypertension, skin and gastrointestinal problems, endocrine disruption, and abnormal development in children (Yan et al., 2022; Amal Raj et al., 2024). Additionally, they can also hinder the growth of aquatic flora. The possibility of a trophic transfer and leaching into the soil system is also an additional aspect to be considered.

While heavy metal pollution is a long-studied issue, concerns over the elevated chloride (Cl^-) concentrations in freshwater bodies have recently been raised among the scientific community. The major sources for this anion are chlorination for sterilization purposes, inclusion of municipal and industrial wastewater into the waterbodies, application of salt for de-icing of roads and seawater mixing due to high tides (Schuler et al., 2017; Hong et al., 2023). Chloride is a beneficial micronutrient in higher plants at lower concentrations. It is involved in photosynthesis as a cofactor at ‘S’ transition state during electron excitation in PSII, and repairing process of photodamaged thylakoid membrane, osmoregulation and maintaining the turgor pressure. However, the higher concentrations can become toxic for the plants by causing chlorosis, disturbing the homeostatic balance in chloroplast and mitochondria, and decreasing the enzymatic activities (Kobayashi et al., 2006; Geilfus, 2018; Raven, 2020). Therefore, it is important to continuously monitor the

pollution levels in the waterbodies to maintain water quality and preserve an overall ecosystem health.

In addition to *in situ* water quality monitoring through bioindicator organisms, the toxicological effects of environmental pollutants can also be modeled to evaluate their overall impact on the ecosystem. According to Hee, (1993), the term bioindicator refers to an organism that indicates the presence of an environmental stressor (e.g., pollutant, excess nutrient) by manifesting a physical, chemical, or behavioral response. These sensitive bioindicator species offer a rapid and economic option to prevent an upcoming catastrophic damage in the ecosystem by acting as an early warning system (Martinez-Haro et al., 2015). Commonly used plants for modelling toxicological effects of chemicals in freshwaters include a wide set of organisms from the higher plant *Myriophyllum spicatum* L. to microalgal species such as *Chlorella vulgaris* Beijerinck and *Pseudokirchneriella subcapitata* Korshikov (Ceschin et al., 2021). Duckweeds are, however, the most popular model organisms due to their fast vegetative growth, low maintenance needs and simple anatomy (Ziegler et al., 2016). Considering their practical advantages, internationally adopted growth inhibition-based test protocols have been developed by the International Standard Organization (ISO) and the Organization for Economic Cooperation and Development (OECD) for testing toxicity of environmental pollutants (ISO, 2005; OECD, 2006).

The underlying concept behind plant ecotoxicity testing is the variable sensitivity of plants to different substances. Usually, the effects of these pollutants are characterized based on how they change the growth rate, biomass or photosynthetic pigment content of the test plants (Ceschin et al., 2021). During these tests, the plants are exposed to the targeted pollutant for a defined duration and the changes in the specified endpoints are measured by comparing their initial and final values. These endpoints were initially limited to the biomass and biochemical contents of the test plants, however, the growing interest in predicting environmental impacts has led to the progressive adoption of further phytotoxicity endpoints. These additional endpoints help to test the hypothesized effects of many substances released into the

environment. These recently developed approaches also promise higher sensitivity and a faster response compared to the commonly used growth inhibition-based ones. These methods, however, also require new culturing procedures that allow monitoring changes and measuring endpoints over time periods other than defined by the OECD (2006) and ISO (2005) standards. In phyto-toxicological studies, amongst others, chlorophyll fluorescence (ChlF) based endpoints are also considered as promising alternatives or accessories to the traditional growth-based endpoints.

Measuring ChlF induction is non-destructive, and therefore can be jointly applied with other approaches. In addition, the method gains information on the functionality of a basic -and very sensitive- metabolic process (i.e., photosynthesis), thus promising faster responsivity to adverse effects, as compared to growth responses that reflect a later stage of organic matter production. Several basic and derived endpoints have already been applied in a variety of ways to measure the response of plants to environmental stress factors (Bhagooli et al., 2021). Despite the increasing application of this technique in plant ecophysiological and toxicological studies, however, a comprehensive comparison of reliability and responsiveness has never been made between the classical growth-based methods and the ChlF-based methods using a wider set of toxicants in duckweeds.

2. Aims and objectives

This thesis is based on two studies involving *Spirodela polyrhiza* (L.) Schleiden and *Lemna gibba* L. The first study with *S. polyrhiza* was aimed to identify the most suitable ChlF-based endpoints while the *L. gibba*-based study was focused on further evaluating the suitability of these endpoints under exposure to various environmentally relevant metals and metalloids. These latter results with *L. gibba* also formed the basis for comparison whether the findings of *S. polyrhiza*-based investigation were general or species specific. Overall, the objectives of the thesis were to address the following questions and hypotheses:

1. ChlF imaging technique is gaining popularity in ecotoxicology due to its rapid and non-invasive measuring principle. Since several endpoints can be derived from the same basic measured parameters, the first aim was to assess which endpoints are the most responsive in duckweed toxicological tests and thus can be recommended in practical applications. The first hypothesis of the study was that the light-adapted parameters are more sensitive than the dark-adapted ones when measured in standard kinetic curves.
2. In order to record a full ChlF induction curve, dark-adaptation of samples is required followed by a continuous measurement until reaching steady-state photosynthesis. In case of a large sample series, however, following this protocol extends the time requirement significantly. Measuring light- and dark-adapted parameters separately without recording a full induction curve could, thus, significantly increase the through-put of such measurements. The second hypothesis of this study was that acquiring the light- and dark-adapted ChlF parameters in two separate steps still yields endpoints with a comparable sensitivity to the full ChlF induction curve.
3. Stress responses of duckweeds are toxicant-dependent and can be measured by means of both growth and ChlF. Here we tested whether ChlF-based phytotoxicity endpoints have comparable sensitivity to those of growth-based ones under exposure to a wide set of heavy metals, and hence, whether they can reliably substitute the growth-based endpoints. The third hypothesis of

the study was that ChlF-based endpoints have a comparable sensitivity to the growth-based ones.

4. The standard duckweed growth inhibition tests are conducted in such volumes of medium that are large enough to support growth of the cultures for seven days. The duration and medium requirements, however, can be significantly reduced by multi-well plate-based experimental setups. The fourth hypothesis of this study was that such multi-well plate-based setups can be adopted for duckweed toxicity testing without compromising the sensitivity.

3. Literature review

3.1. Duckweed morphology, evolutionary history and biogeographical distribution

Duckweeds are the smallest flowering members of the Plant Kingdom belonging to the family Lemnaceae within the monocot order of Alismatales (An et al., 2018). To date, there are 5 recognized genera and 36 species of duckweeds (Sree et al., 2016; Bog et al., 2020). The five genera include *Spirodela*, *Landoltia*, *Lemna*, *Wolffia* and *Wolffiella* (An et al., 2018). Their body primarily consists of a leaf-like frond, having a very simple anatomy. The fronds have a spongy mesophyll contained between an upper and lower epidermis layer. The mother fronds produce the next generation of daughter fronds through meristematic regions. The size of these fronds depends on the duckweed species, but ranges in the mm–cm range (**Figure 1**).

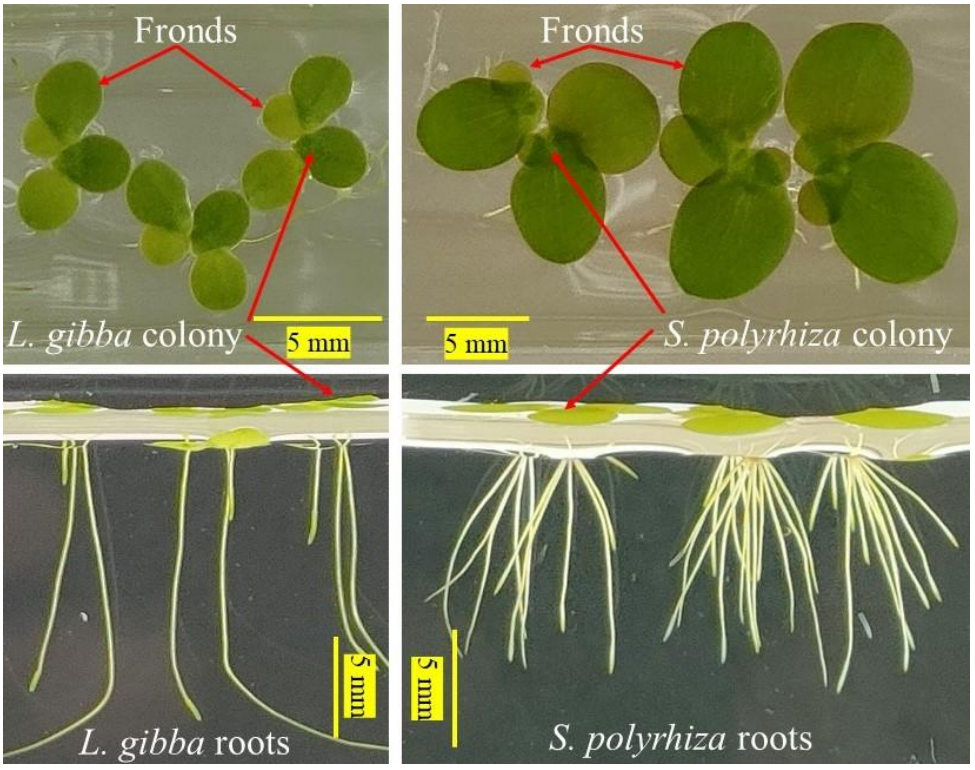

Figure 1. Colonies of the duckweeds *Lemna gibba* and *Spirodela polyrhiza* showing differences in frond size and number of roots (author's own images).

Duckweeds have evolved through a gradual simplification in their anatomical complexity. As a result, a continuous reduction in body size can be observed from *Spirodela* towards *Wolffia*. Duckweed species also reduced the number of roots present per frond over the course of their evolution due to restricted usage of roots in nutrient uptake (Ware et al., 2023). Multiple roots initially present in *Spirodela* and *Landoltia* species were reduced to only a single root in *Lemna* species. As the other extreme, both the *Wolffia* and *Wolffiella* species are rootless (**Figure 2**). Instead of roots, these plants can obtain nutrients from the growth medium predominantly via their abaxial (lower) epidermis and supply them directly to the assimilating tissues (Landolt & Kandeler, 1987; Cedergreen & Madsen, 2002). The genome size, on the other hand, shows an increasing trend from *Spirodela* to *Wolffia* species (Wang et al., 2011).

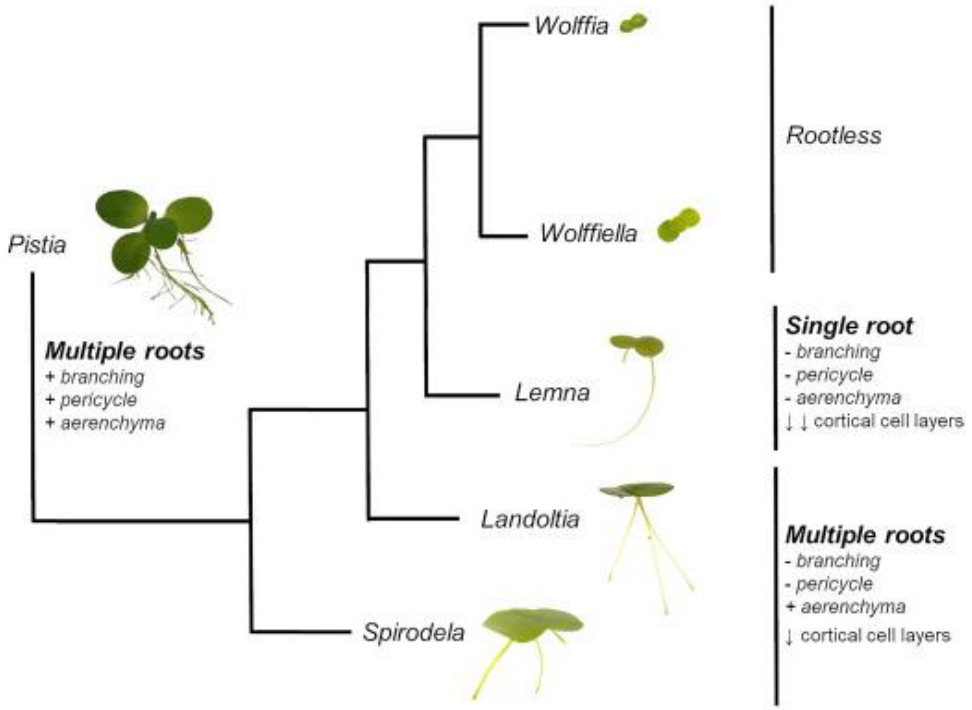

Figure 2. Phylogeny of duckweeds and genera with a progressive morphological and anatomical reduction, and loss of roots (Ware et al., 2023).

Except the polar permafrost regions, duckweeds are widespread all over the globe, and many species are in fact cosmopolite spanning over multiple continents (Landolt, 1986; Tippery & Les, 2020). Some of the most commonly present species are *Landoltia punctata* G. Meyer*, S. polyrhiza* and *Lemna minor* L. *Landoltia punctata* is known to be natively present in Australia and southern Asia while *S. polyrhiza* spreads more widely as it covers most of Europe, Asia and America. *Lemna minor* is mainly present in Europe, America, Africa and in some regions of northern Asia (Landolt, 1986). Apart from these native habitats, some species of duckweeds have also spread into other regions as a result of anthropogenic introduction e.g., *La. punctata* to certain parts of southeastern Europe, North America, South America, *L. minuta* to Europe, *L. gibba* to Japan and *L. minor* to Australasia (Landolt, 1986; Tippery & Les, 2020).

3.2. Applications of duckweeds

Duckweeds are widespread across the globe, however, the first monograph on this plant group was published only in 1839 describing the Lemnaceae family (Schleiden, 1839). Later on, the 1950s marked the initiation of biochemical studies on these plants (Hillman, 1957; Acosta et al., 2021). In ancient times, they were believed to have medicinal benefits in relation to different disorders. For instance, *S. polyrhiza* and *L. minor* were used as a remedy for fever among romans and Chinese while *L. minor* was a component for the ointment against colic in medieval Christian Europe. Their usage was also a part of many rituals in different religions and cultures (Edelman et al., 2022). Nowadays, duckweeds are primarily utilized as a source of feed for water birds, fish and other animals due to their high protein content. They are also used as human food supplement in some regions across the globe (Xu et al., 2015). Additionally, researchers are also studying the possibility of using these cosmopolite plants as biomass and biofuel production source (Cui et al., 2015; Chen et al., 2022; Paolacci et al., 2022; Petersen et al., 2022), and as phyto-remediating agents (Chen et al., 2018; Iqbal et al., 2019; Golob et al., 2021; Szabó et al., 2023).

The global distribution of duckweeds enables their growth in different environmental conditions with variable nutrient availability and salinity (Baek et al.,

2021). Due to their hyperaccumulation capabilities, they have the potential to remove heavy metals, pesticides, and organic compounds from wastewater. Studies have been performed with duckweed for nitrogen and phosphorus removal where 93% removal efficiency was achieved using municipal wastewater (Zhou et al., 2018) and 98% for swine wastewater (Mohedano et al., 2012). Certain *Spirodela* and *Lemna* species have showed the highest growth, biomass production accompanied by efficient nutrient removal from wastewater (Cheng & Stomp, 2009). **Figure 3** summarizes the major potential applications of duckweed species.

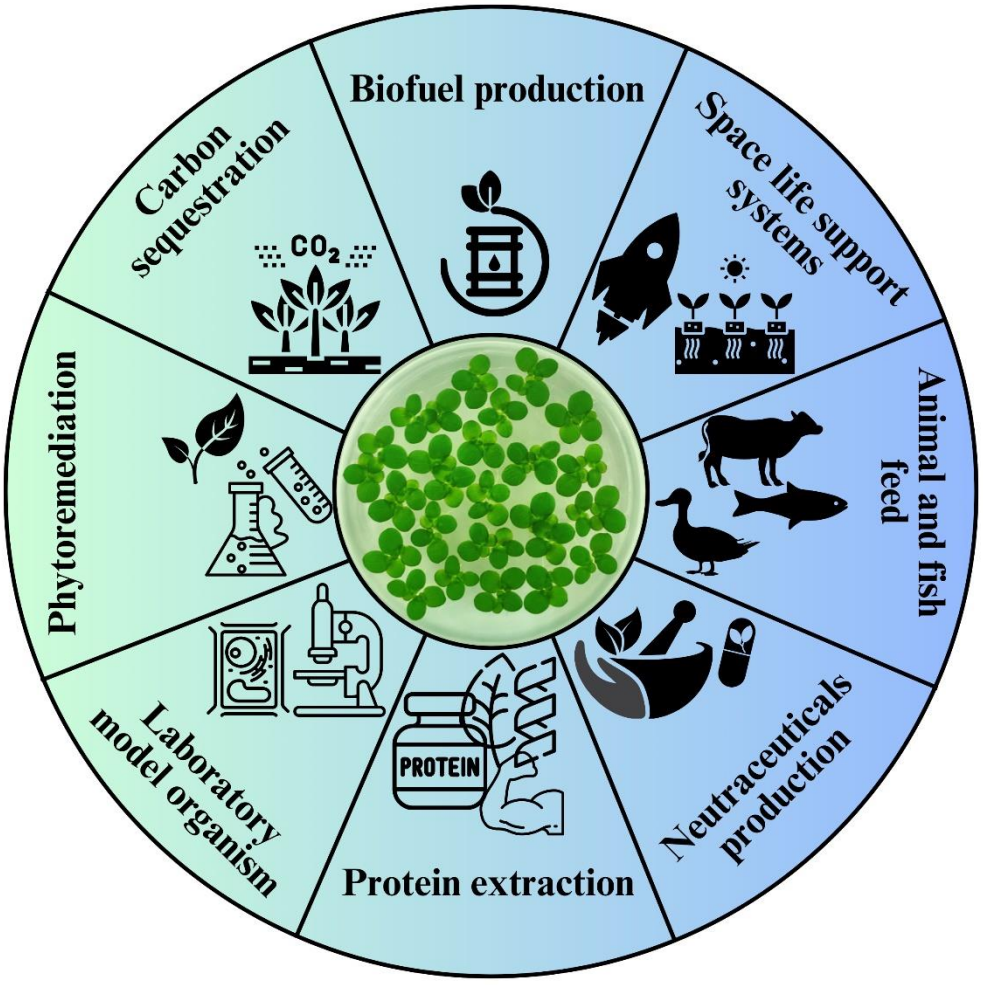

Figure 3. Current and further potential applications of duckweeds (author's own illustration based on the idea from Thingujam et al., 2024).

Besides these large-scale applications, duckweed plants are also being widely used in laboratory-scale studies for research purposes and have gained popularity over the years. They are being studied regarding their genomics, biochemistry and developmental physiology (Acosta et al., 2021; Zhou et al., 2023). Due to the small genome size of *Spirodela*, it is often studied as a reference genome for the monocots (An et al., 2018). Duckweed roots might also be utilized to simulate the molecular and evolutionary processes behind losing vestigial organs in plants (Ware et al., 2023). The members of Lemnaceae family are also excellent for modelling the environmental stress responses in aquatic plants because of their high sensitivity (Zhou et al., 2023).

3.3. Utilization in ecotoxicology

Amongst laboratory scale applications, duckweeds have been extensively used in plant physiology research and their popularity as a model organism comes from a variety of innate fundamental advantages that make them an appealing asset in ecotoxicological research. For instance, their rapid growth rate predominantly by vegetative reproduction enables researchers to conduct toxicity studies in comparatively shorter periods than with other test species (Radić et al., 2011; Acosta et al., 2021; Yahaya et al., 2022). This trait is especially useful when conducting acute toxicity tests, where speedy results can be extremely important. In this regard, duckweeds are advantageous over the other test species for not relying on the root-to-shoot transport but directly absorbing the nutrients from their abaxial surface of fronds (Landolt & Kandeler, 1987; Cedergreen & Madsen, 2002), hence resulting in faster and more direct responses. As duckweeds are relatively easy to grow, require less area and fewer resources, their utilization under laboratory conditions makes experimental techniques simpler with lower maintenance costs. Furthermore, these plants are very sensitive to a variety of pollutants, making them an accurate indicator of environmental stress factors. They can indicate a wide range of toxicants, including heavy metals (Sharma & Lenaghan, 2022), pesticides (Ueda & Nagai, 2021) and medicines (Markovic et al., 2021), highlighting their value in monitoring environmental pollution.

3.3.1. Development of duckweeds toxicity tests

Duckweeds have been used in toxicological testing since the late-19th and early-20th century when scientists began to observe their ability to respond to environmental factors. However, the work of a Swiss geobotanist Dr. Elias Landolt in the 1980s (Landolt, 1986) pioneered in making substantial contributions to the discipline. His extensive research determined the sensitivity of duckweeds to various environmental stresses, particularly on heavy metals which laid the foundation for utilizing duckweeds as bioindicators in toxicological investigations. In the period between the 1990s and 2000s, attempts were made to standardize test methodologies for conducting duckweed toxicity assays. The most popular and widely recognized standardized ecotoxicity tests include the Organization for Economic Cooperation and Development (OECD) guideline 221 (OECD, 2006), and International Standard Organization (ISO) protocols number 20079 and 20227 (ISO, 2005). The availability of these standardized test methodologies encouraged the widespread adoption of duckweeds in ecotoxicological investigations.

These test protocols involve exposing the duckweed test plants to environmental contaminants and their growth and physiological responses are monitored over time. Generally, *Lemna* and *Spirodela* species are preferred due to their ease of availability, larger size, rapid growth rate and high sensitivity to environmental changes. Several types of synthetic media have been recommended for duckweed culturing and toxicological testing including Steinberg medium, Schenk and Hildebrandt medium, N-medium, Bonner-Devirian medium, Bollard medium, Murashige and Skoog medium, and Hoagland medium (Appenroth, 2015). The test solutions are prepared by diluting the studied chemical agent (e.g., a pesticide, household chemical, cosmetic, etc.) in the growth medium by designing a series of concentrations, or by spiking the dilution series of the tested water sample with nutrients of the synthetic medium applied in the control. These concentrations usually span over several orders of magnitude to cover the range of potential toxic effects.

The widely adopted test protocols, including ISO (2005) and OECD (2006), recommend using a minimum of 100 mL growth medium in a single test vessel. In addition to test units, controls are also incorporated to check the optimum growth of duckweed cultures under non-contaminated conditions. Each concentration of the test substance and controls are set up in multiple replicates to ensure the statistical robustness of the tests. It is recommended to perform such growth inhibition tests at a temperature of 24 ± 2 °C, and under continuous warm- or cool-white, fluorescent light source within a light intensity range of 6500-10000 lux. The flux of the photosynthetically active radiation (400-700 nm) should also be kept between 85 to 125 $\mu E^{-2} s^{-1}$ (OECD, 2006). The size and design of the test vessels can vary according to the availability and personal preferences, but commonly used vessels include glass beakers, crystallization dishes and Petri dishes. The recommended duration of the tests by standard ISO and OECD protocols is 7 days but varying exposure durations (3-14 days) have been applied in literature considering the research objectives. However, OECD protocol puts a compulsion to let the test plants grow for several generations and the doubling time of control cultures should be less than 2.5 days for the tests to be adequately sensitive.

3.3.2. Measurement of growth inhibition

The subsequent changes in frond number, surface area and the produced biomass of the duckweed cultures upon exposure to the environmental stressors can be used to calculate growth inhibition (ISO, 2005; OECD, 2006). These changes are typically calculated in terms of relative growth rate (RGR) and yield for a specific growth parameter. For this purpose, the initial frond number, biomass or surface area covered by duckweed plants at the beginning of the tests is measured to establish a baseline for the comparison. Following that, these measurements are repeated periodically throughout the experiment. The natural dynamics of duckweed population growth follow a sigmoid curve (**Figure 4**), and duckweed growth inhibition tests are usually conducted targeting the exponential growth phase.

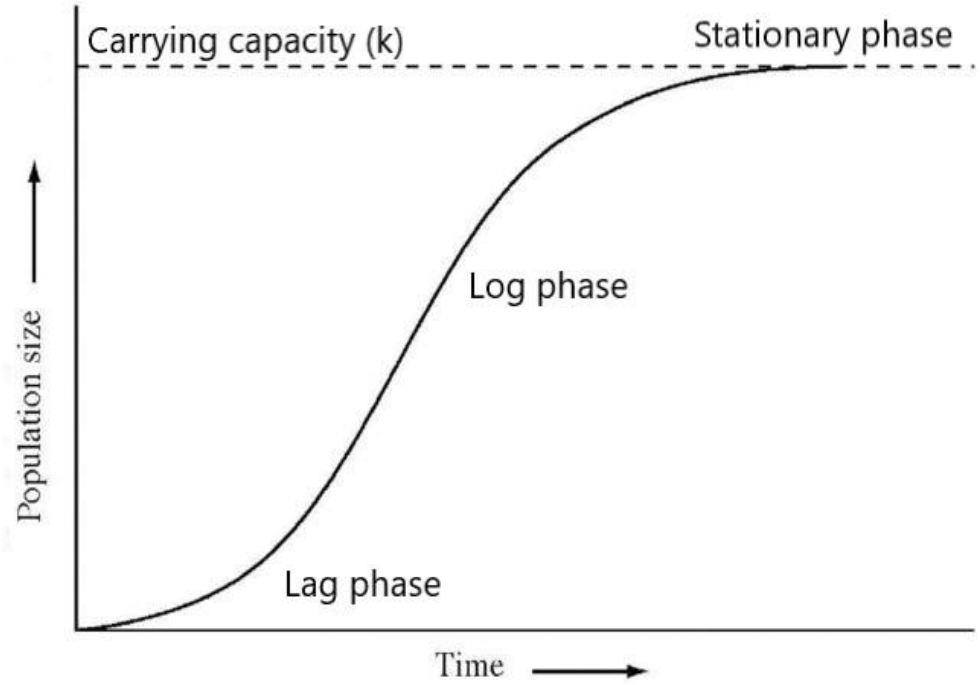

Figure 4. A standard sigmoid curve for duckweed population growth representing different phases of natural growth including lag-, log- and stationary-phase (derived from Yamaguchi, 2014).

Because of the exponential growth of cultures, log-transformation of growth parameters is required to linearize the growth (see section 4.4 in the Materials and methods). These calculated growth rates allow us to estimate the potential effects of harmful compounds on the growth of the test plants in comparison to the control plants. Additionally, the calculation of effective concentrations (EC) in toxicity tests also plays an essential role when evaluating the possible impact of pollutants on the test organism. EC represents the modelled concentration of an applied substance that results in a defined effect, such as a certain degree of growth inhibition, or mortality in a particular proportion of the test population. These concentrations are important for understanding the dose-response relationship and evaluating the toxicity of a chemical.

The most widely used EC is EC_{50}, that is the concentration at which the desired response is achieved by 50% of the population or the studied endpoint reaches

50% of that of the control population. In terms of duckweed toxicity assays, the latter one applies. Similarly, reporting EC_{10} and/or EC_{20} along with EC_{50} is also common in literature. These concentrations are usually calculated by fitting dose-response models in regression analyses. These models give mathematical description of the dose-response relationship thus allowing interpolation of the respective ECs (such as EC_{20} and EC_{50}, **Figure 5**). Besides, these models can also help in visualizing the relationship between the applied concentrations and the observed response in terms of the measured parameters.

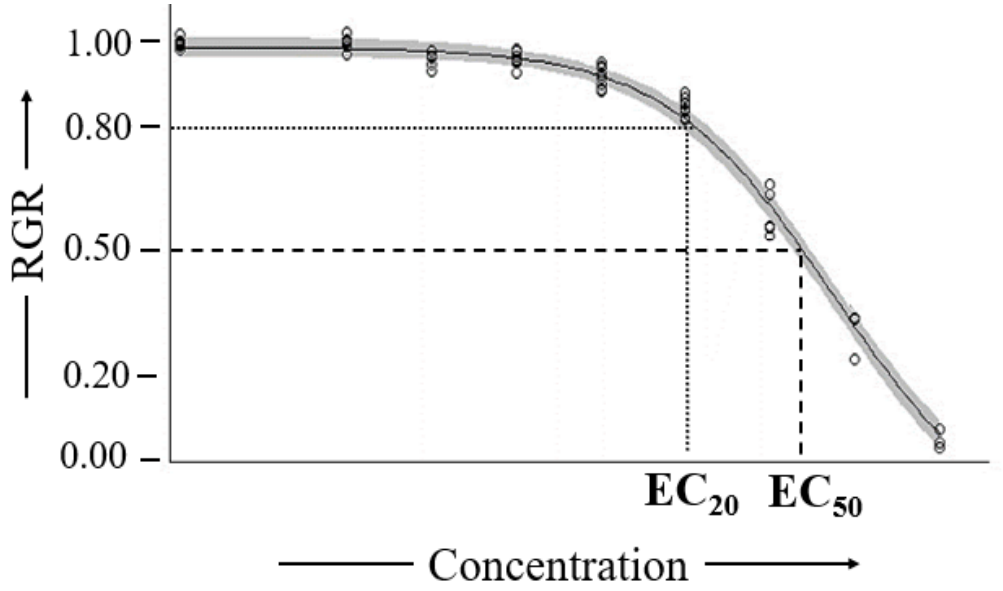

Figure 5. A dose response curve constructed by plotting the control-normalized relative growth rates against the toxicant concentration. EC_{20} and EC_{50} denote the estimated toxicant concentrations resulting in 20 and 50% growth inhibition compared to the control, respectively (author's own data were used for the graph).

3.3.3. Hormesis in toxicity assays

In addition to the typical growth inhibition pattern in **Figure 5.** resulting from toxicity of a pollutant, hormetic responses are also commonly observed in ecotoxicity tests (Cedergreen et al., 2007). Hormesis is a special response type when a known environmental stressor with proven toxicity at high dosage produces stimulatory

effects at a lower concentration (Southam & Chrlich, 1943; Agathokleous et al., 2024). Early observations of hormesis date back to ancient Greeks. However, this peculiar response has attracted research interest again in the late 20th century. Initially, the phenomenon was known as a biphasic growth response, and it was observed that lower concentrations of several toxins enhanced the fungal metabolism but inhibited it at higher concentrations (Schulz, 1887; Calabrese & Baldwin, 2001). Later on, the published works of Calabrese and Baldwin opened the way to the current adoption of this phenomenon (Calabrese & Baldwin, 2000a, 2000b, 2000c, 2000d, 2000e; Henschler, 2006). These authors also published a comprehensively detailed study describing different types of hormesis and interpreted their quantitative attributes (Calabrese & Baldwin, 2002). The stimulation during hormesis can vary but can even be as high as 60% compared to the control cultures.

Dose response relationships are described by fitting mathematical functions. The presence of hormesis, however, may result in poor fittings of the applied models, and underestimate the calculated EC values (Calabrese, 2003). Because of that, specific regression models that include a hormetic component are suggested when hormesis is observed during toxicity tests. These models allow calculating additional information related to hormesis, including No Observed Adverse Effect Level (NOAEL), maximum stimulatory response (MAX) and the associated effective concentrations with maximal stimulation (EC_{max}) (**Figure 6**). To meet the minimum threshold of hormesis and to prefer opting for a hormetic model, the stimulatory effect has been suggested to be more than 5% of the control value under identical conditions (Cedergreen et al., 2007).

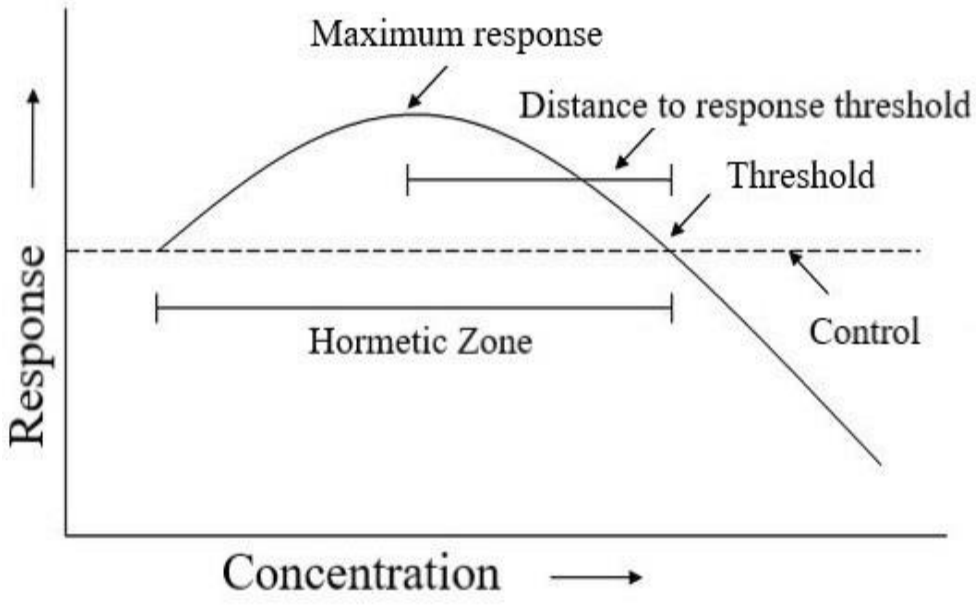

Figure 6. A generalized biphasic dose-response curve illustrating the quantitative features of hormesis (Cornelius et al., 2014).

3.3.4. Limitations of standard duckweed tests and subsequent developments

The most common standard toxicity testing protocols with duckweeds mainly focused on the measurement of growth inhibition based on the biomass production of the cultures. However, with the developments in biochemical analytical methods and availability of advanced imaging techniques, researchers have also started to measure additional parameters during such tests. In this regard, measurement of chlorophyll content (Zhao et al., 2015; Yang et al., 2022; Szabó et al., 2023), carotenoids (Daniel et al., 2020), and enzyme activities (Forni et al., 2012; Obermeier et al., 2015) were the most applied endpoints. Apart from these biochemical endpoints, morphometric parameters, such as colony size (Henke et al., 2011; Oláh et al., 2016) and measurement of the root length (Zhang et al., 2020; Lee et al., 2023) have also been suggested. Another key factor considering the limitations of the common standard protocols was the recommended test duration of 7 days which could lack rapidity and efficiency when test results from a larger number of samples are required over a shorter period. In order to overcome this issue, toxicologists adapted duckweed tests

in multi-well tissue-culture plates (usually 6-, 12- or 24-well plates) using smaller volumes of test medium for 3-7 days (Zhang et al., 2010; De Cesare et al., 2019; O'Brien et al., 2020; Lee et al., 2023). The amount of nutrients present in the wells were found to be sufficient for an optimal growth, and toxic effects were well developed at the end of these experiments. Such setups can be managed in a small space and require fewer resources. These advantages can promote their application as alternative testing systems to the standard ISO/OECD protocol-based systems (Baudo et al., 2015; Kalčíková et al., 2018; Kose et al., 2023). To date, these multi-well-plate-based tests were adopted for a limited number of stressors using only fewer concentrations, but they are gaining popularity. The application of tissue-culture plates also promotes the use of automated high throughput phenotyping systems (Subbaraman et al., 2024) and of chlorophyll fluorescence induction-based techniques as they allow multiple samples to be measured at the same time using such instruments.

3.4. Chlorophyll fluorescence induction method

The concept of chlorophyll fluorescence induction (ChlF) originated in the discovery of dark/light induction of chlorophyll fluorescence in photosynthesizing organisms, widely known as the Kautsky effect (Kautsky & Hirsch, 1931; Banks, 2017). Photons absorbed by photosynthetic pigments result in their excitation. This excitation energy can be used further in either of 3 possible ways. Firstly, a fraction of it operates the photochemistry driving the photosynthetic processes. Secondly, a portion of the remaining excitation energy that was not used in photochemistry dissipates in a regulated way as heat radiation through the xanthophyll cycle. Thirdly, a tiny amount (1-2%) of the excitation energy can be re-emitted in the visible light range as fluorescent light. This fraction is known as chlorophyll fluorescence (Maxwell & Johnson, 2000).

These three processes compete for the excitation energy, i.e., the share of either of them can increase only at the expense of the other two processes. This also means that changes in the share of either process are indicative of changes in the other two mechanisms. Kinetics in the ChlF thus can serve as a proxy of photosynthetic

and photoprotective processes. A combined term 'quenching' is used for all these three energy dissipation pathways. The measurement of ChlF can be performed in three different ways: by applying short light flashes (electron transfer from plastoquinone pool A to B), by using a saturating pulse (to achieve the saturated state of electron transport chain), and by using a continuous illumination (to induce a steady state of photochemistry), respectively (Kalaji et al., 2014). Based on these differences in measurement protocols, several types of fluorometers are available in the market including continuous excitation fluorometers (CEF), OJIP fluorometers and fast repetition rate (FRR) fluorometers, but pulse amplitude modulation (PAM) fluorometers are the most widely used in algae and plant physiology research (Lazár, 2015; Banks, 2017; Zavafer et al., 2020).

The basic principle of measuring ChlF relies on a gradual transition from the dark-adapted state to the light-adapted one of the photosystem complexes. The initial state (O) refers to 'Open state' when all the photosynthetic reaction centers are relaxed, the antennae are in their non-excited state, and the electron transport chain is fully capable of conveying electrons. In this condition, the plastoquinone pool (PQ_A, PQ_B and free PQ) is in a completely oxidized state resulting in ground fluorescence level (F_o). This state allows capturing the maximum number of incoming photons. Upon absorption, the energy from the captured photons is used to split water molecules in PSII and the resulting electrons are transferred to the PQ pool via PQ_A and PQ_B. The electron transport chain then gets partially saturated and further electrons cannot be easily transported from PQ_A to PQ_B thus resulting in the reduction of PQ_A pool. This state is referred to as 'J' and is represented by a rise in the fluorescence yield due to the increasing portion of absorbed but non-utilized light energy. Following PQ_A, the reduction of PQ_B is termed as 'I' state. At the final, maximum peak in the fluorescence (F_m) represents the 'P' state, that is when the entire PQ pool is reduced, and all the absorbed energy is released in the form of fluorescence (Küpper et al., 2019).

This whole transition process takes less than a second under a saturating light pulse and is often referred to as fast kinetics of ChlF. The ground fluorescence of a

sample is measured by a PAM ChlF fluorometer using weak illumination pulses that cannot trigger photochemical charge separation in PSII but is released shortly after its absorbance in the form of chlorophyll fluorescence. The transitional states of this curve and their related fluorescence levels are also measured in detail only when using OJIP fluorometers. However, in the case of the most widely applied PAM fluorometers, this transition is expressed as a high peak value (F_m). After the 'P state', when the saturating light is off, ChlF emission phases out in a few seconds. If the illumination, however, stays continuously on, ChlF is subjected to a subsequent decrease which eventually stabilizes that is called steady-state fluorescence (F_s) (**Figure 7**). This process of decrease in fluorescence is referred to 'fluorescence quenching'. The quenching process occurs due to an increase in the electron transport rate backed by the activation of enzymatic carbon assimilation and stomatal opening (photochemical quenching qP), and heat energy dissipation (non-photochemical quenching qN). A time span of around 15-20 minutes is required to complete this quenching process depending on the plant species and physiological state (Maxwell & Johnson, 2000). When steady-state photochemistry has been achieved, another saturation pulse can be applied to measure the maximum fluorescence level in this state (F'_m). Since the enzymatic reactions and heat dissipation mechanisms are already active under actinic irradiation, this fluorescence level is expected to be lower than the dark-adapted F_m (**Figure 7**).

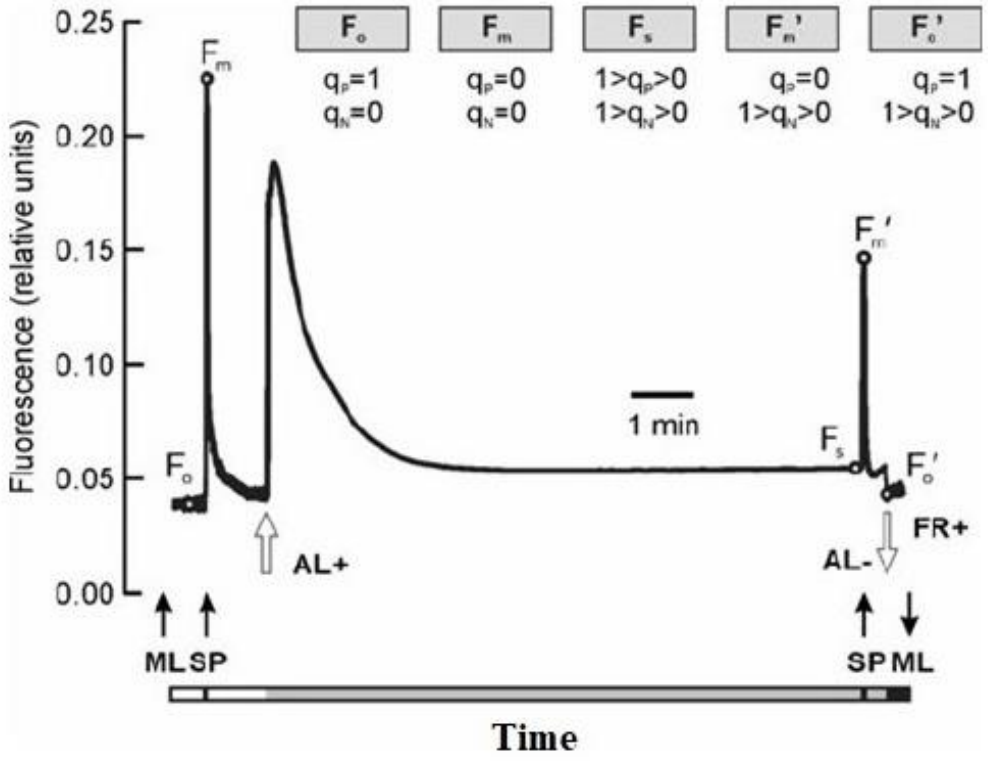

Figure 7. A standard PAM fluorometer ChlF induction curve showing a rapid rise fluorescence curve from F_o to F_m (Kautsky effect) and subsequent quenching as evidenced by the decrease in the fluorescence level (Buonasera et al., 2011). ML, SP, AL and FR denote the application of measuring light, saturation pulse, actinic light and far-red light, respectively.

The basic ChlF parameters recorded during the PAM measurement routine include ground (F_o) and maximal fluorescence yields of the dark-adapted sample (F_m), and steady-state (F_s) and maximal fluorescence yields (F'_m) of the light-adapted sample under actinic irradiation. F'_o denotes ground fluorescence yield of the light-adapted sample without actinic light but applying a far red (FR) illumination to selectively excite PSI. This way, electrons already in the electron transport chain can be "drained" without inducing further charge separation and supplying new electrons into electron transport. Both the photochemical and non-photochemical processes

operate simultaneously, and it is necessary to differentiate between them for estimating the photochemistry of PSII. This resolution was made possible by designing pulse amplitude modulation (PAM) chlorophyll fluorometers based on the principle of "light doubling". Following this principle, a PAM fluorometer applies multiple short-lived saturation pulses with increasing intensities to periodically turn off the photochemical quenching (qP) and measures the variable ChlF until the saturation is reached (Schreiber et al., 1986; Buonasera et al., 2011).

PAM fluorometers also have a clear advantage of allowing measurements even in bright environments (Murchie & Lawson, 2013). The presence of ambient light doesn't interfere with the measurements because the induction light is applied at a known frequency and the detector is synchronized to measure the same frequency. PAM ChlF measurements can be used to generate a variety of indices that can be used as potential indicators of stress or toxicity in plant ecophysiological studies. However, the above mentioned dark- and light-adapted basic ChlF levels i.e., F_o, F_m, F_s, F'_o and F'_m are used to calculate all these available endpoints (**Figure 7**, **Table 1**).

Table 1. Calculation and physiological background of some of the most widely applied ChlF parameters.

Endpoint	Formula	Physiological background	References
F_v/F_m	$(F_m-F_o)/F_m$	Maximum quantum yield of PSII photochemistry	(Roháček, 2002)
F_v/F_o	$(F_m-F_o)/F_o$	Maximum ratio of quantum yields of photochemical and concurrent non-photochemical processes in PSII in dark-adapted state	(Roháček, 2002)
Y(II)	$\Delta F/F'_m$	The effective quantum yield of photochemical energy conversion in PSII; a.k.a. Genty parameter	(Roháček, 2002)
Y(NPQ)	$(F_s/F'_m)-(F_s/F_m)$	Quantum yield of regulated non-photochemical energy loss in PSII	(Klughammer & Schreiber, 2008)
Y(NO)	F_s/F_m	Quantum yield of non-regulated heat dissipation and fluorescence emission	(Klughammer & Schreiber, 2008)
NPQ	$(F_m-F'_m)/F'_m$	Non photochemical ChlF quenching	(Roháček, 2002)
qP	$(F'_m-F_s)/(F'_m-F'_o)$	Photochemical quenching of variable ChlF, i.e., the fraction of open PSII reaction centers in light-adapted state	(Roháček, 2002)
qN	$(F'_m-F'_o)/(F_m-F_o)$	Non photochemical quenching of variable ChlF	(Roháček, 2002)
F'_v/F'_m	$(F'_m-F'_o)/F'_m$	Effective quantum yield of PSII photochemistry in light-adapted state	(Roháček, 2002)
F'_v/F'_o	$(F'_m-F'_o)/F'_o$	Effective ratio of quantum yields of photochemical and concurrent non-photochemical processes in PSII related to light-adapted state	(Roháček, 2002)
Rfd	$(F_m-F_s)/F_s$	Chlorophyll fluorescence decrease ratio proportional to net photosynthesis; a.k.a. “vitality index”	(Lichtenthaler et al., 2005)

3.4.1. Chlorophyll fluorescence imaging in duckweed research

The early works for the development of photosynthesis imaging were carried out during the late 1990s and early 2000s by using a Peltier-cooled CCD-camera and a fluorescence microscope. Later on, compact PAM fluorometers were designed by mounting LED light source, a CCD camera and enabling data transfer to a computer, altogether called as imaging PAM chlorophyll fluorometer (Schreiber et al., 2007). Regarding the applications, assessment of phytotoxic effects in algal species has already been performed using imaging PAM technique (Schreiber et al., 2007; Muller et al., 2008), seagrass (Ralph et al., 2005; Wilkinson et al., 2015), or mosses (Chen et al., 2019). A clear advantage of this technique is the possibility of parallel phenotyping using several samples simultaneously. It is also possible to use multi-well tissue-culture plates during such measurements. Duckweeds' body is essentially 2-dimensional and floats on the surface of the medium, facing directly towards the optical sensor, thus making them suitable for ChlF imaging. Additionally, due to their small size, they can easily be grown and measured in multi-well plates. They take up substances directly into the assimilating tissues without involving root-to-shoot transport, and thus the photosynthetic responses can become faster and more direct. Considering these advantages, ChlF imaging-based techniques have been widely used in duckweed research to evaluate their physiological fitness and morpho-physiological characteristics (Pietrini et al., 2019; Stewart et al., 2020; Liebers et al., 2023; Smith et al., 2024), and even to analyze photosynthetic heterogeneities within the frond (Oláh et al., 2024).

3.4.2. Applications and limitations of the chlorophyll fluorescence induction method

ChlF-based methods have been increasingly utilized in the past decade in various physiological and ecotoxicological studies with plants and algae (Gan et al., 2023; Moustaka & Moustakas, 2023). They have been studied as a promising substitute to the traditional growth-based methods since they offer non-destructive way of measurements (Brain & Cedergreen, 2009). ChlF is directly related to the flow

of energy via electron transport chain that is utilized by the plants for growth. In addition, photosynthesis is a complex biochemical process consisting of many consecutive steps, and some of those show high sensitivity to any disturbance. Therefore, any external stress affecting the plants' metabolism can impact ChlF-derived parameters (Barbagallo et al., 2003; Murchie & Lawson, 2013). Since photosynthesis acts as the basic energy source for plant growth, changes in ChlF can offer an early-warning proxy for the toxicological effects, that potentially outperforms the sensitivity of growth-based phytotoxicity test endpoints even at shorter exposure duration and lower toxicant concentration (Cervantes et al., 2001; Ralph et al., 2007; Ziegler et al., 2019).

Apart from these advantages, this technique also has its limitations concerning applicability. The wide set of measuring conditions that may affect the outcome, and due to the diversity of potentially applicable ChlF endpoints the comparison between different data sources has become a challenge. Many widely used endpoints in literature reflect different aspects of photosynthetic efficiency, such as F_v/F_m, F_v/F_o, Y(II), qP, and ETR (i.e., electron transport rate). Others, contrastingly, describe the efficiency of photoprotective mechanisms and constitutional energy loss processes, such as qN (non-photochemical quenching), NPQ (an alternative to qN without needing F'_o for its calculation), Y(NPQ) (share of the regulated non-photochemical quenching, i.e., heat dissipation), Y(NO) (share of the non-regulated non-photochemical quenching, i.e., ChlF). When it comes to testing the applicability of ChlF-based methods in phytotoxicity compared to the traditional endpoints, most papers in the available literature are focused on a single toxicant or a well-defined group of toxicants. In addition, these case studies apply various test and exposure conditions making the results difficult to compare.

4. Materials and methods

4.1. Test plants and culturing conditions

Axenic cultures of two duckweed species were used for this study. We used *Spirodela polyrhiza* (L.) Schleid. clone #UD0401 (isolated in lake Kis-Balaton, W-Hungary) (Oláh et al., 2018) to compare the sensitivity of different ChlF-based endpoints. As a second test species, we chose *Lemna gibba* L. clone #UD0101 (isolated in Poroszló, E-Hungary) to evaluate the toxicity of metals and metalloids (**Figure 8**). Healthy colonies picked from the main stocks were allowed to grow for 7 days under axenic conditions in 100 mL of Steinberg medium (Environment Canada, 2007). The sub-stocks were kept in the tissue culturing room of the Department of Botany, University of Debrecen under a continuous, white irradiation (60 ± 2 µE m^{-2} s^{-1}) and controlled temperature (24 ± 2°C). These sub-stocks were then used as a starting inoculum for our toxicity experiments.

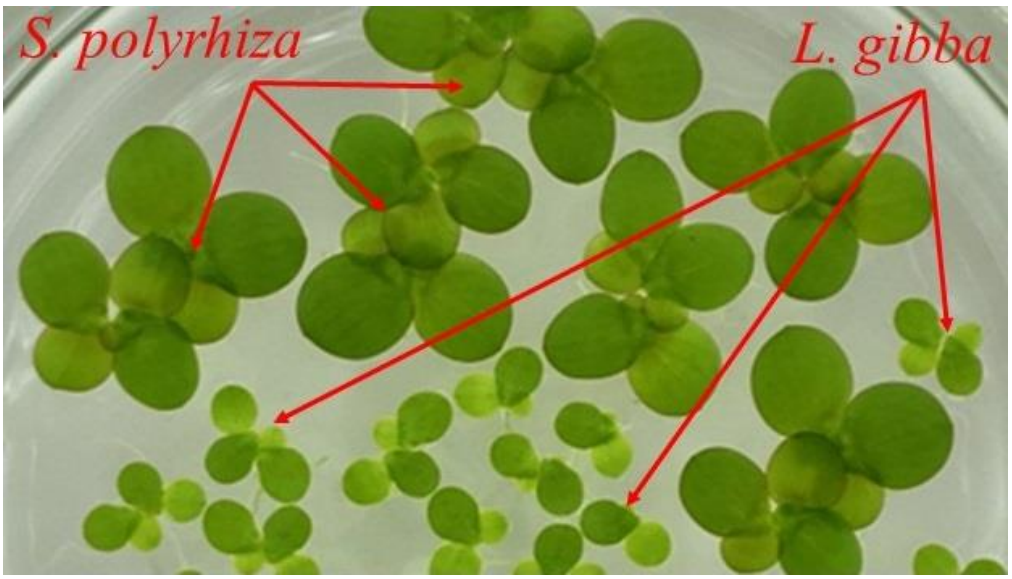

Figure 8. Specimens of the applied duckweed clones UD0401 (*S. polyrhiza*) and UD0101 (*L. gibba*) under laboratory conditions (author's own image).

4.2. Experimental design and preparation of chemicals

For stock culturing and experimental work, modified Steinberg medium was used with a final pH of 6.0 ± 0.2 (Steinberg, 1946; Environment Canada, 2007). The chemical composition and preparation of the medium is supplemented in **appendix III**. The freshly prepared Steinberg medium was autoclaved and stored at room temperature before use. The experimental work was performed under non-axenic conditions, but the sterile medium, axenic stock cultures and short exposure duration ensured that microbial contamination had not affected the plants' responses.

In the experiments with *S. polyrhiza*, we used three chemicals that were suggested for standard duckweed test protocols as reference toxicants in positive controls (Environment Canada, 2007): nickel (Ni as $NiSO_4 \times 7H_2O$), chromate (i.e., Cr(VI) as $K_2Cr_2O_7$) and sodium chloride (NaCl). The applied Ni and Cr(VI) concentrations ranged between 0.039–10.0 mg L^{-1} in a geometric series of 9 consecutive concentrations each doubling the previous one. NaCl was applied in an arithmetic concentration series in the range of 2–16 g L^{-1}, each concentration exceeding the previous one by 2 g L^{-1}. In addition to these treatments with either toxicant concentration, controls with pure Steinberg medium were also included.

After selecting the most sensitive ChlF-based endpoints, we compared their responsivity to the commonly used growth-based ones in *L. gibba*, using 12 environmentally relevant metals and metalloids, including different oxidation states of some metals. Pilot experiments were first run to find the nominal concentration ranges for all the tested elements. On the basis of these pilot experiments, we applied the toxicants in a series designed to cover approximately three magnitudes using at least eight nominal concentrations. The concentrations at every series level were doubled as compared to the previous concentration level. Three elements, namely Ag, Cr(VI) and Se(VI), showed highly divergent response ranges for growth- and ChlF-based endpoints in the pilot experiments, therefore, we introduced additional concentration levels for these metals. We applied the tested elements in the following concentration ranges given in **Table 2**.

Table 2. The studied elements, source chemicals and their respective concentrations.

Element	Symbol	Source chemical	Concentration range
Silver	Ag	$AgNO_3$	0.76 ng L^{-1}–0.25 mg L^{-1}
Arsenite	As(III)	$NaAsO_2$	0.078–10 mg L^{-1}
Arsenate	As(V)	Na_2HAsO_4	0.78–100 mg L^{-1}
Cadmium	Cd	$CdCl_2$	0.078–10 mg L^{-1}
Chromite	Cr(III)	$KCr(SO_4)_2 \times 12H_2O$	0.78–100 mg L^{-1}
Chromate	Cr(VI)	K_2CrO_4	0.0012–10 mg L^{-1}
Copper	Cu	$CuSO_4 \times 5H_2O$	0.078–10 mg L^{-1}
Mercury	Hg	$HgCl_2$	0.078–10 mg L^{-1}
Nickel	Ni	$NiSO_4 \times 7H_2O$	0.078–10 mg L^{-1}
Selenite	Se(IV)	Na_2SeO_3	0.078–10 mg L^{-1}
Selenate	Se(VI)	$Na_2SeO_4 \times 10\ H_2O$	0.002–10 mg L^{-1}
Zinc	Zn	$ZnSO_4 \times 7H_2O$	0.78–100 mg L^{-1}

The experiments with both species were conducted using standard 12-well tissue-culture plates. Each well contained either 4 mL pure Steinberg medium (controls) or the metal-spiked solution (treatments). All the control and treatment wells were paralleled by four replicates. The starting inoculum for each well consisted of a single healthy colony of *S. polyrhiza* (4–5 fronds) or *L. gibba* (3–4 fronds). The exposures lasted for three days (72 ± 2 h) under identical ambient conditions to those of stock culturing. This shorter exposure duration was chosen based on preliminary experiments indicating no nutrient depletion or crowding in the control wells until the end of the test while maintaining the minimum growth rate requirements of standard toxicity tests. The experiments with *S. polyrhiza* were repeated three times applying identical environmental conditions and the same experimental design. The experimental work with *L. gibba* was repeated twice with regard to each metal.

4.3. *In vivo* chlorophyll fluorescence induction measurements

We used a Maxi Imaging-PAM chlorophyll fluorometer (Heinz Walz GmbH, Effeltrich, Germany) to measure the photosynthetic activity of the test plants. The instrument used a built-in, blue-colored LED light source with a peak intensity at 450 nm to illuminate the samples and captured the images using an IMAG–K6 digital camera (2/3" chip with 1392 × 1040 pixels resolution). The unit was operated via

ImagingWin v2.47 software (Heinz Walz GmbH, Effeltrich, Germany). We used slightly different protocols for the two parts of the investigation as detailed in the following subsections.

4.3.1. Standard chlorophyll fluorescence induction curve measuring routine

The following protocol was applied to compare sensitivities of different ChlF-derived endpoints in *S. polyrhiza* to the reference toxicants:

1. Before starting ChlF measurements, we allowed the test plants to achieve fully oxidized state of PSII photochemistry by dark-adapting them for 20 minutes.
2. F_o i.e., ground fluorescence level of plants was determined immediately after dark-adaption using a weak, non-inductive measuring light (intensity: 2, frequency: 1 s^{-1}).
3. The dark-adapted maximum fluorescence level (F_m) of the test plants was then measured using a single saturating light pulse for 720 ms (intensity: ~ 4000 µE m^{-2} s^{-1}).
4. Afterwards, light-adapted state of the plants was induced using a continuous actinic irradiation for 10 minutes (intensity: ~77 µE m^{-2} s^{-1}). The intensity of this applied irradiation aimed at mimicking the light climate during the stock culturing and experimental treatments of the plants. In the light-adapted state of plants, F_s (i.e., steady-state ChlF level) was measured. Also, the maximum fluorescence level under light-adapted state (F'_m) was measured by means of a second saturating pulse with the same settings as for determining F_m. We were unable to directly measure F'_o (i.e., ground ChlF level under the light-acclimated state) using the imaging PAM due to absence of far-red light source to selectively excite PSI. Instead, it was calculated using the following formula (Heinz Walz GmbH, 2019):

$$F'_o = \frac{F_o}{(\frac{F_v}{F_m} + \frac{F_o}{F'_m})}$$

5. Right after obtaining the ChlF induction curve using the above-mentioned measurement protocol, we recorded a so-called rapid light curve (RLC) in the light-adapted plants (see also in section 4.3.2). This RLC characterized the functional state of PSII photochemistry along with 15 consecutively increasing illumination intensities ranging from 0–530 µE m^{-2} s^{-1}, with each light step lasting for 30 s. At the end of each light step, quasi steady-state chlorophyll fluorescence (F_s) and the light-adapted maximal chlorophyll fluorescence yield (F'_m) was determined under the ambient light intensity according to the previous point #4.
6. Finally, different ChlF-based endpoints were calculated using the formulas provided in **Table 1**. All those endpoints were used for *S. polyrhiza*, however, we used only the two most sensitive endpoints from the dark- and light-adapted states i.e., F_v/F_o and Y(II) in the investigations with *L. gibba*.

4.3.2. Rapid light curve (RLC) induction and calculation of ETR

The electron transport rate (ETR) of *S. polyrhiza* plants was calculated using F_s and F'_m according to the given formula (Heinz Walz GmbH, 2019):

$$ETR\ (\mu mol\ electrons\ m^{-2}s^{-1}) = Y(II) \times PPFD \times 0.84 \times 0.5$$

Where PPFD = the photosynthetic photon flux density of the incident light (µE m^{-2} s^{-1}), and the two constant values refer to the incident light absorption efficiency of the plants (i.e., 84%) and the assumed proportion of light absorbed by PSII (i.e., 50%) assuming equal stoichiometric distribution of the absorbed light between PSI and PSII (Ralph et al., 2005; Murchie & Lawson, 2013; Kalaji et al., 2017; Park et al., 2017).

The calculated ETR values corresponding to 15 incident PPFD levels were then used for plotting the rapid light curve (**Figure 9**) in order to determine ETR_{max} and **α**. ETR_{max} shows the highest calculated value of ETR along the curve while **α** refers to the initial slope of the curve representing the maximum photon-use efficiency under the applied ambient conditions. The following mathematical equation was applied to calculate **α**:

$$\alpha\ (electron\ photon^{-1}) = ETR/11 \quad \mu E\ m^{-2}s^{-1}$$

where 11 corresponds to the lowest light intensity applied in the course of the RLC measurements (**Figure 9**).

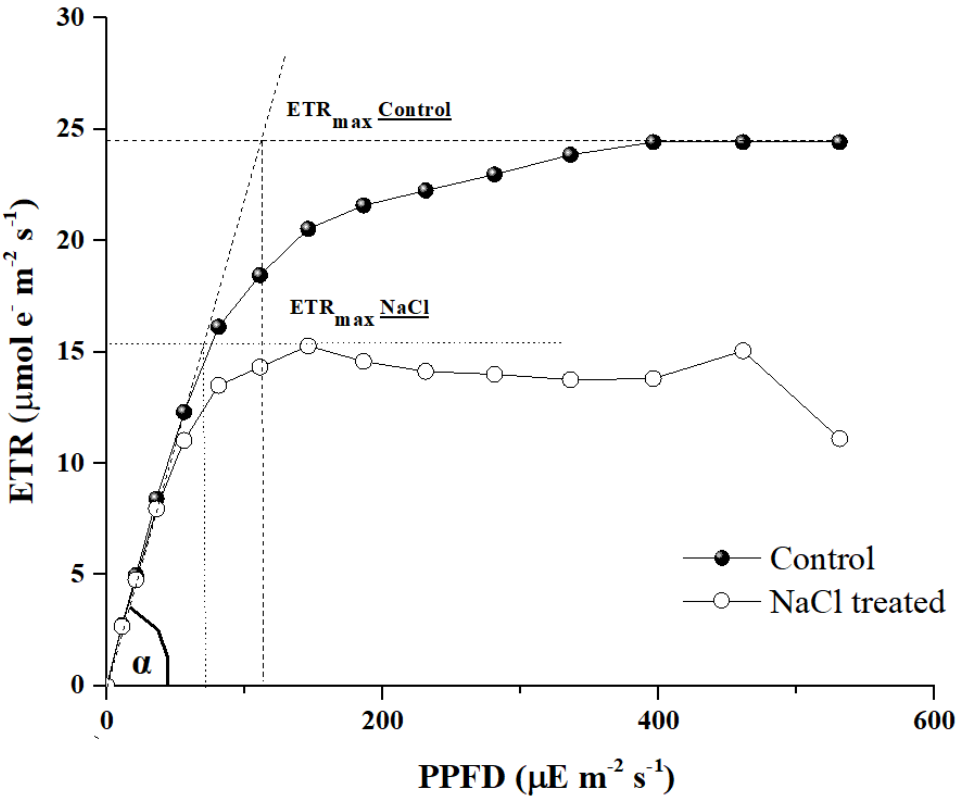

Figure 9. Rapid Light Curves of control and treated plants showing the saturation of the electron transport against the applied light intensities (PPFD). Parameters α and ETR_{max} denote the initial slopes and the maximal values of the saturation curves, respectively (author's own graph).

4.3.3. Customized protocol to obtain basic chlorophyll fluorescence parameters

The standard ChlF induction protocol measures all the basic ChlF levels along with a continuous sequence. During this routine, firstly the dark-adapted indicators (F_o and F_m) are measured, then the plants are continuously illuminated until

steady-state photosynthesis, and eventually the light-adapted indicators, such as F'_s, F'_o, F'_m are measured in this state. We shortened this process by reversing the order of the measurements: Since the test plants were already light-adapted when taken for the measurements from the tissue culturing room, the light-adapted ChlF parameters could hence be measured by maintaining this state. Following that, as a second step, the plants were darkened to measure the dark-adapted ChlF parameters. This way, the time-consuming induction of photosynthetic processes could be spared while still obtaining the 4 basic parameters. This shortened, 2-step routine was used for *L. gibba* to compare phytotoxic potential of different metals and metalloids following the below protocol:

1. As a first step, the test plants were swiftly transferred from the tissue-culturing room into the instrument's measurement chamber. In order to maintain the light-acclimated state of the plants, letting them stop floating around in the wells and to adapt them to the instrument's actinic light conditions, we illuminated them for 60 s using a continuous actinic light (~77 $\mu E\ m^{-2}\ s^{-1}$).
2. Before the continuous actinic light was timed-out, F_s was measured followed by a saturating light pulse (~4000 $\mu E\ m^{-2}\ s^{-1}$) to measure F'_m.
3. After the measurement of light-adapted ChlF levels, the test plants were put into 20 minutes of dark-adaptation to fully oxidize PSII. Subsequently, we measured the dark-adapted ChlF levels (i.e., F_o and F_m) following the same protocol given in steps 2–3 of section 4.3.1.
4. The calculation of the ChlF-based endpoints including F_v/F_o and Y(II) followed the same protocol as given in **Table 1**.

4.4. Measurement of growth inhibition

We used ChlF images of *L. gibba* cultures taken by the ImagingWin software v2.47 (Heinz Walz GmbH, Germany) to calculate the relative growth rates (RGR). These images were taken on the 0^{th} and 3^{rd} days under the dark-adapted conditions representing F_m of the cultures. In order to obtain the total surface area and frond numbers of the cultures, the exported images (JPEG with 640 × 480 pixels resolution)

were then processed using ImageJ software v1.54d (Schneider et al., 2012). The function 'Analyze Particles' was applied to measure plant area within manually defined selections. Another plugin, namely 'cell counter' was applied to help the visual counting of the fronds. These calculated values for the surface area and total frond number were then utilized to calculate the relative growth rates (RGRs) in terms of both the measured parameters i.e., RGR_{area} and RGR_{frond}. The calculations were performed according to the below formula (OECD, 2006):

$$RGR_X = \frac{ln(X_f) - \ln(X_i)}{3}$$

where X denotes the growth parameter (area or number of fronds), X_i is the initial value of the respective growth parameter on day 0 and X_f is the final value of the respective growth parameter on day 3.

Based on RGR, the doubling time of the cultures was also calculated using the following formula (OECD, 2006):

$$Doubling\ time = \ln(2)/\mathrm{RGR}$$

4.5. Data processing and statistical analyses

During data processing for experiments with *S. polyrhiza*, we normalized the averages (mean) values of four internal replicates to their respective control averages. As the tests with each reference toxicant were triplicated, thus a total of n = 3 data for each applied concentration was used per toxicant. For the experiment with *L. gibba*, on the other hand, the data from two individual experiments were pooled to produce a total of n = 8 samples for each concentration level. We fitted non-linear regression models to the data for determining the concentration-dependent responses of ChlF- and RGR-based parameters by means of the "drc"-package (v. 2.5-12) (Ritz et al., 2015), in R statistical environment (v.3.2) (R Core Team, 2015) and in RStudio (RStudio Team, 2023). The lower limits for these log-logistic models were fixed to zero considering the assumption that the calculated ChlF-based endpoints –specifically depicting the efficiency of PSII photochemistry– can theoretically decrease to zero.

Primarily, we used 3-parameter log-logistic function "LL.3" of the drc package to model most –all in the case of *L. gibba*– of the ChlF-based responses. However, the modified log-logistic functions developed by Brain & Cousens, (1989) ("BC"-model) and by Cedergreen et al., (2005) ("CRS"-model) were also utilized. Thus, besides the 3-parameter log-logistic function, we also fitted the 4-parameter models ("BC.4" and "CRS.4") to the datasets in order to include a hormetic component at the lower concentration range. Firstly, the suitability of the applied models was visually evaluated and then compared according to their Akaike information criterion (AIC) score. For AIC comparison, we used the "mselect" function of the "drc"-package. Additionally, we also performed further suitability checks by applying the lack-of-fit test using the "modelFit" function and calculating the pseudo-R^2 using the "cor" function of the "drc"-package. During these investigations, hormetic models were only applied to describe stress responses in *S. polyrhiza*. However, toxic effects of metals and metalloids in *L. gibba* were only modelled by using 3-parameter log-logistic functions. Models with an additional hormetic component were opted in case of the former species because we observed hormetic-like responses for multiple endpoints in Ni and NaCl treatments. On the other hand, we didn't observe any significant hormesis (MAX >105% of control, (Calabrese, 2010)) in the majority of concentration-response relationships in treatments with *L. gibba*. Therefore, due to ensure uniformity in data processing within this study, we chose to apply the simplest model to describe plant responses. The applied models were then used to estimate the effective concentrations (EC) resulting in 20% (EC_{20}) and 50% (EC_{50}) inhibition of the respective endpoint by applying the 'ED' function of the 'drc' package. In the case when a hormetic model was applied, we also calculated the corresponding "No Observable Adverse Effect Concentration" (NOAEC), after fading of the hormetic effect. Similarly, the highest level of the hormetic response ("max"), and the concentration associated with this level were also extracted using the "MAX" function. The available literature also favors the calculation of maximum response since hormesis should be considered significant only when the max value exceeds that of control response by at least 5% (Calabrese, 2010).

We evaluated the sensitivity of ChlF-based endpoints based on the calculated mean ranks for both EC_{20} and EC_{50} values during the *S. polyrhiza* investigation. To calculate mean ranks, each of the eight measured endpoints was assigned with a rank based on the calculated EC values (lowest to highest) for each reference toxicant. These individual EC_{20} and EC_{50} ranks were then averaged to calculate mean ranks for the respective endpoint.

Similarly, the sensitivity of measured growth- and ChlF- based endpoints in the study with *L. gibba* was compared by their median EC_{20} and EC_{50} values calculated by paired sample Wilcoxon test using OriginPro 2016 (v. b9.3.226; Academic). A correlation matrix (Spearman's correlation) of the calculated EC_{50} values of the measured endpoints for *L. gibba* was also constructed using the 'corrplot' package (Wei & Simko, 2021) in RStudio in order to evaluate the interdependency in the sensitivity of both growth- and ChlF-based endpoints.

5. Results

5.1. Comparative responsiveness of ChlF-based endpoints

As a result of the treatments, ChlF parameters of *S. polyrhiza* were affected in the applied concentration range in terms of all the three reference toxicants (**Figures 10–12**). In general, the actual inhibition of ChlF-based endpoints in Ni treatments was recorded from 1.25 mg L^{-1}. Afterwards, these inhibitory effects were observed in a concentration-dependent manner till the maximum inhibition was achieved for each endpoint (**Figure 10**, for overall results and summary statistics refer to **Table S1**).

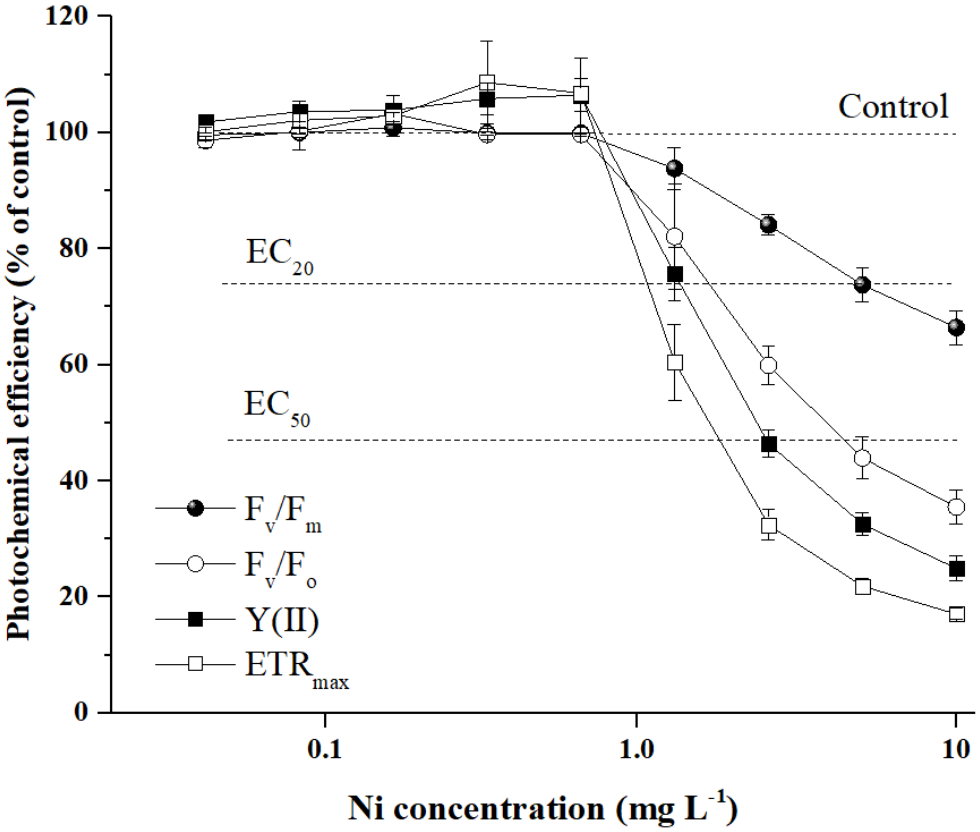

Figure 10. Concentration-dependent response curves of the most applied ChlF-based endpoints F_v/F_m, F_v/F_o, Y(II) and ETR_{max} in Ni treated *S. polyrhiza* UD0401 test plants. Symbols and error bars denote grand means ± SE of n = 3 samples.

Overall, the calculated EC_{20} and EC_{50} values for different ChlF-based endpoints showed considerable differences ranging between 1.0–3.7 mg L^{-1} (EC_{20}) and 1.8–20.6 mg L^{-1} (EC_{50}), respectively. Due to insufficient inhibitory effects, EC_{50} values for 4 out of the 9 studied parameters were higher than the maximal applied Ni concentration (that is 10 mg L^{-1}, **Table 3**). According to our results, ETR_{max} and Y(II) were the most responsive endpoints (i.e., those had the lowest EC_{20} and EC_{50}) while F_v/F_m and Rfd were the least responsive in Ni-treated *S. polyrhiza* plants.

A hormetic effect, on the other hand, was observed for most of the ChlF parameters when the Ni concentration was <1.25 mg L^{-1} (**Table 3**, RStudio-exported drc-model fittings are presented in **Figure S1**). This stimulatory effect ranged up to 10% as compared to control in the case of calculated ETR_{max}. In general, non-linear models including a hormetic component described the dose-response relationship in a better way even when the maximum stimulation was <5% compared to control, with the only exception of F_v/F_m. A NOAEC range for Ni was observed between 0.6–0.7 mg L^{-1} after the hormetic effect phased out. In general, EC_{max} for Ni was calculated to be in the range of 0.1–0.3 mg L^{-1} (**Table 3**).

Table 3. The basic parameters of non-linear regression model fittings (i.e., model type, degree of freedom (DF), residual sum of squares (RSS), F-value, Pseudo-R^2) using drc-package in RStudio, the calculated elements of hormesis (maximum value of observed hormesis (Max) and the associated concentration (EC_{max}), No Observed Adverse Effect Concentration (NOAEC)), and calculated EC values with 95% confidence interval (CI) for the measured ChlF-based endpoints after 72 h exposure to Ni in *S. polyrhiza* UD0401 test plants. Models "LL.3" and "BC.4" denote 3-parameter log-logistic and 4-parameter Brain-Cousens models, respectively. The corresponding values in the case of a significant hormetic effect (MAX >105% of control) are highlighted in Bold style.

Endpoint	Model	DF	RSS	F-Value	Pseudo-R^2	Max	EC_{max}	NOAEC (95% CI)	EC_{20} (95% CI)	EC_{50} (95% CI)
F_v/F_m	LL.3	27	323.56	1.7206	0.9286	NA	NA	NA	3.72 (2.87–4.57)	18.6* (13.8–23.4)
F_v/F_o	BC.4	26	914.79	0.5439	0.9522	102.5	0.2	0.52 (0.16–0.88)	1.41 (1.10–1.72)	4.2 (3.36–5.03)
Y(II)	BC.4	26	679	3.6103	0.9775	**108.3**	**0.26**	**0.67 (0.49–0.84)**	1.22 (1.05–1.38)	2.68 (2.35–3.01)
F'_v/F'_m	BC.4	26	404.32	1.4081	0.96	102.6	0.21	0.61 (0.30–0.91)	2.03 (1.65–2.41)	10.8*(7.55–14.0)
F'_v/F'_o	BC.4	26	1051.19	1.3835	0.9554	**105.6**	**0.23**	**0.64 (0.38–0.89)**	1.3 (1.04–1.56)	3.4 (2.74–4.07)
Rfd	BC.4	26	302.72	3.8371	0.9602	103.4	0.13	0.38 (0.05–0.71)	2.13 (1.69–2.57)	20.59* (12.0–29.2)
α	BC.4	26	747.14	0.3612	0.9267	103.3	0.23	0.68 (0.25–1.11)	2.2 (1.66–2.75)	11.4* (6.70–16.1)
ETR_{max}	BC.4	26	1671.24	2.5494	0.96	**110**	**0.28**	**0.66 (0.47–0.85)**	1.02 (0.85–1.19)	1.84 (1.56–2.13)

The extrapolated effective concentrations (i.e., higher than the maximum applied Ni concentration (10mg L^{-1}) and mathematically calculated using drc models) are represented with asterisk (*). Absence of hormetic response in terms of the respective parameter is indicated using NA (Not Applicable) as a value. **Figure S1** presents the RStudio-exported drc-model fittings and **Table S1** provides the summary statistics of the original data.

The experiments with Cr(VI) showed a similar lowest threshold level to that of Ni. Most of the ChlF parameters showed inhibition starting at 1.25 mg L^{-1}. However, ETR_{max} and F'_v/F'_o were already affected (~10% decrease) even at 0.625 mg L^{-1} (**Figure 11**), though this effect was not significant ($p = 0.0525$). Even if the calculated AIC scores indicated that concentration-based responses for most ChlF parameters were better modelled with a hormetic component than the three-parameter log-logistic models, Cr(VI) did not cause "true" (i.e., >105%) hormetic response in most of the cases (**Figure S2**). The only exception that even exceeded 102% of the control was Rfd (**Table 4**). The derived EC_{20} values for Cr(VI) were found to be ranging between 0.7–2.5 mg L^{-1} and EC_{50} values to be between 1.8–9.0 mg L^{-1}. Cr(VI) resembled the effects of Ni in that ETR_{max} was the most sensitive endpoint while Rfd and F_v/F_m were the least sensitive ones (**Table 4**).

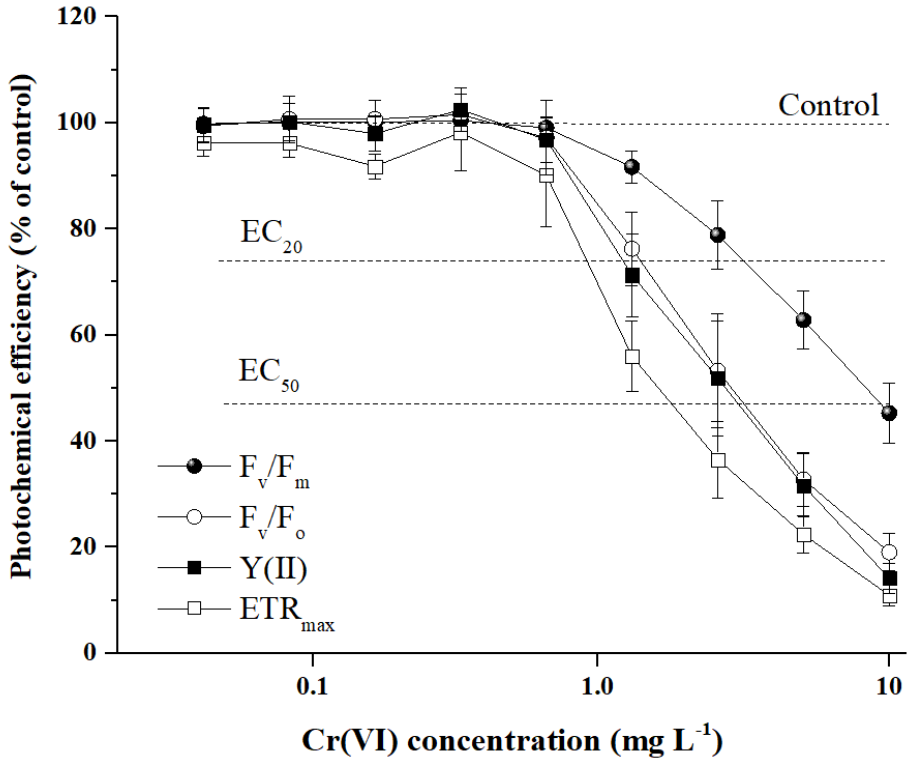

Figure 11. Concentration-dependent response curves of the most applied ChlF-based endpoints F_v/F_m, F_v/F_o, Y(II) and ETR_{max} in Cr(VI) treated *S. polyrhiza* UD0401 test plants. Symbols and error bars denote grand means ± SE of n = 3 samples.

Table 4. The basic parameters of non-linear regression model fittings (i.e., model type, degree of freedom (DF), residual sum of squares (RSS), F-value, Pseudo-R^2) using drc-package in RStudio, the calculated elements of hormesis (maximum value of observed hormesis (Max) and the associated concentration (EC_{max}), No Observed Adverse Effect Concentration (NOAEC)), and calculated EC values with 95% confidence interval (CI) for the measured ChlF-based endpoints after 72 h exposure to Cr(VI) in *S. polyrhiza* UD0401 test plants. Models "LL.3", "BC.4" and "CRS.4" denote 3-parameter log-logistic, 4-parameter Brain-Cousens, and 4-parameter Cedergreen-Ritz-Streibig models, respectively. The corresponding values in the case of a significant hormetic effect (MAX >105% of control) are highlighted in Bold style.

Endpoint	Model	DF	RSS	F-Value	Pseudo-R^2	Max	EC_{max}	NOAEC (95% CI)	EC_{20} (95% CI)	EC_{50} (95% CI)
F_v/F_m	BC.4	26	727.5	0.0317	0.9336	100.5	0.18	0.45 (0.58–1.47)	2.46 (1.89–3.03)	8.26 (6.25–10.3)
F_v/F_o	BC.4	26	1783.9	0.0571	0.9382	102.1	0.21	0.49 (0.02–1.00)	1.21 (0.89–1.53)	2.77 (2.24–3.30)
Y(II)	CRS.4b	26	1873.8	0.2508	0.9395	102.2	0.24	0.4 (0.03–0.83)	1.06 (0.72–1.40)	2.54 (2.00–3.09)
F'_v/F'_m	BC.4	26	984.35	0.066	0.9426	100.3	0.13	0.32 (0.36–1.00)	1.48 (1.09–1.87)	4.7 (3.74–5.67)
F'_v/F'_o	BC.4	26	2127.9	0.1227	0.9307	100.9	0.14	0.33 (0.16–0.82)	0.93 (0.63–1.23)	2.25 (1.75–2.74)
Rfd	BC.4	26	1537.2	0.2505	0.8784	**105.3**	**0.34**	**0.98 (0.37–1.58)**	2.47 (1.77–3.17)	9.02 (5.12–12.9)
α	LL.3	27	918.75	0.2719	0.9357	NA	NA	NA	1.88 (1.34–2.43)	6.13 (5.11–7.15)
ETR_{max}	LL.3	27	2303.1	1.0996	0.9344	NA	NA	NA	0.72 (0.47–0.98)	1.85 (1.45–2.24)

Absence of hormetic response in terms of the respective parameter is indicated using NA (Not Applicable) as a value. **Figure S2** presents the RStudio-exported drc-model fittings and **Table S2** provides the summary statistics of the original data.

After 72 h of exposure, different ChlF parameters responded very differently to NaCl treatments (**Figure 12**). After the hormetic effects were wearing down, the actual inhibitory effects could be first observed in terms of Rfd from 6 g L^{-1} NaCl, followed by the inhibition of Y(II) and ETR_{max} from 8 g L^{-1}. The rest of the ChlF-based endpoints including F_v/F_m, F_v/F_o, F'_v/F'_m, F'_v/F'_o and the maximal photon use efficiency (i.e., α) were inhibited at the maximum applied concentration of NaCl (16 g L^{-1}). Similar to Ni treatments, hormetic responses were observed for several ChlF-based endpoints including F_v/F_o, Y(II), F'_v/F'_o, and ETR_{max} at lower NaCl concentrations (**Figures 12** and **S3**, **Table 5**).

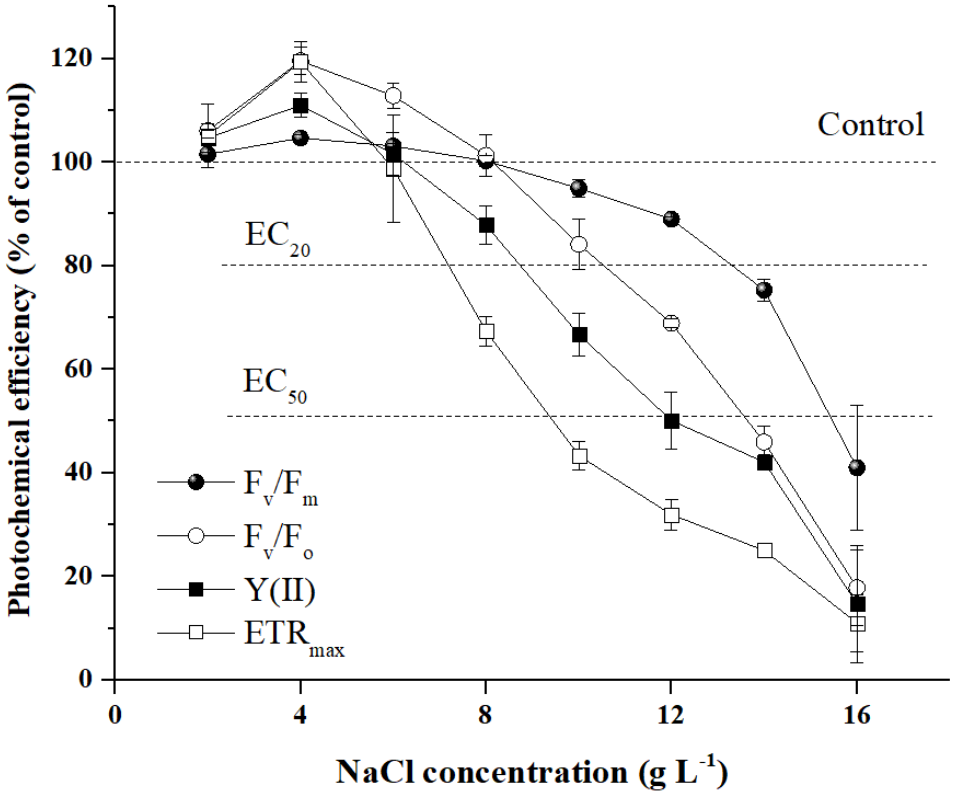

Figure 12. Concentration-dependent response curves of the most applied ChlF-based endpoints F_v/F_m, F_v/F_o, Y(II) and ETR_{max} in NaCl treated *S. polyrhiza* UD0401 test plants. Symbols and error bars denote grand means ± SE of n = 3 samples.

With an estimated EC_{max} of 3.2–4.6 g L^{-1}, or 50–57% of the predicted NOAEC, the maximal hormetic stimulation varied between 108 and 125% of the corresponding control values (**Table 5**). Additionally, despite the better fit of three-parameter log-logistic models, some parameters showed stimulation of 2–7% at lower concentrations ranges (2–4 g L^{-1}, **Figure S3**). The calculated EC_{20} and EC_{50} values for NaCl treatments ranged between 7.4–13.2 g L^{-1} and 9.7–15.5 g L^{-1}, respectively (**Table 5**). In line with our heavy metal treatments, the highest sensitivity was recorded for ETR_{max}, whereas Rfd and F_v/F_m were the least sensitive endpoints.

Table 5. The basic parameters of non-linear regression model fittings (i.e., model type, degree of freedom (DF), residual sum of squares (RSS), F-value, Pseudo-R^2) using drc-package in RStudio, the calculated elements of hormesis (maximum value of observed hormesis (Max) and the associated concentration (EC_{max}), No Observed Adverse Effect Concentration (NOAEC)), and calculated EC values with 95% confidence interval (CI) for the measured ChlF-based endpoints after 72 h exposure to NaCl in *S. polyrhiza* UD0401 test plants. Models "LL.3", "BC.4" and "CRS.4" denote 3-parameter log-logistic, 4-parameter Brain-Cousens and and 4-parameter Cedergreen-Ritz-Streibig models, respectively. The corresponding values in the case of a significant hormetic effect (MAX >105% of control) are highlighted in Bold style.

Endpoint	Model	DF	RSS	F-Value	Pseudo-R^2	Max	EC_{max}	NOAEC (95% CI)	EC_{20} (95% CI)	EC_{50} (95% CI)
F_v/F_m	LL.3	24	1109.59	0.5767	0.8996	NA	NA	NA	13.2 (12.4–14.0)	15.5 (15.0–15.9)
F_v/F_o	CRS.4a	23	1273.78	2.8564	0.9554	**113.2**	**4.55**	**8.78 (7.47–10.1)**	10.7 (9.96–11.5)	13.2 (12.6–13.8)
Y(II)	CRS.4a	23	1771.4	1.3314	0.9381	**108.2**	**3.2**	**6.48 (4.34–8.61)**	8.95 (7.87–10.0)	12 (11.1–12.8)
F'_v/F'_m	LL.3	24	1546.45	1.983	0.8844	NA	NA	NA	11.8 (10.7–13.0)	15.1 (14.4–15.9)
F'_v/F'_o	BC.4	23	2031	3.5422	0.9333	**124.6**	**4.63**	**8.57 (7.52–9.61)**	10.2 (9.37–11.1)	13.3 (12.2–14.3)
Rfd	LL.3	24	1206.4	1.4771	0.9374	NA	NA	NA	10.1 (9.09–11.2)	13.4 (12.8–14.0)
α	LL.3	24	1479	0.8038	0.9053	NA	NA	NA	11.9 (10.9–12.9)	14.6 (14.1–15.2)
ETR_{max}	BC.4	23	1632.4	0.9605	0.9595	**115.8**	**3.45**	**6.06 (5.12–7.00)**	7.44 (6.76–8.11)	9.71 (9.06–10.4)

Absence of hormetic response in terms of the respective parameter is indicated using NA (Not Applicable) as a value. **Figure S3** presents the RStudio-exported drc-model fittings and **Table S3** provides the summary statistics of the original data.

We compared the overall sensitivity of tested ChlF endpoints in *S. polyrhiza* exposed to three reference toxicants using the mean ranks of the calculated EC_{20} and EC_{50} values. In terms of both EC_{20} and EC_{50}, the order of sensitivity indicated ETR_{max}, Y(II) and F'_v/F'_o to be the most responsive endpoints followed by F_v/F_o (**Figure 13**). $F_v/F_{m,}$ on the other hand, was the least responsive endpoint along with other light-adapted endpoints including F'_v/F'_m, Rfd and α (**Figure 13**). According to the calculated mean ranks, Rfd proved to be more responsive than α in terms of EC_{20} values, but this order was reversed for EC_{50} values.

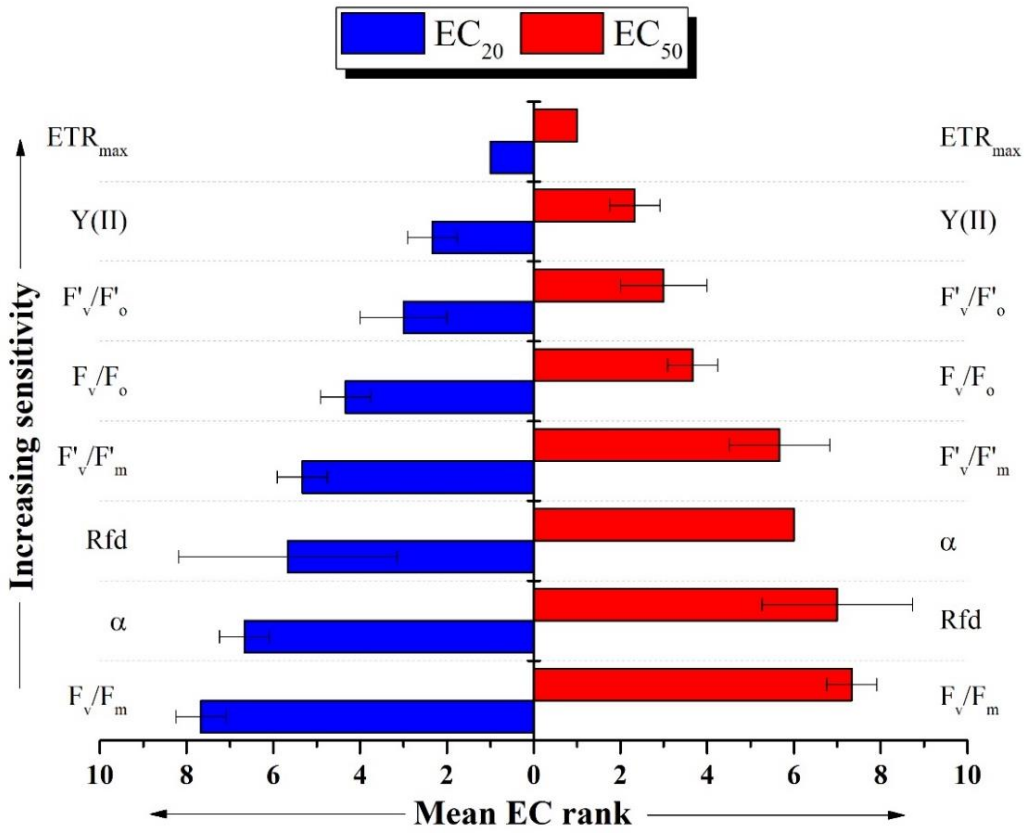

Figure 13. Sensitivity order of the tested ChlF-based endpoints according to their mean EC_{20} (blue bars spreading to the left) and EC_{50} ranks (red bars spreading to the right) after 72 h long exposures to Ni, Cr(VI) and NaCl in *S. polyrhiza* UD0401 test plants.

5.2. Applicability of the customized ChlF measurement protocol

After selecting F_v/F_o and Y(II) as the most sensitive endpoints derived from the rapid (dark-adapted) and slow (light-adapted) kinetics of the ChlF induction curve, we compared the sensitivity of these endpoints after obtaining them from a customized ChlF measuring protocol. In this part of the investigation, we exposed *L. gibba* to 12 different toxicants and calculated their respective EC_{20} and EC_{50} values in terms of Y(II) and F_v/F_o (**Table S4**). Photosynthetic inhibition was recorded in terms of both ChlF-based endpoints after the exposure duration for each applied toxicant (**Figure S4, S5**). Based on the calculated EC_{50} values, the following order of phytotoxicity was established for the tested metals and metalloids:

F_v/F_o: Cr(VI)>Cu>Ag>As(III)>Cd>Hg>Ni>Se(IV)>Se(VI)>Cr(III)>Zn> As(V)
Y(II): Ag>Cr(VI)>Cu>As(III)>Cd>Hg>Ni>Se(VI)>Se(IV)>Cr(III)>As(V)>Zn

The computed EC_{20} for the two ChlF-based endpoints did not differ substantially according to the paired sample Wilcoxon signed ranks test ($p = 0.176$, $Z = 1.412$). The calculated medians were 2.665 mg L^{-1} (interquartile range: 0.47–7.13 mg L^{-1}) for F_v/F_o and 3.210 mg L^{-1} (interquartile range: 0.81–11.06 mg L^{-1}) for Y(II). However, in terms of EC_{50}, a significant difference was observed ($p = 0.021$, $Z = 2.275$) in their sensitivity. Overall, F_v/F_o proved to have a higher sensitivity to the tested elements with a calculated median EC_{50} of 5.340 mg L^{-1} (interquartile range: 1.41–11.86 mg L^{-1}) as compared to 5.755 mg L^{-1} for Y(II) (interquartile range: 2.09–17.37 mg L^{-1}), respectively. Y(II) had lower EC values than F_v/F_o for Ag, Hg and Se(VI) treatments, while F_v/F_o was a more sensitive endpoint for the rest of the applied toxicants (**Figure 14**, **Table S4**). It should also be noted that the calculated EC values did not fit into the applied concentration ranges of Ag, Se(VI) and Zn, and thus the models had to be extrapolated due to predict EC_{50} or even EC_{20} (**Table S4**). Ag proved to be so poisonous that it resulted in death of the test plants within 3 days, even before reaching 20% inhibition in any ChlF-based endpoint. Hormetic effects were observed in the case of Ag, Hg, Se(IV) and Se(VI) for F_v/F_o. However, as

maximal hormesis stayed below 105% of the respective control, we opted for non-hormetic 3-parameter log-logistic model in case of these metals too.

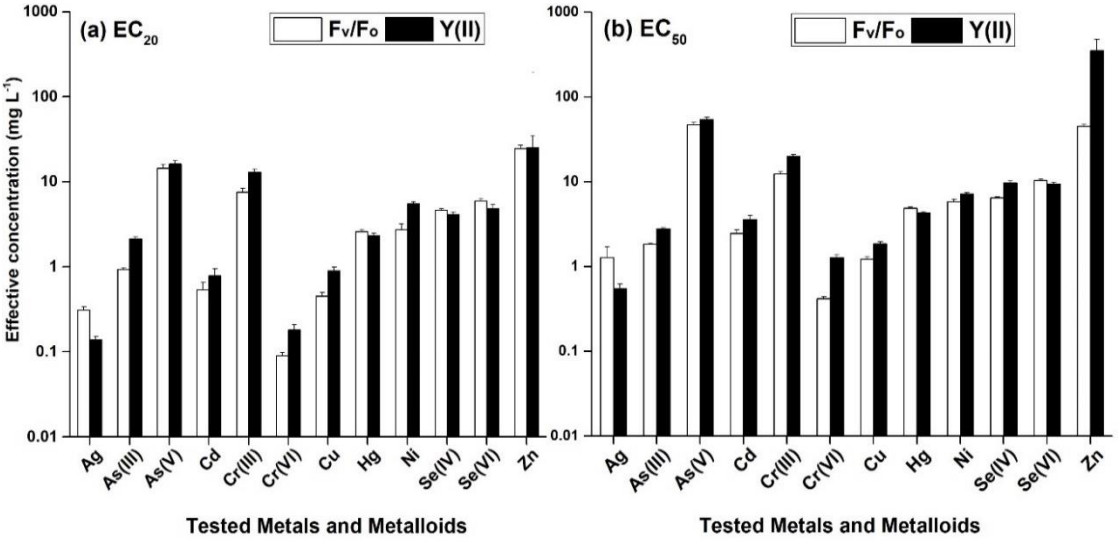

Figure 14. Bar plots representing the calculated effective concentrations and standard errors (±SE) resulting in (a) 20% (EC_{20}) and (b) 50% inhibition (EC_{50}) of the ChlF-based endpoints F_v/F_o (white bars) and Y(II) (black bars) in *L. gibba* exposed to 12 tested metals and metalloids. The EC values were calculated using 3-parameter log-logistic models using drc package in RStudio environment. Note the logarithmic scale of the y-axis.

5.3. Comparison of the growth- and ChlF-based endpoints

In the control wells, an average control growth rate of 0.37 ± 0.04 and 0.39 ± 0.05 day^{-1} was recorded over the 3 days-long experiments in terms of frond area and frond number, respectively. Similar to ChlF-based endpoints, clearly developed growth inhibitory effects were recorded in our *L. gibba* test plants exposed to the applied toxicants for 3 days (**Figure S6, S7**). Hormesis was observed in terms of growth-based parameters including As(III), As(V), Cu, Ni, Se(IV) and Se(VI). However, to keep data processing uniform within the dataset, we modelled the responses using 3-parameter log-logistic model without a hormetic component. As a total, we tested 12 metals and metalloids using *L. gibba*, out of which the lowest ECs (i.e., highest toxicity) in terms of both RGR_{area} and RGR_{frond} were recorded for Ag. Following Ag, we found Hg to be the second most toxic element in terms of RGR_{area}. Similarly, after Ag and Hg, Cu and Cd were also among the most toxic elements in our experiments. The tested elements showed a wide range of calculated effective concentrations spreading over around 3 magnitudes (**Figure 15**). The sensitivity of RGR_{area} was found to be comparatively higher than that of RGR_{frond} based on both EC_{20} and EC_{50} values. The paired sample Wilcoxon signed ranks tests showed highly significant differences for both EC_{20} and EC_{50} ($p < 0.001$, $Z = 3.02$). The resulting median values for EC_{20} were 2.64 mg L^{-1} (interquartile range: 0.81–5.32 mg L^{-1}) for RGR_{frond} and 0.365 mg L^{-1} (interquartile range: 0.13–3.45 mg L^{-1}) for RGR_{area}, respectively. Similarly, in terms of EC_{50}, the corresponding medians were 4.065 mg L^{-1} (interquartile range: 1.74–7.96 mg L^{-1}) for RGR_{frond} and 1.75 mg L^{-1} (interquartile range: 0.38–4.28 mg L^{-1}) for RGR_{area}. The least toxic elements included As(V) and Cr(III) according to the calculated EC_{50} values. RGR_{frond} proved to be less responsive to As(V) with the maximum growth inhibition within the applied concentration range being less than 50% (supplementary **Table S4** and **Figure S7**). Similar to As(V), Zn also had higher EC_{50} values in terms of RGR_{frond}, however, a medium-level growth inhibition was recorded with respect to RGR_{area}. Overall, the following order of phytotoxic potential of the applied toxicants was observed based on the calculated EC_{50} values:

RGR_{frond}: Ag>Cu>Hg>Cd>As(III)>Ni>Cr(VI)>Se(IV)>Se(VI)>Cr(III)>Zn>As(V)

RGR_{area}: Ag>Hg>Cu>Cr(VI)>Cd>Se(VI)>As(III)>Ni>Zn>Se(IV)>Cr(III)>As(V)

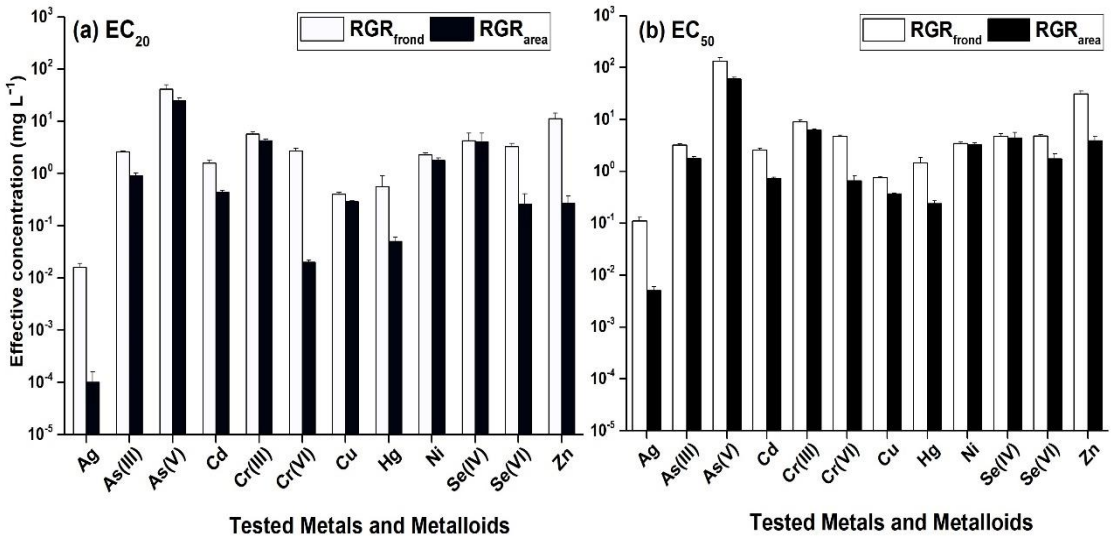

Figure 15. Bar plots representing the calculated effective concentrations and standard errors (±SE) resulting in (a) 20% (EC_{20}) and (b) 50% inhibition (EC_{50}) of the growth-based endpoints RGR_{frond} (white bars) and RGR_{area} (black bars) in *L. gibba* exposed to 12 tested metals and metalloids. The EC values were calculated using 3-parameter log-logistic models using drc package in RStudio environment. Note the logarithmic scale of the y-axis.

In terms of the tested metals and metalloids, we obtained a similar order of sensitivity for the more sensitive growth- and ChlF-based parameters i.e., RGR_{area} and F_v/F_o, respectively. The median EC_{20} values for RGR_{area} and F_v/F_o were 0.365 mg L^{-1} (interquartile range: 0.13–3.45 mg L^{-1}) and 2.665 mg L^{-1} (interquartile range: 0.47–7.13 mg L^{-1}), respectively, showing a seven-fold difference (paired sample Wilcoxon signed ranks tests p = 0.042, Z = 2.045). Similarly, median values in case of EC_{50} for RGR_{area} and F_v/F_o, showed a three-fold difference with the respective values of 1.75 mg L^{-1} (interquartile range: 0.38–4.28 mg L^{-1}) and 5.340 mg L^{-1} (interquartile range: 1.41–11.86 mg L^{-1}) according to the paired sample Wilcoxon signed ranks tests (p = 0.042, Z = 2.045). In addition to the generally higher sensitivity of RGR_{area}, some toxicant-specific patterns were also observed. For instance, F_v/F_o proved to be more

sensitive than RGR_{area} when we compared EC_{50} in the case of Cr(VI). Additionally, in the case of As(V), both the EC_{20} and EC_{50} for F_v/F_o were lower than those for RGR_{area}. Similarly, As(III) treatments resulted in comparable sensitivities of RGR_{area} and F_v/F_o in terms of the calculated EC_{20} and EC_{50} values (**Figure 16**, **Table S4**).

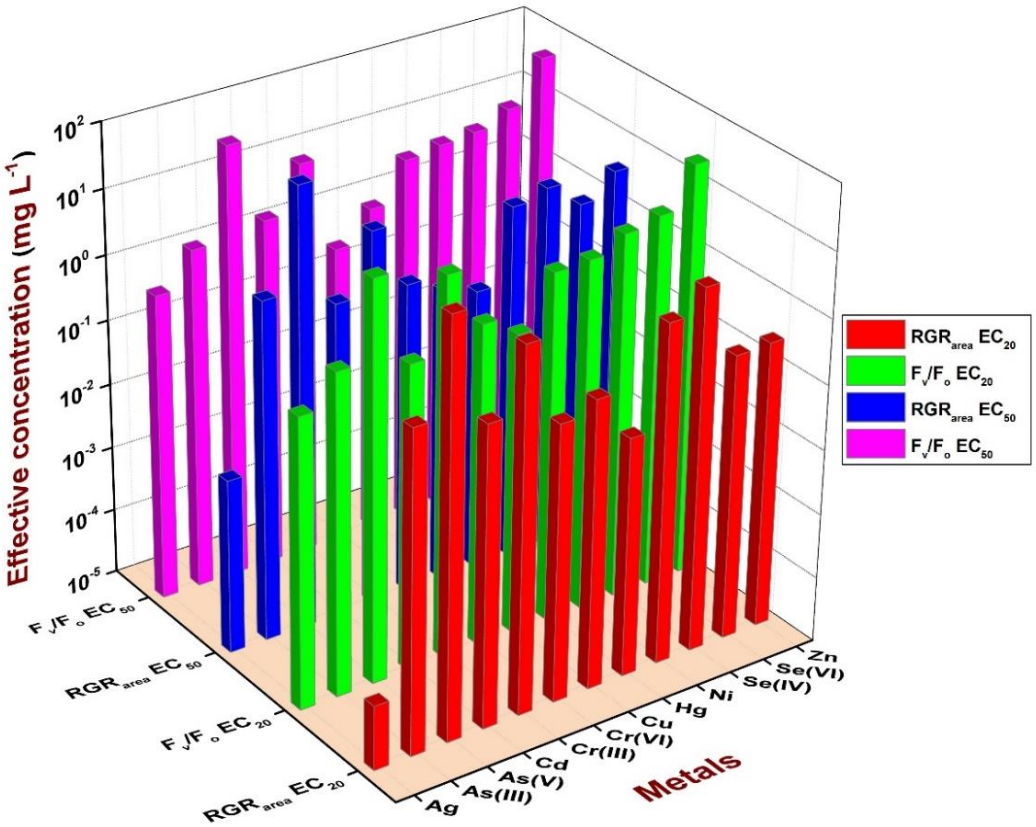

Figure 16. 3D bar plot graph representing EC_{20} and EC_{50} values growth-based RGR_{area} and ChlF-based F_v/F_o values for *L. gibba* in terms of 12 tested metals and metalloids.

5.4. Multi-well plate-based vs ISO/OECD standard duckweed tests

We also compared the sensitivity of our multi-well plate-based test setup to the reported results by a previous study with a standardized growth inhibition test protocol (Naumann et al., 2007) that used *L. minor*. We found that our setup was less sensitive than the standardized one conducted in accordance with the ISO protocol (ISO, 2005). Their toxicity experiments lasted for 7 days and had 9 metals common with our *L. gibba*-based study including Ag, As(III), As(V), Cd, Cr(VI), Cu, Hg, Ni and Zn. The median EC_{20} and EC_{50} values of the 9 tested metals were significantly lower in the study by Naumann et al., (2007) compared to ours (**Table 6**). The calculated EC_{20} values in the two studies showed only weak correlation (Spearman's $\rho = 0.55$, $p = 0.125$), while this correlation was comparatively stronger between the EC_{50} values (Spearman's $\rho = 0.78$, $p = 0.012$).

Table 6. The sensitivity of the multi-well plate-based setup (present study) compared to previously reported study by Naumann et al., (2007) using ISO-standard (ISO, 2005) based on the effective concentrations of 9 tested elements in common.

Median Effective Concentration RGR_{frond} (mg L^{-1})				
	L. gibba (present study)	*L. minor* (Naumann et al., 2007)	W	p
EC_{20}	2.27	0.086	2	0.023
EC_{50}	3.21	0.683	3	0.02

6. Discussion

6.1. Overall sensitivity of ChlF-based toxicity endpoints

The results with *S. polyrhiza* indicated that ChlF imaging-based endpoints could be utilized efficiently to characterize acute phytotoxicity of various chemicals. However, selection of the most suited and responsive endpoints is a crucial decision to be made prior to the investigation (Kalaji et al., 2017). We found a wide range of sensitivity in terms of ChlF-based endpoints for the 3 reference toxicants used in *S. polyrhiza*-based study. The calculated highest EC_{50} value was 11 times higher than the lowest one in the case of Ni, while this difference was 5-fold in case of Cr(VI). Such a difference between the two metals may be due to the essentiality of Ni, while Cr has no known physiological function in plants (Wani et al., 2022). The narrowest range in the calculated EC_{50} values was found in NaCl treatments, corresponding to 1.6 times. It should also be noted, on the other hand, that in this case the entire applied concentration range was much narrower as compared to the above metals. These differences show a highly variable range of responsiveness using different ChlF-based endpoints.

In general, F_v/F_m and Rfd are amongst the frequently used parameters in plant ecophysiology research. In fact, F_v/F_m is the most frequently applied parameter in the literature related to ChlF analyses (Guidi et al., 2019; Vidaković-Cifrek & Tkalec, 2023). However, in our study, both F_v/F_m and Rfd were among the least sensitive endpoints. On the other hand, F_v/F_o proved to be more sensitive than F_v/F_m even though both ratios were calculated using the same basic ChlF levels, i.e., F_o and F_m. Therefore, it is the calculation method and not the measured basic parameter which makes F_v/F_o perform over a larger dynamic range than F_v/F_m (Lichtenthaler et al., 2005). Plotting these two endpoints against each other shows the non-linear relationship (**Figure 17**) that makes F_v/F_o more sensitive in the physiologically near-optimum ranges (Láposi et al., 2009; Oláh et al., 2010; Pietrini et al., 2016). Therefore, careful consideration must be taken into account when relying exclusively on F_v/F_m in a toxicological study as this endpoint proved to be quite robust when it comes to plant responses to toxic effects. It can also be a possible reason of why F_v/F_o,

and the other more sensitive endpoints, were more likely to show hormetic patterns than F_v/F_m.

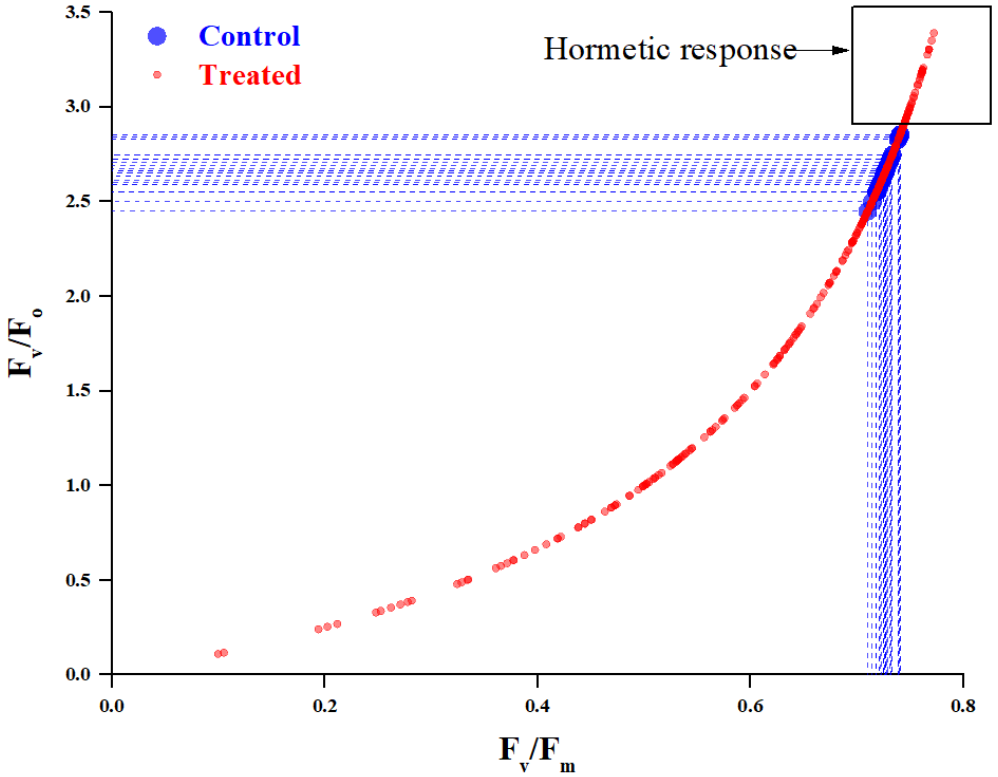

Figure 17. The non-linear relationship between F_v/F_m and F_v/F_o resulting in a larger dynamic range and higher sensitivity of the latter endpoint. The presented data were obtained from Ni-, Cr(VI)- and NaCl-treated *S. polyrhiza* plants.

Hormesis has been discussed extensively in recent years as a possible outcome of the plants' growth under mild environmental stress (Calabrese & Blain, 2009; Agathokleous, 2018). Similarly, exposure of duckweeds to multiple organic and inorganic toxicants has also resulted in hormetic responses (Cedergreen et al., 2005, 2007; Belz et al., 2008; Zhong et al., 2016; Agathokleous, 2018). Hormesis in duckweeds' photosynthetic reactions, on the other hand, has received little attention. (Agathokleous, 2021). We observed hormesis in many ChlF-based endpoints when we studied the effects of reference toxicants on *S. polyrhiza*. According to the applied regression models, definite stimulation was found at lower concentrations of Ni and

NaCl in terms of various ChlF-based endpoints. We found that Ni and NaCl treatments were more likely to result in hormesis in the more sensitive endpoints (such as F_v/F_o, Y(II), F'_v/F'_o, and ETR_{max}). We also observed that hormetic models fit better in case of Cr(VI) than the non-hormetic log-logistic one, despite the fact that MAX was <3%, which was lower than the commonly accepted criterion (>5%) for hormetic responses (Cedergreen et al., 2007). This lower-than-threshold stimulation was valid for all the measured ChlF endpoints under Cr(VI)-stress except the least sensitive Rfd with a stimulation exceeding 105% of the control.

The calculated values for EC_{max} (concentrations associated with the maximal hormetic response level EC_{max}) lied within 2–15% of the calculated EC_{50} values for Ni-treated *S. polyrhiza*, and ranged between 25–35% for the NaCl-treated ones. These results were similar to EC_{max} of terbuthylazine-treated aquatic macrophytes that ranged within 20–25% of the calculated EC_{50} values (Cedergreen et al., 2005). The maximal hormetic effect was associated with 5–10% stimulation in Ni and 10–25% in NaCl, being in agreement with previously reported studies (Calabrese & Blain, 2009; Agathokleous, 2021). Ni is essential for plants, but it is not intendedly added to Steinberg's medium during its preparation. Subsequently, nickel's physiological function explains how it stimulates plant metabolism (DalCorso, 2012). Similar to this, it has been observed that at low concentrations, NaCl also boosts plant photosynthesis (Hasanuzzaman et al., 2013). Particularly interesting, we discovered that in the current study, stimulating concentrations of Ni and NaCl for ChlF-based endpoints were within the range of growth inhibition-based EC_{50}s derived from 7 days-long exposures using the same *S. polyrhiza* clone (Oláh et al., 2015; Hepp et al., 2018). Whether these hormetic patterns were intermittent or ChlF-specific, therefore, would require further research.

If actinic irradiation is used, variations in the photochemical efficiency can be more clearly identified compared to the ChlF-based endpoints measured in the dark-adapted state. Irradiating the plants could be more informative as it puts the limiting steps of photochemistry under pressure (Ralph et al., 2005; Kumar & Han, 2010; Perreault et al., 2010; Lahive et al., 2012; Flores et al., 2013; Dewez et al.,

2018). The results of this investigation with *S. polyrhiza* were also in line with this fact as Y(II) proved to be a very responsive endpoint in our experiments. Other endpoints representing the light-adapted state, e.g., F'_v/F'_m and F'_v/F'_o, also had higher sensitivities as compared to their dark-adapted analogues i.e., F_v/F_m and F_v/F_o, respectively. Rapid light curves (RLC), according to a number of studies, provide also particularly sensitive endpoints for determining herbicide and heavy metal toxicity in duckweed (Oláh et al., 2010; Kumar & Han, 2010; Park et al., 2017; Pietrini et al., 2019; Park et al., 2020; Lee et al., 2021). In agreement with these studies, our results supported ETR_{max} to be a sensitive endpoint. The sensitivity of photochemical apparatus thus seemed to favor measurement of performance under a high physiological pressure. Therefore, ETR_{max} measured under high illumination intensity proved to be the most sensitive endpoint for our reference toxicants. Based on these outcomes, we conducted further investigations with the most sensitive dark- and light-adapted ChlF-based endpoints, i.e., F_v/F_o and Y(II) in *L. gibba*.

6.2. Applicability of the customized ChlF measuring protocol

The calculated EC values for the dark- and light-adapted ChlF-based endpoints (i.e., F_v/F_o and Y(II), respectively) derived from the customized 2-step measurement protocol showed an overall strong correlation (Spearman's $\rho = 0.97$) indicating their strong interdependence despite being measured separately. This interdependence between the measured endpoints has been already proven in multiple studies using ChlF, and comes from using the limited set of basic parameters (F_o, F_m, F_s, F'_m and F'_o, respectively) for their calculations. Similar to our results, a strong co-dependence was recorded between F_v/F_m and F_v/F_o when ChlF was measured in *Cunninghamia lanceolata* under different photoperiod durations and light spectra (Xu et al., 2020). F_v/F_o and F_v/F_m were also significantly correlated ($p < 0.01$) while depicting the effects of *Bacillus subtilis* and different potassium ion (K^+) levels on cucumber (*Cucumis sativus* L.) seedlings (Li et al., 2024). Similarly, when Cu toxicity was monitored in *L. minor* in terms of ChlF, F_v/F_o and F_v/F_m were found to be strongly co-dependent (Singh et al., 2022).

Apparently, our results pointed to the fact that measuring light-adapted samples directly without the gradual build-up of different quenching processes after the dark-adapted state affected the sensitivity of light-adapted parameters. The order of sensitivity of the dark- and light-adapted ChlF-based endpoints in *L. gibba* was the opposite for most of the tested elements contrasting to our results with *S. polyrhiza*. Since we measured the dark-adapted F_v/F_o following the same darkening period (20 minutes) to reach relaxed state of photochemistry, this measurement was practically not influenced by adopting the customized protocol. Therefore, it should have been the applied light-adapted endpoint i.e., Y(II) that showed decreased responsivity. Y(II) is considered to be an accurate indicator of PSII efficiency under ambient conditions. A possible reason for its altered sensitivity is that it can be significantly affected by even slight differences in the measuring conditions (Murchie & Lawson, 2013). It is well known that acclimation to the spectral composition of ambient light can significantly affect photosynthetic performance and other physiological processes of plants (e.g., Ahlman et al., 2017; Yang et al., 2018; Li et al., 2022). Similarly, our results with various duckweed species had confirmed that the plants displayed different photosynthetic efficiency depending on whether the culturing light was provided by red, blue or white LEDs (Irfan et al., unpublished data). During the standard measurement protocol, the dark-light transition and steady state light-adapted photochemistry of *S. polyrhiza* was achieved in the measuring chamber of the instrument, by using 10-minutes long illumination period with the blue LED source. In addition, the plants were dark-adapted for 20 min before the measurements. Hence, the carry-over effect from the previous light acclimation could be much weaker. During the customized measurement protocol, on the other hand, we measured *L. gibba* that was originally light-adapted under a comparable PPFD from white, fluorescent tubes. Although we allowed the plants to adapt to the blue LED source for 60 s before applying the saturation pulse, still this shorter period could lead to a different state of PSII photochemistry as compared to the standard protocol.

The fact that basic ChlF parameters (F_o, F_m, F_s and F'_m) obtained from our customized protocol were not interchangeable with those measured during the

standard kinetic curve was further supported by our attempts to calculate ChlF parameters that relied on both the dark- and the light-adapted states. Calculation of Y(NPQ) and Y(NO), as examples, uses F_m from the dark-adapted state and F_s and F'_m from the light-adapted one (see **Table 1**). Deriving these parameters from the customized protocol sometimes resulted in negative values or summing up the 3 quenching parameters contradicted to the theoretical expectation of Y(II)+Y(NPQ)+Y(NO) = 1 (Irfan et al., unpublished results). These observations pointed to the unsuitability of the customized protocol in such calculations. Therefore, even if our customized approach may yield valuable information on different aspects of photosynthesis, it cannot fully replace protocols that use the standard ChlF induction curve.

Based on the results of this study, measuring the dark-adapted ChlF-based endpoints, especially F_v/F_o, would be preferable in phytotoxicity studies when a quick comparison is required in terms of toxicity potential of different environmental stressors. F_v/F_o has been studied for a long time to measure the photosynthetic efficiency of stressed plants (Xu et al., 2010; Zhong et al., 2016; Cen et al., 2017; Alp et al., 2023). Generally, besides higher sensitivity in our experiments, measuring the rapid ChlF kinetics (i.e., dark-adapted state) would ensure a certain level of standardization, and thus, higher comparability of the results as those would not be affected by such lab-specific conditions as the intensity, spectrum and length of the actinic irradiation, or the ambient temperature, respectively.

6.3. Comparative sensitivity of growth- and ChlF- based endpoints

We also applied two common growth inhibition-based endpoints in our *L. gibba* investigation in addition to using the most sensitive ChlF-based endpoints. From this perspective, we found an overall lower range of the calculated EC_{50} values for RGR_{area} as compared to those for RGR_{frond}. These results were consonant with metal phytotoxicity literature where the former endpoint was comparatively more sensitive than the later one in duckweeds (Oláh et al., 2018; Markovic et al., 2021). Frond area is a continuous variable as an opposite to the quantile nature of frond number. This difference contributes significantly to the higher sensitivity of the area-based RGR. A typical duckweed response is that daughter fronds may reach smaller size under stress since less resources can be devoted to frond expansion, or due to stress-induced morphogenic responses (Potters et al., 2007). This way, the newly-formed but smaller fronds have a relatively less contribution to the increment in total frond area resulting in stronger growth inhibition, while frond number growth may still be less inhibited.

The ecotoxicological potential also depends on the chemical properties and mode of action of different toxicants, thus influencing the selection of appropriate toxicity endpoints. Amongst the three reference toxicants used in the case of *S. polyrhiza*, Ni stimulates plant development at low concentrations because it is a necessary cofactor for the urease enzyme participating in the N-metabolism (Rampazzo et al., 2022). However, at higher concentrations, it causes problems with N-metabolism, water balance, and nutritional absorption, which eventually results in decreased fitness and growth suppression (DalCorso, 2012). Higher concentration of Ni can halt photosynthesis in several ways, mainly by reducing the chlorophyll content, and changing the structure of chloroplasts due to Mg displacement in chlorophyll and RuBisCo (Appenroth et al., 2010; Yusuf et al., 2011; Andresen et al., 2013). The reduction in chlorophyll content and changes in chloroplasts then inhibit the electron transport chain responsible for the energy transfer between the two photosystems. Additionally, in the worst case, both photosystems can be inactivated. Based on spatially resolved ChlF analyses, younger tissues, that is young fronds and

basal parts of the still forming fronds, are especially prone to Ni-induced photosynthetic disorders (Oláh et al., 2024). In aqueous environments, its prevalent oxidation form is Ni^{2+} ion, and it disturbs duckweed growth starting from 0.1 mg L^{-1} concentration range (Naumann et al., 2007; Oláh et al., 2015).

Contrary to Ni, chromium has no proven physiological benefits in plants (Wani et al., 2022). The hexavalent form of chromium, i.e., Cr(VI), exists in waters as CrO_4^{2-} and $Cr_2O_7^{2-}$ oxyanions, and the sulfate transport system allows plants to actively absorb those forms (Shanker et al., 2005). Due to the suppression of enzymes such as Fe(III)-reductase, nitrate reductase, and plasma membrane H^+-ATPase, Cr(VI) poisoning can result in the disruption of the nutritional balance. According to DalCorso (2012), Cr(VI) can react with macromolecules in cells, causing oxidative stress as it is converted to Cr(III). At the level of photosynthesis, Cr(VI) depletes chlorophyll content, obstructs electron transport during photosynthetic reactions, inactivates Calvin-Benson cycle enzymes, and disarrays the ultrastructure of the chloroplasts (Shanker et al., 2005). The frond edges and interveinal regions of duckweeds are particularly affected by Cr(VI)-induced photosynthetic impairment (Oláh et al., 2024). For duckweed, Cr(VI) reduces growth in the range of 0.1-1.0 mg L^{-1} (Naumann et al., 2007; Oláh et al., 2015).

In addition to the osmotic stress caused by NaCl, the toxicity of Na^+ and Cl^- ions hinders plant growth. According to Hasanuzzaman et al., (2013), salinity stress changes protein structure, disrupts mineral feeding and water interactions, and causes reactive oxygen species (ROS) to develop. It has been observed that NaCl alters the ultrastructure of chloroplasts, decreases the amount of chlorophyll, and blocks electron transport (Jajoo, 2013). Generally, the growth of various duckweed species is inhibited upon exposure to NaCl in the concentration range of 1–10 g L^{-1} (Sree et al., 2015). Besides the recommended reference toxicants tested with *S. polyrhiza*, various elements in the study with *L. gibba* also had distinct toxic effects in duckweeds. The most toxic element -i.e., Ag- caused oxidative stress in duckweed *L. minor* and was also associated with cellular damage (Li et al., 2020). Similarly, in *S. polyrhiza* it suppressed biomass production along with causing root abscission and

fragmentation of fronds from the plant colony (Jiang et al., 2012). The second most toxic element, Hg had caused reduction in the 'chlorophyll a' content and oxidative damage. It also demonstrated potential to cause DNA damage leading to cellular mortality (Zhang et al., 2017). Likewise, it was discovered that Cu and Cd were linked to the disruption of photosynthetic pigments and the weakening of duckweed's antioxidant defense mechanism (Hou et al., 2007).

Despite the lower sensitivity of ChlF-based endpoints, the calculated EC_{50} values for F_v/F_o and Y(II) in *L. gibba* were strongly correlated to the ones for the growth-based endpoints (i.e., RGR_{frond} and RGR_{area}) (**Figure 18**). A similar correlation was observed between Y(II) and growth rate inhibition in duckweed toxicological tests with common PSII inhibiting herbicides (e.g., atrazine and diuron) (Park et al., 2017). *L. minor* exposed to Bisphenol A and Cu also showed a high sensitivity in terms of ChlF-based endpoints along with a strong observed correlation with fresh weight changes (Liang et al., 2022; Singh et al., 2022). This interdependence was also proven by no changes in ChlF-based endpoints under perfluorooctanoic acid and dimethyl phthalate treatments parallel to no observed growth inhibition in the cultures (Pietrini et al., 2019, 2023).

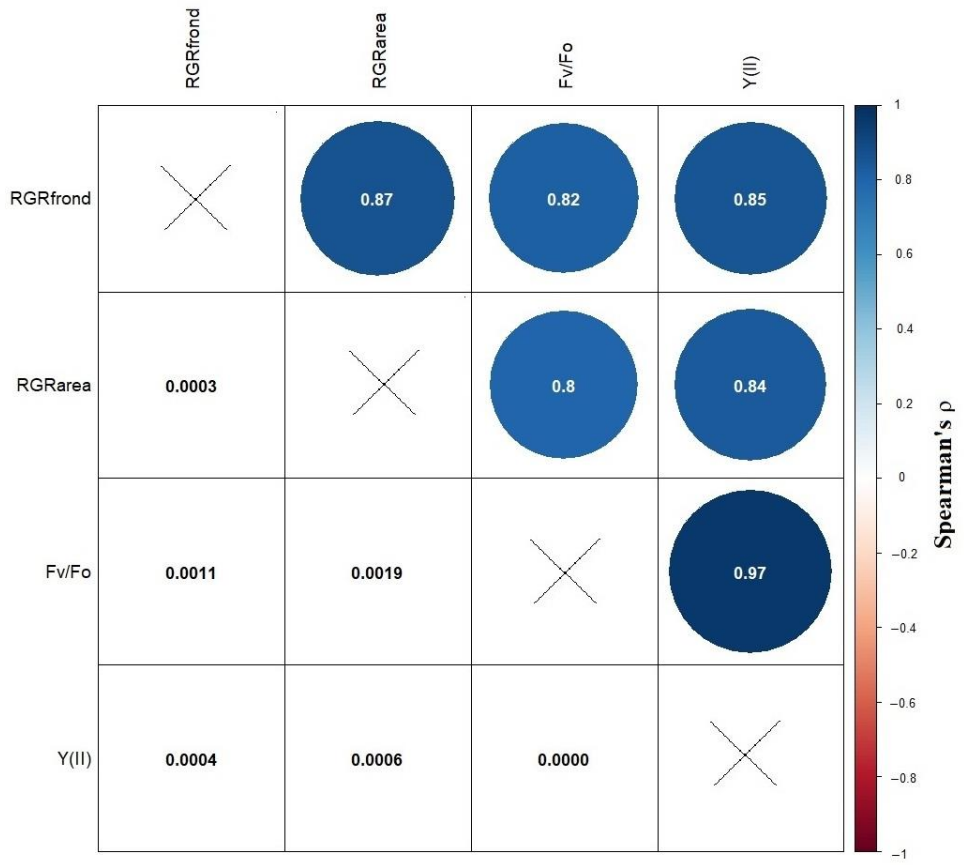

Figure 18. Spearman's ρ (upper triangle) and the accompanying p-values (lower triangle) for the estimated EC_{50} values for the growth- and ChlF-based endpoints in *L. gibba* test plants.

Interpreting inhibition of ChlF-based endpoints is not as simple as growth-based endpoints as the former group indicates operability of certain physiological processes of the plants. Thus, if those physiological processes are not affected directly by the applied toxicant, a weaker or delayed sensitivity may occur in the ChlF-based endpoints (Brain & Cedergreen, 2009; Alkimin et al., 2019). Additionally, the sensitivity of ChlF-based endpoints can also be influenced by irradiation conditions as the test plants exposed to toxicants under sub-saturating irradiance promote up-regulation of PSII repair and ROS scavenging systems compared to higher irradiation levels (Christensen et al., 2003; Wilkinson et al., 2015). As a result of these

comparisons, it could be concluded that ChlF- and growth rate-based endpoints might not have same sensitivity pattern to a specific concentration range. Based on our results, therefore, it is recommended to be very thoughtful before using ChlF-based endpoints as sole method to measure phytotoxic effects.

Moreover, as a non-destructive way to determine surface area or frond number, digital image analysis is commonly used. In our study, these measurements were performed using ChlF-based images taken by the fluorometer at maximum fluorescence level (F_m images). Measurement of the surface area and frond number using F_m images provide easy and time efficient ways of morphometric analyses, however, chlorotic areas of fronds could significantly bias the calculated frond area. Camera photos capture both the healthy and the chlorotic parts of the fronds. Due to no or low ChlF signal from chlorotic regions, on the other hand, ChlF-based images do not indicate plant surface in these parts. Because of these undetected regions, the total surface area could appear to be considerably lower while still maintaining the frond count. This can result in a widening gap between the sensitivities of the two growth-based endpoints. An observed decrease in the comparability of RGR_{area} and RGR_{frond} at lower and higher concentration ranges of Ag, Se(VI) and Zn could be attributed to this virtual surface area loss due to chlorosis.

Using a ChlF imaging-based method in toxicological assays also comes with some measurement limitations. Similarly to other chlorophyll fluorometers, the instrument in our study reduced noise by thresholding the signal (Heinz Walz GmbH, 2019). This, in turn, makes poorly photosynthesizing frond areas undetectable either under the measuring light or during the saturating light pulse. Omission of these low-performing regions from the final calculations of F_v/F_o and Y(II) allowed these indicators to represent only those frond parts that retained higher photochemical functionality (**Figure 19**). Sometimes, in case of extreme stress, duckweeds detach their premature fronds from the mother frond as a survival strategy (Henke et al., 2011; Ziegler et al., 2023). This separation was noted in our investigation under the highest concentration treatments and in the presence of extremely hazardous elements (e.g., Ag and Hg). Even though the majority of these early-separated fronds did not

significantly increase in size, they still persevered in some level of photosynthetic activity. Overall, all these factors including chlorosis, weaker photochemical performance of some regions and suppressed growth of separated fronds supported a cautious interpretation of ChlF-based endpoints in duckweed tests.

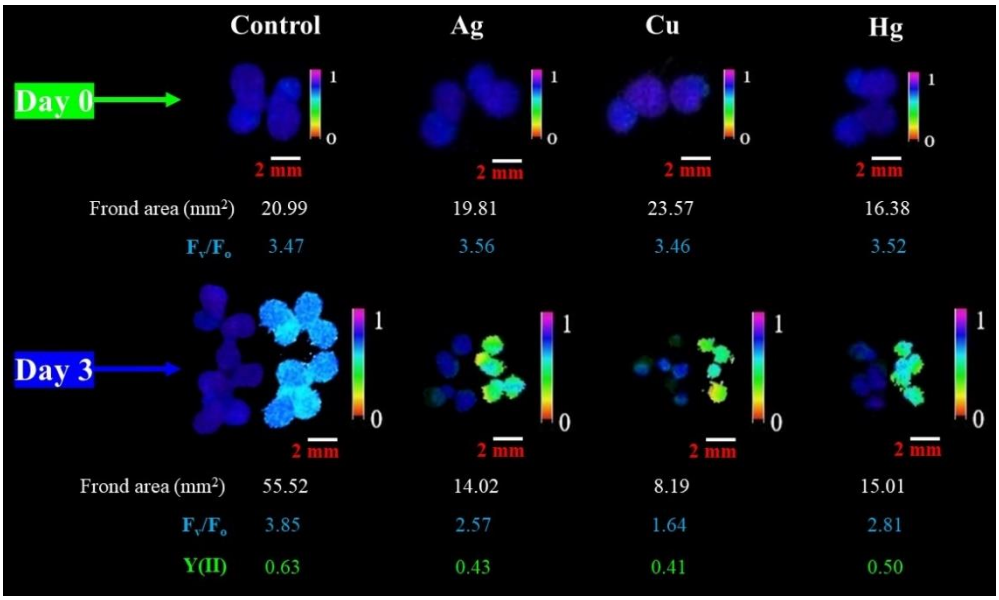

Figure 19. The chlorophyll fluorescence images taken by using imaging-PAM at the beginning (day 0) and final day (day 3) of the exposures showing the same control and metal-treated *L. gibba* colonies. Treatments with 3.125 µg L^{-1} Ag, 1.25 mg L^{-1} Cu, and 2.5 mg L^{-1} Hg are indicated by the symbols Ag, Cu, and Hg, respectively. F_v/F_m images are displayed in the upper row (day 0), and for the corresponding treatments, Y(II) imagery is represented on the right side and F_v/F_m on the left side in the lower row (day 3).

6.4. Multi-well plate vs ISO/OECD standard duckweed tests

The standard validity criterion for a duckweed toxicological experiment requires its control cultures to double in less than 2.5 days (OECD, 2006). In our experiments with *L. gibba*, this criterion was clearly fulfilled in the plate-based setup. The control cultures doubled in terms of frond area within 1.90 ± 0.24 days and a doubling time of 1.80 ± 0.22 days was recorded based on the frond number.

In terms of both the ChlF- and growth-based endpoints, our findings on the toxicity of the applied metals and metalloids in *L. gibba* were similar to the data from the previously published literature. For Ag, As(III), and Cu, the effective concentrations of RGR_{frond} in *L. gibba* were similar to the corresponding values in *L. minor* (Naumann et al., 2007; Khellaf & Zerdaoui, 2009). Similarly, As(V) showed the lowest phytotoxicity of 10 heavy metals in *L. minor* with respect to both the growth-based endpoints and chlorophyll content (Naumann et al., 2007). Another element in our study, Zn was also moderately toxic up to an applied concentration of 10 mg L^{-1}, reported by Lahive et al., (2011) and Lanthemann & van Moorsel (2022).

The RGR_{frond} and RGR_{area} EC_{50} values in the present study, when compared to the values previously obtained in our lab following the OECD, (2006) protocol, were considerably higher. Subsequent RGR_{area} EC_{50} values were much lower in those earlier experiments conducted with the same *S. polyrhiza* clone (UD0401). The calculated EC_{50} values for those treatments were 0.184, 0.188, 0.104 and 0.137 mg L^{-1} for Ni, Cr(VI), Cd and Hg, respectively (Oláh et al., 2015, 2016; Hepp et al., 2016). In comparison to the present investigation with *L. gibba*, EC_{50} was calculated to be 1.33 mg $L^{-1}$and 25.04 mg L^{-1} in *S. polyrhiza* under As(III) and As(V) treatments, respectively (Hepp et al., unpublished data). In our multi-well-plate-based setup with *L. gibba*, Ni also turned out to be 3–4 times less toxic than data reported for the same species using the OECD protocol (Khellaf & Zerdaoui, 2010). The EC50 values for Cu, however, from our multi-well plate-based research, were similar to those published using *L. gibba* in accordance with the OECD protocol (Khellaf & Zerdaoui, 2010). A shorter exposure and lower toxicant-to-biomass ratio in our plate-based setup, therefore, probably lead to such differences in addition to species-specific

stress responses. In our plate-based setup, the tests were performed using 4 mL of medium volume for a total exposure time of 3 days as compared to 100 mL vessels used for treatments lasting for 7 days in standard OECD and ISO protocols. Firstly, the plate-based test may result in lower dose (that is toxicant to biomass ratio) at the same nominal toxicant concentrations. Secondly, a shorter exposure time may also cause lower sensitivity of phytotoxicity assays. Regarding different exposures, three-day-long Cd treatments in *S. polyrhiza* resulted in three times higher calculated EC_{50} values for the growth-based endpoints than the seven-days-long treatments under the same experimental conditions (Oláh et al., 2014).

In aquatic plants, ChlF endpoints are typically thought to be comparably sensitive to growth-based endpoints (Ralph et al., 2007; Brain & Cedergreen, 2009). Higher sensitivity of these endpoints was also reported in some cases. For example, herbicide and phenol treatments resulted in comparatively higher sensitivity of F_v/F_m and ETR_{max} than the corresponding growth-based endpoints (Kumar & Han, 2010; Park et al., 2012). However, our results with *S. polyrhiza* contradicted these observations. Regardless of being the most responsive endpoints, the calculated EC_{50} values for ETR_{max} and Y(II) were considerably higher in the present study as compared to growth-based endpoints using the same *S. polyrhiza* clone (**Figure 20**). The calculated EC_{50} values for the most responsive ETR_{max} in the case of Ni and Cr(VI) were 10-fold higher than EC_{50}s of growth-based endpoints in OECD-conform tests, that ranged between 0.18–0.2 mg L^{-1} (Oláh et al., 2015). Similarly, in NaCl treatments, the present EC_{50} values for ETR_{max} were 2-3 times higher than those for the growth-based endpoints corresponding to 3.45 and 4.51 g L^{-1} for RGR_{area} and RGR_{frond}, respectively (Hepp et al., 2018).

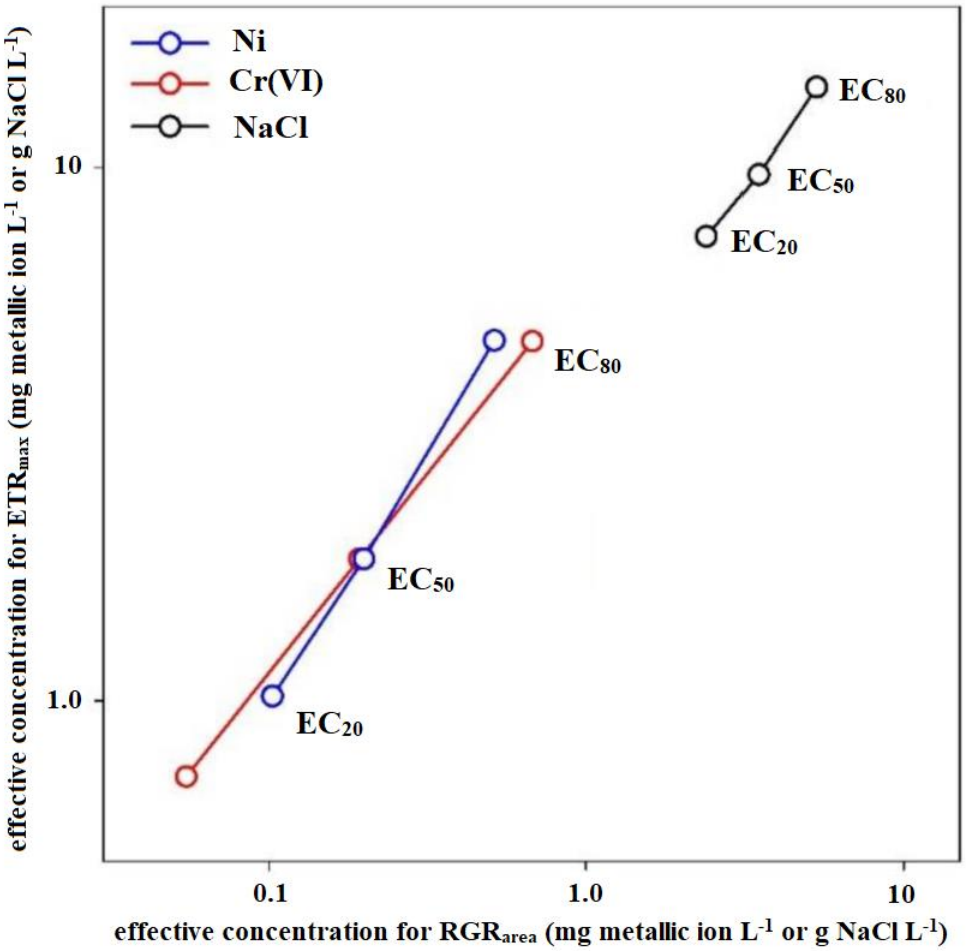

Figure 20. Correlations between the maximal electron transport rates (ETR_{max}) measured in three-day long multi-well-plate-based phytotoxicity tests and the 20, 50, and 80% inhibiting concentrations (EC_{20}, EC_{50}, and EC_{80}, respectively) of Cr(VI), Ni, and NaCl calculated in terms of frond area-based relative growth rates (RGR_{area}) using the same *S. polyrhiza* clone UD0401 in seven-day long growth tests. Data for ETR_{max} is based on the present study while the frond area-based growth inhibition data were reported by Oláh et al., (2015) and Hepp et al., (2018), respectively.

7. Summary

Increasing freshwater pollution due to anthropogenic activities have resulted in an immediate need for *in situ* water quality monitoring for management and conservation purposes. Different bioindicator organisms are being used to monitor water quality and model the toxicological effects of environmental pollutants. Using duckweeds in toxicological studies is becoming common due to their superior characteristics including fast growth rate, easy management, and faster response rate. In addition to classical growth-based toxicological assays, chlorophyll fluorescence (ChlF) induction-based methods are also becoming popular in duckweed toxicity tests as non-destructive, fast and easily applicable way to measure photosynthetic inhibition under toxicant exposure. In the growth-based toxicological assays, the adverse effects of the applied toxicants are mainly characterized as changes in the growth rates of surface area or production of new fronds. The ChlF-based methods, on the other hand, rely on the measurement of ground and maximum fluorescence levels under dark- and light-adapted states of the photosystem. These basic parameters are then used to derive many ChlF-based endpoints for the measurement of toxic effects.

In this research, two duckweed species, namely *Spirodela polyrhiza* and *Lemna gibba* were used to assess the most sensitive endpoints using Pulse Amplitude Modulated (PAM) ChlF method and to possibly reduce the required measurement duration. The sensitivity of ChlF-based endpoints was then compared with the most applicable and most sensitive surface area growth-based endpoint to check the potential of ChlF alone to substitute the growth-based endpoints. Another aim of this research was to measure these endpoints from a small, less resource intensive and comparatively short-term tissue-culture plate-based system instead of the standardized duckweed testing system with higher infrastructure and resource requirements. For this purpose, plants were grown in smaller volume of test solutions for a shorter period. In short, the efforts were made to significantly reduce the time and effort required for the standard assay methods while producing higher throughput and increasing the efficiency of the tests.

According to our findings with *S. polyrhiza*, many ChlF-endpoints responded to the applied treatments with varying degrees of sensitivity. Out of the tested ChlF-based endpoints, the sensitivity of dark-adapted chlorophyll fluorescence endpoint F_v/F_o was notably higher than that of the widely used F_v/F_m. On the other hand, Y(II) proved to be amongst the most sensitive light-adapted endpoints. The results emphasized the importance to consider reporting information on F_v/F_o as well in addition to F_v/F_m. The sensitivity of the selected highly responsive endpoints (i.e., Y(II) and F_v/F_o) were then subjected to comparative toxicity tests using different metals and metalloids in duckweed *L. gibba*. During these tests, the ChlF-generated images were also used to simultaneously measure the growth-based parameters of the test cultures.

On the one hand, the results with *L. gibba* supported the fact that using the small-scale, multi-well-plate-based testing system could come in handy in terms of saving space, growth- and analysis-duration and required smaller volumes of testing solutions. On the other hand, the sensitivity of such growth inhibition tests was lower as compared to standard tests. Despite such lower sensitivity, the tested elements showed comparable order of phytotoxicity to previously conducted OECD- and ISO-conform tests. The responsiveness of individual tested endpoints, based on their calculated effective concentrations, were also noticeably different. The results of this study also supported the higher sensitivity of growth-inhibition-based endpoints and hence ruled out their complete substitution by ChlF-based phytotoxicity endpoints in duckweed toxicity testing. Another observation of this study was the underestimation of photosynthesis-inhibiting effects due to the exclusion of chlorotic frond parts when exposed to an element with high acute phytotoxic potential. The results of this study also suggested that changes in the photochemical efficiency of duckweeds were not necessarily corresponding to the growth responses due to such exclusions.

Another attempt to make the measurements shorter, that is using ChlF-based F_m images to measure growth-based parameters of the test cultures, also proved to bias the measurement. This was due to chlorotic regions in fronds that appeared as virtual loss in total surface area causing an underestimation in this growth parameter.

Despite the comparatively lower sensitivity and methodological constraints, ChlF-based phenotyping techniques can increase the throughput of toxicity assays by providing a non-invasive tool for physiological monitoring. Furthermore, the utilization of imaging techniques in ChlF allowed for the simultaneous measurement of duckweed growth and photosynthetic responses in phytotoxicity studies, resulting in a considerable reduction in testing duration. Finally, using the small-scale multi-well-plate-based testing system in combination with ChlF imaging technique, duckweed phytotoxicity assays can facilitate simultaneous screening of large sample series or multiple duckweed species/clones within a short duration.

8. New scientific results

1. This study compared the most widely used ChlF-based endpoints to evaluate their suitability to replace classic growth-based endpoints. The results didn't support the replacement of growth-based endpoints by the ChlF-based ones, but rather favored joint measurement of both endpoint groups to maximize the information obtained from toxicological tests.
2. The results of this study proved that F_v/F_o is a more sensitive endpoint than the frequently used F_v/F_m and, hence, reporting F_v/F_o should also be promoted instead or in addition to the latter parameter.
3. Measuring ChlF using our customized protocol significantly affected the sensitivity order of the endpoints and resulted in an overall lesser sensitivity of the light-adapted Y(II) as compared to the dark-adapted F_v/F_o. This fact, together with the more standardized way of measuring dark-adapted ChlF parameters, favors using those parameters as endpoints in duckweed-based phytotoxicity tests.
4. Hormetic patterns were found to be prevalent in our results with duckweeds in case of both growth- and ChlF-based endpoints, though even the maximal stimulation was relatively low with the metallic elements. These results suggest that hormesis, especially in case of the more responsive parameters, may play a considerable role in shaping the concentration-response patterns and thus should be considered when analyzing duckweed responses to environmental stimuli.
5. The short-term and less cost-intensive tissue-culture plate-based toxicity test system can be applied in duckweed toxicity assay in case a large number of species/ecotypes/chemical agents is to be tested within a limited timescale and limited space availability. However, the sensitivity of the tests is lower as compared to standard OECD or ISO test protocols.
6. As a baseline for further research of this kind, this study produced a detailed phytotoxicity dataset for *L. gibba* obtained in a multi-well-plate-based configuration for 12 environmentally significant metals and metalloids.

9. Acknowledgments

I would like to express my deepest gratitude to my research supervisor Dr. Viktor Oláh for entrusting me with an opportunity to be a part of his team. Throughout this journey, not only he has been very helpful but also a kind and supportive mentor. His invaluable patience and constructive feedback made this milestone accomplishable. Big thanks to the Tempus Public Foundation and the Higher Education Commission of Pakistan for their Stipendium Hungaricum Scholarship Program. Without this scholarship it wouldn't be possible for me to be in this institute. I would like to extend my sincere thanks to Dr. Ilona Mészáros for providing critical and insightful guidance. Many appreciations to the whole faculty of the Department of Botany, especially Prof. Dr. Gábor Vasas, Prof. Dr. Csaba Máthé, Dr. Gábor Sramkó and Dr. Tamás Garda for always considering me a part of the institute and helping me in every possible situation. Also, none of this work would have been possible without the help of our laboratory colleagues, namely Judit Juhászné Kovács and Dorottya Magi. All the research students of the duckweed research lab, especially Zsuzsanna Barnáné Szabó, Nguyen Phuong Bach, Pham Thi Hong Xuan, and Raja Amri are also appreciated for their help and creating a friendly environment. Lastly, I am highly indebted to all my family members and friends for believing in me and encouraging me at every stage of my educational journey.

This work would also not have been possible without financial supports by the National Research, Development and Innovation Office —NKFIH— of the Hungarian Ministry for Innovation and Technology through the research grant OTKA FK 134296, the János Bolyai Research Scholarship of the Hungarian Academy of Sciences, and the ÚNKP-23-5 New National Excellence Program of the Ministry for Culture and Innovation provided for Viktor Oláh. Last but not least, we greatly appreciate the invaluable contribution of the Agora Science Centre (Debrecen, Hungary) by providing us the opportunity to use the Maxi Imaging-PAM instrument.

10. References

Acosta, K., Appenroth, K.-J., Borisjuk, L., Edelman, M., Heinig, U., Jansen, M. A. K., Oyama, T., Pasaribu, B., Schubert, I., Sorrels, S., Sree, K. S., Xu, S., Michael, T. P., & Lam, E. (2021). Return of the Lemnaceae: Duckweed as a model plant system in the genomics and postgenomics era. *The Plant Cell*, *33*(10), 3207–3234. https://doi.org/10.1093/plcell/koab189

Agathokleous, E. (2018). Environmental hormesis, a fundamental non-monotonic biological phenomenon with implications in ecotoxicology and environmental safety. *Ecotoxicology and Environmental Safety*, *148*, 1042–1053. https://doi.org/10.1016/j.ecoenv.2017.12.003

Agathokleous, E. (2021). The rise and fall of photosynthesis: Hormetic dose response in plants. *Journal of Forestry Research*, *32*(2), 889–898. https://doi.org/10.1007/s11676-020-01252-1

Agathokleous, E., Calabrese, E. J., & Barceló, D. (2024). Environmental hormesis: New developments. *Science of The Total Environment*, *906*, 167450. https://doi.org/10.1016/j.scitotenv.2023.167450

Ahlman, L., Bånkestad, D., & Wik, T. (2017). Using chlorophyll a fluorescence gains to optimize LED light spectrum for short term photosynthesis. *Computers and electronics in agriculture, 142*, 224-234. https://doi.org/10.1016/j.compag.2017.07.023

Alkimin, G. D., Daniel, D., Frankenbach, S., Serôdio, J., Soares, A. M. V. M., Barata, C., & Nunes, B. (2019). Evaluation of pharmaceutical toxic effects of non-standard endpoints on the macrophyte species *Lemna minor* and *Lemna gibba*. *The Science of the Total Environment*, *657*, 926–937. https://doi.org/10.1016/j.scitotenv.2018.12.002

Alp, F. N., Arikan, B., Ozfidan-Konakci, C., Gulenturk, C., Yildiztugay, E., Turan, M., & Cavusoglu, H. (2023). Hormetic activation of nano-sized rare earth element terbium on growth, PSII photochemistry, antioxidant status and phytohormone regulation in *Lemna minor*. *Plant Physiology and Biochemistry, 194*, 361-373. https://doi.org/10.1016/j.plaphy.2022.11.031

Amal Raj, A. R., Mylsamy, P., Sivasankar, V., Kumar, B. S., Omine, K., & Sunitha, T. G. (2024). Heavy metal pollution of river water and eco-friendly remediation using potent microalgal species. *Water Science and Engineering*, *17*(1), 41–50. https://doi.org/10.1016/j.wse.2023.04.001

An, D., Li, C., Zhou, Y., Wu, Y., & Wang, W. (2018). Genomes and Transcriptomes of Duckweeds. *Frontiers in Chemistry*, *6*, p. 230 https://www.frontiersin.org/articles/10.3389/fchem.2018.00230

Andresen, E., Opitz, J., Thomas, G., Stärk, H.-J., Dienemann, H., Jenemann, K., Dickinson, B. C., & Küpper, H. (2013). Effects of Cd & Ni toxicity to *Ceratophyllum demersum* under environmentally relevant conditions in soft & hard water including a German lake. *Aquatic Toxicology*, *142–143*, 387–402. https://doi.org/10.1016/j.aquatox.2013.09.016

Appenroth, K.-J. (2015). Useful methods 3: Media for in vitro-cultivation of duckweed. *Duckweed Forum*, *3*(4), 180-186. http://www.ruduckweed.org/uploads/1/0/8/9/10896289/iscdra_issue11-2015-11_final.pdf

Appenroth, K.-J., Krech, K., Keresztes, Á., Fischer, W., & Koloczek, H. (2010). Effects of nickel on the chloroplasts of the duckweeds *Spirodela polyrhiza* and *Lemna minor* and their possible use in biomonitoring and phytoremediation. *Chemosphere*, *78*(3), 216–223. https://doi.org/10.1016/j.chemosphere.2009.11.007

Baek, G., Saeed, M., & Choi, H.-K. (2021). Duckweeds: Their utilization, metabolites and cultivation. *Applied Biological Chemistry*, *64*(1), 73. https://doi.org/10.1186/s13765-021-00644-z

Banks, J. M. (2017). Continuous excitation chlorophyll fluorescence parameters: A review for practitioners. *Tree Physiology*, *37*(8), 1128–1136. https://doi.org/10.1093/treephys/tpx059

Baudo, R., Foudoulakis, M., Arapis, G., Perdaen, K., Lanneau, W., Paxinou, A.-C., Kouvdou, S., & Persoone, G. (2015). History and sensitivity comparison of the *Spirodela polyrhiza* microbiotest and *Lemna* toxicity tests. *Knowledge and Management of Aquatic Ecosystems*, *416*, 23.

https://doi.org/10.1051/kmae/2015019

Belz, R. G., Cedergreen, N., & Sørensen, H. (2008). Hormesis in mixtures—Can it be predicted? *Science of The Total Environment*, *404*(1), 77–87. https://doi.org/10.1016/j.scitotenv.2008.06.008

Bhagooli, R., Mattan-Moorgawa, S., Kaullysing, D., Louis, Y. D., Gopeechund, A., Ramah, S., ... & Baker, A. C. (2021). Chlorophyll fluorescence–A tool to assess photosynthetic performance and stress photophysiology in symbiotic marine invertebrates and seaplants. *Marine pollution bulletin*, *165*, 112059. https://doi.org/10.1016/j.marpolbul.2021.112059

Bog, M., Sree, K. S., Fuchs, J., Hoang, P. T. N., Schubert, I., Kuever, J., Rabenstein, A., Paolacci, S., Jansen, M. A. K., & Appenroth, K.-J. (2020). A taxonomic revision of *Lemna* sect. Uninerves (Lemnaceae). *Taxon*, *69*(1), 56–66. https://doi.org/10.1002/TAX.12188

Brain, P., & Cousens, R. (1989). An equation to describe dose responses where there is stimulation of growth at low doses. *Weed Research*, *29*(2), 93–96. https://doi.org/10.1111/j.1365-3180.1989.tb00845.x

Brain, R. A., & Cedergreen, N. (2009). Biomarkers in aquatic plants: Selection and utility. *Reviews of Environmental Contamination and Toxicology*, *198*, 49–109. https://doi.org/10.1007/978-0-387-09647-6_2

Buonasera, K., Lambreva, M., Rea, G., Touloupakis, E., & Giardi, M. T. (2011). Technological applications of chlorophyll a fluorescence for the assessment of environmental pollutants. *Analytical and Bioanalytical Chemistry*, *401*(4), 1139–1151. https://doi.org/10.1007/s00216-011-5166-1

Calabrese, E. J. (2003). The maturing of hormesis as a credible dose-response model. Nonlinearity in biology, toxicology, medicine, 1(3), 319–343. https://doi.org/10.1080/154014203902499

Calabrese, E. J. (2010). Hormesis is central to toxicology, pharmacology and risk assessment. *Human & Experimental Toxicology*, *29*(4), 249–261. https://doi.org/10.1177/0960327109363973

Calabrese, E. J., & Baldwin, L. A. (2000a). Chemical hormesis: Its historical foundations as a biological hypothesis. *Human & Experimental Toxicology*, *19*(1), 2–31. https://doi.org/10.1191/096032700678815585

Calabrese, E. J., & Baldwin, L. A. (2000b). Radiation hormesis: Its historical foundations as a biological hypothesis. *Human & Experimental Toxicology*, *19*(1), 41–75. https://doi.org/10.1191/096032700678815602

Calabrese, E. J., & Baldwin, L. A. (2000c). Radiation hormesis: The demise of a legitimate hypothesis. *Human & Experimental Toxicology*, *19*(1), 76–84. https://doi.org/10.1191/096032700678815611

Calabrese, E. J., & Baldwin, L. A. (2000d). Tales of two similar hypotheses: The rise and fall of chemical and radiation hormesis. *Human & Experimental Toxicology*, *19*(1), 85–97. https://doi.org/10.1191/096032700678815620

Calabrese, E. J., & Baldwin, L. A. (2000e). The marginalization of hormesis. *Human & Experimental Toxicology*, *19*(1), 32–40. https://doi.org/10.1191/096032700678815594

Calabrese, E. J., & Baldwin, L. A. (2001). U-shaped dose-responses in biology, toxicology, and public health1. *Annual Review of Public Health*, *22*, 15–33. https://doi.org/10.1146/annurev.publhealth.22.1.15

Calabrese, E. J., & Baldwin, L. A. (2002). Defining hormesis. *Human & Experimental Toxicology*, *21*(2), 91–97. https://doi.org/10.1191/0960327102ht217oa

Calabrese, E. J., & Blain, R. B. (2009). Hormesis and plant biology. *Environmental Pollution*, *157*(1), 42–48. https://doi.org/10.1016/j.envpol.2008.07.028

Cedergreen, N., & Madsen, T. V. (2002). Nitrogen uptake by the floating macrophyte *Lemna minor*. *New Phytologist*, *155*(2), 285–292. https://doi.org/10.1046/j.1469-8137.2002.00463.x

Cedergreen, N., Ritz, C., & Streibig, J. C. (2005). Improved empirical models describing hormesis. *Environmental Toxicology and Chemistry*, *24*(12), 3166–3172. https://doi.org/10.1897/05-014R.1

Cedergreen, N., Streibig, J. C., Kudsk, P., Mathiassen, S. K., & Duke, S. O. (2007). The occurrence of hormesis in plants and algae. *Dose-Response*, *5*(2), dose-response.06-008.Cedergreen. https://doi.org/10.2203/dose-response.06-008.Cedergreen

Cen, H., Weng, H., Yao, J., He, M., Lv, J., Hua, S., ... & He, Y. (2017). Chlorophyll fluorescence imaging uncovers photosynthetic fingerprint of citrus Huanglongbing. Frontiers in plant science, 8, 1509. https://doi.org/10.3389/fpls.2017.01509

Ceschin, S., Bellini, A., & Scalici, M. (2021). Aquatic plants and ecotoxicological assessment in freshwater ecosystems: A review. *Environmental Science and Pollution Research*, *28*(5), 4975–4988. https://doi.org/10.1007/s11356-020-11496-3

Chen, G., Fang, Y., Huang, J., Zhao, Y., Li, Q., Lai, F., Xu, Y., Tian, X., He, K., Jin, Y., Tan, L., & Zhao, H. (2018). Duckweed systems for eutrophic water purification through converting wastewater nutrients to high-starch biomass: Comparative evaluation of three different genera (*Spirodela polyrhiza*, *Lemna minor* and *Landoltia punctata*) in monoculture or polyculture. *RSC Advances*, *8*(32), 17927–17937. https://doi.org/10.1039/C8RA01856A

Chen, G., Zhao, K., Li, W., Yan, B., Yu, Y., Li, J., Zhang, Y., Xia, S., Cheng, Z., Lin, F., Li, L., Zhao, H., & Fang, Y. (2022). A review on bioenergy production from duckweed. *Biomass and Bioenergy*, *161*, 106468–106468. https://doi.org/10.1016/J.BIOMBIOE.2022.106468

Chen, Y.-E., Wu, N., Zhang, Z.-W., Yuan, M., & Yuan, S. (2019). Perspective of monitoring heavy metals by moss visible chlorophyll fluorescence parameters. *Frontiers in Plant Science*, *10,* 35. https://doi.org/10.3389/fpls.2019.00035

Cheng, J. J., & Stomp, A.-M. (2009). Growing duckweed to recover nutrients from wastewaters and for production of fuel ethanol and animal feed. *CLEAN – Soil, Air, Water*, *37*(1), 17–26. https://doi.org/10.1002/clen.200800210

Christensen, M. G., Teicher, H. B., & Streibig, J. C. (2003). Linking fluorescence induction curve and biomass in herbicide screening. *Pest Management Science*, *59*(12), 1303–1310. https://doi.org/10.1002/ps.763

Cornelius, C., Koverech, G., Crupi, R., Di Paola, R., Koverech, A., Lodato, F., Scuto, M., Salinaro, A. T., Cuzzocrea, S., Calabrese, E. J., & Calabrese, V. (2014). Osteoporosis and alzheimer pathology: Role of cellular stress response and hormetic redox signaling in aging and bone remodeling. *Frontiers in Pharmacology*, *5,* 91364. https://doi.org/10.3389/fphar.2014.00120

Cui, W., Cheng, J. J., & Cui, C. W. (2015). Growing duckweed for biofuel production: A review. *Plant Biology*, *17*, 16–23. https://doi.org/10.1111/plb.12216

DalCorso, G. (2012). Heavy metal toxicity in plants. *In: Furini, A. (eds) Plants and Heavy Metals. SpringerBriefs in Molecular Science*. Springer, Dordrecht. https://doi.org/10.1007/978-94-007-4441-7_1

Daniel, D., de Alkimin, G. D., & Nunes, B. (2020). Single and combined effects of the drugs salicylic acid and acetazolamide: Adverse changes in physiological parameters of the freshwater macrophyte, *Lemna gibba*. *Environmental Toxicology and Pharmacology*, *79*, 103431. https://doi.org/10.1016/j.etap.2020.103431

De Cesare, F., Pietrini, F., Zacchini, M., Scarascia Mugnozza, G., & Macagnano, A. (2019). Catechol-loading nanofibrous membranes for eco-friendly iron nutrition of plants. *Nanomaterials*, *9*(9), 1315. https://doi.org/10.3390/nano9091315

Dewez, D., Goltsev, V., Kalaji, H. M., & Oukarroum, A. (2018). Inhibitory effects of silver nanoparticles on photosystem II performance in *Lemna gibba* probed by chlorophyll fluorescence. *Current Plant Biology*, *16*, 15–21. https://doi.org/10.1016/j.cpb.2018.11.006

Edelman, M., Appenroth, K.-J., Sree, K. S., & Oyama, T. (2022). Ethnobotanical history: Duckweeds in different civilizations. *Plants*, *11*(16), 2124. https://doi.org/10.3390/plants11162124

Eid, M. H., Eissa, M., Mohamed, E. A., Ramadan, H. S., Tamás, M., Kovács, A., & Szűcs, P. (2024). New approach into human health risk assessment associated

with heavy metals in surface water and groundwater using Monte Carlo Method. *Scientific Reports*, *14*(1), 1008. https://doi.org/10.1038/s41598-023-50000-y

Environment Canada. (2007). Biological test method for measuring the inhibition of growth using freshwater macrophyte, *Lemna minor*. https://www.canada.ca/en/environment-climate-change/services/wildlife-research-landscape-science/biological-test-method-publications/inhibition-growth-freshwater-macrophyte.html

Flores, F., Collier, C. J., Mercurio, P., & Negri, A. P. (2013). Phytotoxicity of four photosystem ii herbicides to tropical seagrasses. *PLOS ONE*, *8*(9), e75798. https://doi.org/10.1371/journal.pone.0075798

Forni, C., Braglia, R., Harren, F. J. M., & Cristescu, S. M. (2012). Stress responses of duckweed (*Lemna minor* L.) and water velvet (*Azolla filiculoides* Lam.) to anionic surfactant sodium-dodecyl-sulphate (SDS). *Aquatic Toxicology (Amsterdam, Netherlands)*, *110–111*, 107–113. https://doi.org/10.1016/J.AQUATOX.2011.12.017

Geilfus, C. M. (2018). Chloride: from nutrient to toxicant. *Plant and Cell Physiology*, *59*(5), 877-886. https://doi.org/10.1093/pcp/pcy071

Golob, A., Vogel-Mikuš, K., Brudar, N., & Germ, M. (2021). Duckweed (*Lemna minor* L.) successfully accumulates selenium from selenium-impacted water. *Sustainability 2021, Vol. 13, Page 13423*, *13*(23), 13423–13423. https://doi.org/10.3390/SU132313423

Guidi, L., Lo Piccolo, E., & Landi, M. (2019). Chlorophyll fluorescence, photoinhibition and abiotic stress: Does it make any difference the fact to be a C3 or C4 species? *Frontiers in Plant Science*, *10*. https://doi.org/10.3389/fpls.2019.00174

Hasanuzzaman, M., Nahar, K., & Fujita, M. (2013). Plant response to salt stress and role of exogenous protectants to mitigate salt-induced damages. *Ecophysiology and Responses of Plants under Salt Stress*, 25–87. https://doi.org/10.1007/978-1-4614-4747-4_2

Hee, S. Q. (1993). *Biological monitoring: An introduction*. *Van Nostrand Reinhold*, New York, NY. Pp. 650. ISBN 0-442-23677-8.

Heinz Walz GmbH. (2019). *IMAGING-PAM M-Series chlorophyll fluorometer: instrument description and information for users* (5th edition). *Heinz Walz GmbH.* https://www.walz.com/files/downloads/manuals/imaging-pam_ms/imag-m-series0e_3Dg.pdf

Henke, R., Eberius, M., & Appenroth, K.-J. (2011). Induction of frond abscission by metals and other toxic compounds in *Lemna minor*. *Aquatic Toxicology*, *101*(1), 261–265. https://doi.org/10.1016/j.aquatox.2010.10.007

Henschler, D. (2006). The origin of hormesis: Historical background and driving forces. *Human & Experimental Toxicology*, *25*(7), 347–351. https://doi.org/10.1191/0960327106ht642oa

Hepp, A., Oláh, V., Sipos, O., Adorján, B., & Mészáros, I. (2018). *Békalencse fitotoxikológiai tesztek eredményét befolyásoló tényez˝ok vizsgálata* (Assessment of factors affecting the results of duckweed phytotoxicity tests). *Proceedings of the XIV Environmental Scientific Conference of the Carpathian Basin; Gödöllő, Hungary, 5–7 April 2018*. pp. 127–131.

Hepp, A., Vaca, N. Y. G., Kovács, F., Tamás, M., Oláh, V., & Mészáros, I. (2016). Effects of Hg on growth of active and resting (turions) fronds of giant duckweed (*Spirodela polyrhiza* (L.) Schleiden). *Proceedings of 12th Environmental Science Conference of the Carpathian Basin, Pécs, Hungary, 1-4 June 2016. 126*, pp. 94–103. https://m2.mtmt.hu/gui2/?mode=browse&params=publication;3331908

Hillman, W. S. (1957). Nonphotosynthetic light requirement in *Lemna minor* and its partial satisfaction by kinetin. *Science*, *126*(3265), 165–166. https://doi.org/10.1126/science.126.3265.165

Hong, Y., Zhu, Z., Liao, W., Yan, Z., Feng, C., & Xu, D. (2023). Freshwater water-quality criteria for chloride and guidance for the revision of the water-quality standard in China. *International journal of environmental research and public health*, *20*(4), 2875.

https://doi.org/10.3390/ijerph20042875

Hou, W., Chen, X., Song, G., Wang, Q., & Chi Chang, C. (2007). Effects of copper and cadmium on heavy metal polluted waterbody restoration by duckweed (*Lemna minor*). *Plant Physiology and Biochemistry*, *45*(1), 62–69. https://doi.org/10.1016/J.PLAPHY.2006.12.005

Iqbal, J., Javed, A., & Baig, M. A. (2019). Growth and nutrient removal efficiency of duckweed (*Lemna minor*) from synthetic and dumpsite leachate under artificial and natural conditions. *PLoS ONE*, *14*(8). https://doi.org/10.1371/JOURNAL.PONE.0221755

ISO (2005). Water quality—Determination of the toxic effect of water constituents and waste water on duckweed (*Lemna minor*)—Duckweed growth inhibition test. https://www.iso.org/standard/34074.html

Jafarzadeh, N., Heidari, K., Meshkinian, A., Kamani, H., Mohammadi, A. A., & Conti, G. O. (2022). Non-carcinogenic risk assessment of exposure to heavy metals in underground water resources in Saraven, Iran: Spatial distribution, Monte-Carlo simulation, sensitive analysis. *Environmental Research*, *204*, 112002. https://doi.org/10.1016/j.envres.2021.112002

Jajoo, A. (2013). Changes in photosystem II in response to salt stress. In: Ahmad, P., Azooz, M., Prasad, M. (eds) *Ecophysiology and responses of plants under salt stress*. *Springer*, New York, NY, pp. 149-168. https://doi.org/10.1007/978-1-4614-4747-4_5

Jiang, H.-S., Li, M., Chang, F.-Y., Li, W., & Yin, L.-Y. (2012). Physiological analysis of silver nanoparticles and $AgNO_3$ toxicity to *Spirodela polyrhiza*. *Environmental Toxicology and Chemistry*, *31*(8), 1880–1886. https://doi.org/10.1002/etc.1899

Kalaji, H. M., Schansker, G., Brestic, M., Bussotti, F., Calatayud, A., Ferroni, L., Goltsev, V., Guidi, L., Jajoo, A., Li, P., Losciale, P., Mishra, V. K., Misra, A. N., Nebauer, S. G., Pancaldi, S., Penella, C., Pollastrini, M., Suresh, K., Tambussi, E., … Bąba, W. (2017). Frequently asked questions about chlorophyll fluorescence, the sequel. *Photosynthesis Research*, *132*(1), 13–66. https://doi.org/10.1007/s11120-016-0318-y

Kalaji, H. M., Schansker, G., Ladle, R. J., Goltsev, V., Bosa, K., Allakhverdiev, S. I., Brestic, M., Bussotti, F., Calatayud, A., Dąbrowski, P., Elsheery, N. I., Ferroni, L., Guidi, L., Hogewoning, S. W., Jajoo, A., Misra, A. N., Nebauer, S. G., Pancaldi, S., Penella, C., … Zivcak, M. (2014). Frequently asked questions about in vivo chlorophyll fluorescence: Practical issues. *Photosynthesis Research*, *122*(2), 121–158. https://doi.org/10.1007/s11120-014-0024-6

Kalčíková, G., Marolt, G., Kokalj, A. J., & Gotvajn, A. Ž. (2018). The use of multiwell culture plates in the duckweed toxicity test—A case study on Zn nanoparticles. *New Biotechnology*, *47*, 67–72. https://doi.org/10.1016/J.NBT.2018.06.002

Kautsky, H., & Hirsch, A. (1931). Neue Versuche zur Kohlensäureassimilation. *Naturwissenschaften*, *19*(48), 964–964. https://doi.org/10.1007/BF01516164

Khellaf, N., & Zerdaoui, M. (2009). Growth response of the duckweed *Lemna minor* to heavy metal pollution. *Iranian Journal of Environmental Health Science & Engineering*, *6*(3), 161–166. https://www.bioline.org.br/abstract?id=se09024

Khellaf, N., & Zerdaoui, M. (2010). Growth response of the duckweed *Lemna gibba* L. to copper and nickel phytoaccumulation. *Ecotoxicology*, *19*(8), 1363–1368. https://doi.org/10.1007/S10646-010-0522-Z/TABLES/3

Klughammer, C., & Schreiber, U. (2008). Complementary PS II quantum yields calculated from simple fluorescence parameters measured by PAM fluorometry and the Saturation Pulse method. *PAM Application Notes*, *1*(2), 201–247. https://www.walz.com/files/downloads/pan/PAN078007.pdf

Kobayashi, M., Katoh, H., & Ikeuchi, M. (2006). Mutations in a putative chloride efflux transporter gene suppress the chloride requirement of photosystem II in the cytochrome c550-deficient mutant. *Plant and cell physiology*, *47*(6), 799-804. https://doi.org/10.1093/pcp/pcj052

Kose, T., Lins, T. F., Wang, J., O'Brien, A. M., Sinton, D., & Frederickson, M. E. (2023). Accelerated high-throughput imaging and phenotyping system for small organisms. *PLOS ONE*, *18*(7), e0287739.

https://doi.org/10.1371/journal.pone.0287739

Kumar, K. S., & Han, T. (2010). Physiological response of *Lemna* species to herbicides and its probable use in toxicity testing. *Toxicology and Environmental Health Sciences*, *2*(1), 39–49. https://doi.org/10.1007/BF03216512

Küpper, H., Benedikty, Z., Morina, F., Andresen, E., Mishra, A., & Trtílek, M. (2019). Analysis of OJIP chlorophyll fluorescence kinetics and QA reoxidation kinetics by direct fast imaging. *Plant Physiology*, *179*(2), 369–381. https://doi.org/10.1104/pp.18.00953

Lahive, E., O'Callaghan, M. J. A., Jansen, M. A. K., & O'Halloran, J. (2011). Uptake and partitioning of zinc in Lemnaceae. *Ecotoxicology (London, England)*, *20*(8), 1992–2002. https://doi.org/10.1007/s10646-011-0741-y

Lahive, E., O'Halloran, J., & Jansen, M. A. K. (2012). Frond development gradients are a determinant of the impact of zinc on photosynthesis in three species of Lemnaceae. *Aquatic Botany*, *101*, 55–63. https://doi.org/10.1016/j.aquabot.2012.04.003

Landolt, E. (1986). *The family of "Lemnaceae": a monographic study - Biosystematic Investigations in the Family of Duckweeds ('Lemnaceae').* Geobotanisches Institut der ETH, Zürich, Switzerland.

Landolt, E., & Kandeler, R. (1987). *Biosystematic investigations in the family of duckweeds (Lemnaceae), Vol. 4: The family of "Lemnaceae" - a monographic study, Vol. 2 (phytochemistry, physiology, application, bibliography). Veroeffentlichungen Des Geobotanischen Instituts Der ETH, Stiftung Ruebel (Switzerland)*, *95*.

Lanthemann, L., & van Moorsel, S. J. (2022). Species interactions in three Lemnaceae species growing along a gradient of zinc pollution. *Ecology and Evolution*, *12*(2), e8646–e8646. https://doi.org/10.1002/ECE3.8646

Láposi, R., Veres, S., Lakatos, G., Oláh, V., Fieldsend, A., & Mészáros, I. (2009). Responses of leaf traits of European beech (*Fagus sylvatica* L.) saplings to supplemental UV-B radiation and UV-B exclusion. *Agricultural and Forest Meteorology*, *149*(5), 745–755.

https://doi.org/10.1016/j.agrformet.2008.10.023

Lazár, D. (2015). Parameters of photosynthetic energy partitioning. *Journal of Plant Physiology*, *175*, 131–147. https://doi.org/10.1016/j.jplph.2014.10.021

Lee, H., De Saeger, J., Bae, S., Kim, M., Depuydt, S., Heynderickx, P. M., Wu, D., Han, T., & Park, J. (2023). Giant duckweed (*Spirodela polyrhiza*) root growth as a simple and sensitive indicator of copper and chromium contamination. *Toxics*, *11*(9), Article 9. https://doi.org/10.3390/toxics11090788

Lee, H., Depuydt, S., Shin, K., Choi, S., Kim, G., Lee, Y. H., Park, J. T., Han, T., & Park, J. (2021). Assessment of various toxicity endpoints in duckweed (*Lemna minor*) at the physiological, biochemical, and molecular levels as a measure of diuron stress. *Biology*, *10*(7), Article 7. https://doi.org/10.3390/biology10070684

Li, C., Zeng, Q., Han, Y., Zhou, X., & Xu, H. (2024). Effects of *Bacillus subtilis* on cucumber seedling growth and photosynthetic system under different potassium ion levels. *Biology, 13*(5), 348. https://doi.org/10.3390/biology13050348

Li, H., Mo, F., Li, Y., Wang, M., Li, Z., Hu, H., Deng, W., & Zhang, R. (2020). Effects of silver(I) toxicity on microstructure, biochemical activities, and genic material of *Lemna minor* L. with special reference to application of bioindicator. *Environmental Science and Pollution Research*, *27*(18), 22735–22748. https://doi.org/10.1007/s11356-020-08844-8

Li, Q., Yi, Z., Yang, G., Xu, Y., Jin, Y., Tan, L., ... & Fang, Y. (2022). Effects of various spectral compositions on micro-polluted water purification and biofuel feedstock production using duckweed. *Environmental Science and Pollution Research, 29*(34), 52003-52012. https://doi.org/10.1007/s11356-022-19488-1

Liang, J., Li, Y., Xie, P., Liu, C., Yu, L., & Ma, X. (2022). Dualistic effects of bisphenol A on growth, photosynthetic and oxidative stress of duckweed

(*Lemna minor*). *Environmental Science and Pollution Research*, *29*(58), 87717–87729. https://doi.org/10.1007/s11356-022-21785-8

Lichtenthaler, H. K., Buschmann, C., & Knapp, M. (2005). How to correctly determine the different chlorophyll fluorescence parameters and the chlorophyll fluorescence decrease ratio Rfd of leaves with the PAM fluorometer. *Photosynthetica*, *43*(3), 379–393. https://doi.org/10.1007/s11099-005-0062-6

Liebers, M., Hommel, E., Grübler, B., Danehl, J., Offermann, S., & Pfannschmidt, T. (2023). Photosynthesis in the biomass model species *Lemna minor* displays plant-conserved and species-specific features. *Plants*, *12*(13), Article 13. https://doi.org/10.3390/plants12132442

Markovic, M., Neale, P. A., Nidumolu, B., & Kumar, A. (2021). Combined toxicity of therapeutic pharmaceuticals to duckweed, *Lemna minor*. *Ecotoxicology and Environmental Safety*, *208*, 111428. https://doi.org/10.1016/j.ecoenv.2020.111428

Martinez-Haro, M., Beiras, R., Bellas, J., Capela, R., Coelho, J. P., Lopes, I., Moreira-Santos, M., Reis-Henriques, A. M., Ribeiro, R., Santos, M. M., & Marques, J. C. (2015). A review on the ecological quality status assessment in aquatic systems using community based indicators and ecotoxicological tools: What might be the added value of their combination? *Ecological Indicators*, *48*, 8–16. https://doi.org/10.1016/j.ecolind.2014.07.024

Maxwell, K., & Johnson, G. N. (2000). Chlorophyll fluorescence—A practical guide. *Journal of Experimental Botany*, *51*(345), 659–668. https://doi.org/10.1093/jexbot/51.345.659

Mohedano, R. A., Costa, R. H. R., Tavares, F. A., & Belli Filho, P. (2012). High nutrient removal rate from swine wastes and protein biomass production by full-scale duckweed ponds. *Bioresource Technology*, *112*, 98–104. https://doi.org/10.1016/j.biortech.2012.02.083

Muller, R., Schreiber, U., Escher, B. I., Quayle, P., Bengtson Nash, S. M., & Mueller, J. F. (2008). Rapid exposure assessment of PSII herbicides in surface water

using a novel chlorophyll a fluorescence imaging assay. *Science of The Total Environment*, *401*(1), 51–59. https://doi.org/10.1016/j.scitotenv.2008.02.062

Murchie, E. H., & Lawson, T. (2013). Chlorophyll fluorescence analysis: A guide to good practice and understanding some new applications. *Journal of Experimental Botany*, *64*(13), 3983–3998. https://doi.org/10.1093/jxb/ert208

Naumann, B., Eberius, M., & Appenroth, K.-J. (2007). Growth rate based dose-response relationships and EC-values of ten heavy metals using the duckweed growth inhibition test (ISO 20079) with *Lemna minor* L. clone St. *Journal of Plant Physiology*, *164*(12), 1656–1664. https://doi.org/10.1016/J.JPLPH.2006.10.011

Obermeier, M., Schröder, C. A., Helmreich, B., & Schröder, P. (2015). The enzymatic and antioxidative stress response of *Lemna minor* to copper and a chloroacetamide herbicide. *Environmental Science and Pollution Research*, *22*(23), 18495–18507. https://doi.org/10.1007/S11356-015-5139-6

O'Brien, A. M., Laurich, J., Lash, E., & Frederickson, M. E. (2020). Mutualistic outcomes across plant populations, microbes, and environments in the duckweed *Lemna minor*. *Microbial Ecology*, *80*(2), 384–397. https://doi.org/10.1007/S00248-019-01452-1/FIGURES/4

OECD. (2006). OECD guidelines for the testing of chemicals, revised proposal for a new guideline 221, *Lemna sp.* growth inhibition test. https://doi.org/10.1787/9789264016194-en

Oláh, V., Hepp, A., Gaibor Vaca, N. Y., Tamás, M., & Mészáros, I. (2018). Retrospective analyses of archive phytotoxicity test data can help in assessing internal dynamics and stability of growth in laboratory duckweed cultures. *Aquatic Toxicology*, *201*, 40–46. https://doi.org/10.1016/j.aquatox.2018.05.022

Oláh, V., Hepp, A., Lakatos, G., & Mészáros, I. (2014). Cadmium-induced turion formation of *Spirodela polyrhiza* (L.) Schleiden. *Acta Biologica Szegediensis*, *58*(2), Article 2. https://abs.bibl.u-szeged.hu/index.php/abs/article/view/2824

Oláh, V., Hepp, A., & Mészáros, I. (2015). Comparative study on the sensitivity of turions and active fronds of giant duckweed (*Spirodela polyrhiza* (L.) Schleiden) to heavy metal treatments. *Chemosphere*, *132*, 40–46. https://doi.org/10.1016/j.chemosphere.2015.01.050

Oláh, V., Hepp, A., & Mészáros, I. (2016). Assessment of giant duckweed (*Spirodela polyrhiza* L. Schleiden) turions as model objects in ecotoxicological applications. *Bulletin of Environmental Contamination and Toxicology*, *96*(5), 596–601. https://doi.org/10.1007/s00128-016-1765-z

Oláh, V., Kosztankó, K., Irfan, M., Barnáné Szabó, Z., Jansen, M. A. K., Szabó, S., & Mészáros, I. (2024). Frond-level analyses reveal functional heterogeneity within heavy metal-treated duckweed colonies. *Plant Stress*, *11*, 100405. https://doi.org/10.1016/j.stress.2024.100405

Oláh, V., Lakatos, G., Bertók, C., Kanalas, P., Szőllősi, E., Kis, J., & Mészáros, I. (2010). Short-term chromium(VI) stress induces different photosynthetic responses in two duckweed species, *Lemna gibba* L. and *Lemna minor* L. *Photosynthetica*, *48*(4), 513–520. https://doi.org/10.1007/s11099-010-0068-6

Paolacci, S., Stejskal, V., Toner, D., & Jansen, M. A. K. (2022). Wastewater valorisation in an integrated multitrophic aquaculture system; assessing nutrient removal and biomass production by duckweed species. *Environmental Pollution*, *302*, 119059. https://doi.org/10.1016/j.envpol.2022.119059

Park, J., Brown, M. T., Depuydt, S., Kim, J. K., Won, D.-S., & Han, T. (2017). Comparing the acute sensitivity of growth and photosynthetic endpoints in three *Lemna* species exposed to four herbicides. *Environmental Pollution*, *220*, 818–827. https://doi.org/10.1016/j.envpol.2016.10.064

Park, J., Lee, H., & Han, T. (2020). Comparative paraquat sensitivity of newly germinated and mature fronds of the aquatic macrophyte *Spirodela polyrhiza*. *American Journal of Plant Sciences*, *11*(7), Article 7. https://doi.org/10.4236/ajps.2020.117072

Park, J.-S., Brown, M. T., & Han, T. (2012). Phenol toxicity to the aquatic macrophyte *Lemna paucicostata*. *Aquatic Toxicology*, *106–107*, 182–188. https://doi.org/10.1016/j.aquatox.2011.10.004

Perreault, F., Oukarroum, A., Pirastru, L., Sirois, L., Gerson Matias, W., & Popovic, R. (2010). Evaluation of copper oxide nanoparticles toxicity using chlorophyll a fluorescence imaging in *Lemna gibba*. *Journal of Botany*, *2010*, e763142. https://doi.org/10.1155/2010/763142

Petersen, F., Demann, J., Restemeyer, D., Olfs, H.-W., Westendarp, H., Appenroth, K.-J., & Ulbrich, A. (2022). Influence of light intensity and spectrum on duckweed growth and proteins in a small-scale, re-circulating indoor vertical farm. *Plants*, *11*(8), Article 8. https://doi.org/10.3390/plants11081010

Pietrini, F., Bianconi, D., Massacci, A., & Iannelli, M. A. (2016). Combined effects of elevated CO_2 and Cd-contaminated water on growth, photosynthetic response, Cd accumulation and thiolic components status in *Lemna minor* L. *Journal of Hazardous Materials*, *309*, 77–86. https://doi.org/10.1016/j.jhazmat.2016.01.079

Pietrini, F., Passatore, L., Carloni, S., & Zacchini, M. (2023). Non-standard physiological endpoints to evaluate the toxicity of emerging contaminants in aquatic plants: A case study on the exposure of *Lemna minor* L. and *Spirodela polyrhiza* (L.) Schleid. to dimethyl phthalate (DMP). In T. Aftab (Ed.), *Emerging contaminants and plants: interactions, adaptations and remediation technologies* (pp. 87–108). *Springer International Publishing*. https://doi.org/10.1007/978-3-031-22269-6_4

Pietrini, F., Passatore, L., Fischetti, E., Carloni, S., Ferrario, C., Polesello, S., & Zacchini, M. (2019). Evaluation of morpho-physiological traits and contaminant accumulation ability in *Lemna minor* L. treated with increasing perfluorooctanoic acid (PFOA) concentrations under laboratory conditions. *Science of The Total Environment*, *695*, 133828. https://doi.org/10.1016/j.scitotenv.2019.133828

Potters, G., Pasternak, T. P., Guisez, Y., Palme, K. J., & Jansen, M. A. K. (2007). Stress-induced morphogenic responses: Growing out of trouble? *Trends in Plant Science*, *12*(3), 98–105. https://doi.org/10.1016/j.tplants.2007.01.004

R Core Team. (2015). A language and environment for statistical computing: Vienna, Austria. *Available online:* https://www.gbif.org/tool/81287/r-a-language-and-environment-for-statistical-computing

Radić, S., Stipaničev, D., Cvjetko, P., Marijanović Rajčić, M., Širac, S., Pevalek-Kozlina, B., & Pavlica, M. (2011). Duckweed *Lemna minor* as a tool for testing toxicity and genotoxicity of surface waters. *Ecotoxicology and Environmental Safety*, *74*(2), 182–187. https://doi.org/10.1016/J.ECOENV.2010.06.011

Ralph, P. J., Macinnis-Ng, C. M. O., & Frankart, C. (2005). Fluorescence imaging application: Effect of leaf age on seagrass photokinetics. *Aquatic Botany*, *81*(1), 69–84. https://doi.org/10.1016/j.aquabot.2004.11.003

Ralph, P. J., Smith, R. A., Macinnis-Ng, C. M. O., & Seery, C. R. (2007). Use of fluorescence-based ecotoxicological bioassays in monitoring toxicants and pollution in aquatic systems: Review. *Toxicological & Environmental Chemistry*, *89*(4), 589–607. https://doi.org/10.1080/02772240701561593

Rampazzo, M. V., Cunha, M. L. O., de Oliveira, L. C. A., Silva, V. M., Lanza, M. G. D. B., de Melo, A. A. R., & dos Reis, A. R. (2022). physiological roles of nickel on antioxidant and nitrogen metabolism increasing the yield of sugarcane plants. *Journal of Soil Science and Plant Nutrition*, *22*(4), 4438–4448. https://doi.org/10.1007/s42729-022-01045-x

Raven, J. A. (2020). Chloride involvement in the synthesis, functioning and repair of the photosynthetic apparatus in vivo. *New Phytologist*, *227*(2), 334-342. https://doi.org/10.1111/nph.16541

Reid, A. J., Carlson, A. K., Creed, I. F., Eliason, E. J., Gell, P. A., Johnson, P. T. J., Kidd, K. A., MacCormack, T. J., Olden, J. D., Ormerod, S. J., Smol, J. P., Taylor, W. W., Tockner, K., Vermaire, J. C., Dudgeon, D., & Cooke, S. J. (2019). Emerging threats and persistent conservation challenges for

freshwater biodiversity. *Biological Reviews*, *94*(3), 849–873. https://doi.org/10.1111/brv.12480

Ritz, C., Baty, F., Streibig, J. C., & Gerhard, D. (2015). Dose-response analysis using R. *PLOS ONE*, *10*(12), e0146021–e0146021. https://doi.org/10.1371/JOURNAL.PONE.0146021

Roháček, K. (2002). Chlorophyll fluorescence parameters: The definitions, photosynthetic meaning, and mutual relationships. *Photosynthetica 2002 40:1*, *40*(1), 13–29. https://doi.org/10.1023/A:1020125719386

RStudio Team. (2023). RStudio Desktop IDE (Version 2023.06.0-421) [Computer software]. *PBC.* https://posit.co/products/open-source/rstudio/

Schleiden, M. J. (1839). *Prodromus monographiae Lemnacearum oder conspectus generum atque specierum*. *Linnaea* 13(4), 385–392

Schneider, C. A., Rasband, W. S., & Eliceiri, K. W. (2012). NIH Image to ImageJ: 25 years of image analysis. *Nature Methods 2012 9:7*, *9*(7), 671–675. https://doi.org/10.1038/nmeth.2089

Schreiber, U., Quayle, P., Schmidt, S., Escher, B. I., & Mueller, J. F. (2007). Methodology and evaluation of a highly sensitive algae toxicity test based on multiwell chlorophyll fluorescence imaging. *Biosensors and Bioelectronics*, *22*(11), 2554–2563. https://doi.org/10.1016/j.bios.2006.10.018

Schreiber, U., Schliwa, U., & Bilger, W. (1986). Continuous recording of photochemical and non-photochemical chlorophyll fluorescence quenching with a new type of modulation fluorometer. *Photosynthesis Research*, *10*(1), 51–62. https://doi.org/10.1007/BF00024185

Schuler, M. S., Hintz, W. D., Jones, D. K., Lind, L. A., Mattes, B. M., Stoler, A. B., ... & Relyea, R. A. (2017). How common road salts and organic additives alter freshwater food webs: in search of safer alternatives *Journal of Applied Ecology*, *54*(5), 1353-1361. https://doi.org/10.1111/1365-2664.12877

Schulz, H. (1887). Zur lehre von der arzneiwirkung. *Archiv Für Pathologische Anatomie Und Physiologie Und Für Klinische Medicin*, *108*(3), 423–445.

Shanker, A. K., Cervantes, C., Loza-Tavera, H., & Avudainayagam, S. (2005). Chromium toxicity in plants. *Environment International*, *31*(5), 739–753. https://doi.org/10.1016/j.envint.2005.02.003

Sharma, R., & Lenaghan, S. C. (2022). Duckweed: A potential phytosensor for heavy metals. *Plant Cell Reports*, *41*(12), 2231–2243. https://doi.org/10.1007/s00299-022-02913-7

Singh, H., Kumar, D., & Soni, V. (2022). Performance of chlorophyll a fluorescence parameters in *Lemna minor* under heavy metal stress induced by various concentration of copper. *Scientific Reports*, *12*(1), 10620. https://doi.org/10.1038/s41598-022-14985-2

Smith, K. E., Cowan, L., Taylor, B., McAusland, L., Heatley, M., Yant, L., & Murchie, E. H. (2024). Physiological adaptation to irradiance in duckweeds is species and accession specific and depends on light habitat niche. *Journal of Experimental Botany*, *75*(7), 2046–2063. https://doi.org/10.1093/jxb/erad499

Southam, C. M., & Ehrlich, J. (1943). Effects of extract of western bed-cedar heart-wood on certain wood-decaying fungi in culture. *Phytopathology, 33*(6), 517-524

Sree, K. S., Adelmann, K., Garcia, C., Lam, E., & Appenroth, K.-J. (2015). Natural variance in salt tolerance and induction of starch accumulation in duckweeds. *Planta*, *241*(6), 1395–1404. https://doi.org/10.1007/s00425-015-2264-x

Sree, K. S., Bog, M., & Appenroth, K.-J. (2016). Taxonomy of duckweeds (Lemnaceae), potential new crop plants. *Emirates Journal of Food and Agriculture*, *28*. https://doi.org/10.9755/ejfa.2016-01-038

Steinberg, R. A. (1946). Mineral requirements of *Lemna minor*. *Plant Physiology*, *21*(1), 42–48. https://doi.org/10.1104/pp.21.1.42

Stewart, J. J., Adams, W. W., Escobar, C. M., López-Pozo, M., & Demmig-Adams, B. (2020). Growth and essential carotenoid micronutrients in *Lemna gibba* as a function of growth light intensity. *Frontiers in Plant Science*, *11*. https://doi.org/10.3389/fpls.2020.00480

Subbaraman, B., Lange, O. de, Ferguson, S., & Peek, N. (2024). The duckbot: a system for automated imaging and manipulation of duckweed. *PLOS ONE*, *19*(1), e0296717. https://doi.org/10.1371/journal.pone.0296717

Szabó, S., Zavanyi, G., Koleszár, G., del Castillo, D., Oláh, V., & Braun, M. (2023). Phytoremediation, recovery and toxic effects of ionic gadolinium using the free-floating plant *Lemna gibba*. *Journal of Hazardous Materials*, *458*, 131930. https://doi.org/10.1016/j.jhazmat.2023.131930

Thingujam, D., Pajerowska-Mukhtar, K. M., & Mukhtar, M. S. (2024). Duckweed: Beyond an efficient plant model system. *Biomolecules*, *14*(6), 628. https://doi.org/10.3390/biom14060628

Tippery, N. P., & Les, D. H. (2020). Tiny plants with enormous potential: phylogeny and evolution of duckweeds. In X. H. Cao, P. Fourounjian, & W. Wang (Eds.), *The Duckweed Genomes* (pp. 19–38). *Springer International Publishing*. https://doi.org/10.1007/978-3-030-11045-1_2

Ueda, K., & Nagai, T. (2021). Relative sensitivity of duckweed *Lemna minor* and six algae to seven herbicides. *Journal of Pesticide Science*, *46*(3), 267–273. https://doi.org/10.1584/jpestics.D21-018

Vidaković-Cifrek, Ž., & Tkalec, M. (2023). Chlorophyll a fluorescence in evaluation of plant responses to environmental signals. In *chlorophyll a fluorescence measurements in Croatia – First twenty years* (pp. 19–27). https://www.poljinos.hr/wp-content/uploads/2023/10/Chlorophyll-a-Fluorescence-Measurements-in-Croatia-First-Twenty-Years.pdf

Wang, W., Kerstetter, R. A., & Michael, T. P. (2011). Evolution of genome size in duckweeds (Lemnaceae). *Journal of Botany*, *2011*(1), 570319. https://doi.org/10.1155/2011/570319

Wani, K. I., Naeem, M., & Aftab, T. (2022). Chromium in plant-soil nexus: speciation, uptake, transport and sustainable remediation techniques. *Environmental Pollution*, *315*, 120350. https://doi.org/10.1016/j.envpol.2022.120350

Ware, A., Jones, D. H., Flis, P., Chrysanthou, E., Smith, K. E., Kümpers, B. M. C., Yant, L., Atkinson, J. A., Wells, D. M., Bhosale, R., & Bishopp, A. (2023).

Loss of ancestral function in duckweed roots is accompanied by progressive anatomical reduction and a re-distribution of nutrient transporters. *Current Biology*, *33*(9), 1795-1802.e4. https://doi.org/10.1016/j.cub.2023.03.025

Wei, T., & Simko, V. R. (2021). *Package 'corrplot': Visualization of a correlation matrix (version 0.90).*

Wilkinson, A. D., Collier, C. J., Flores, F., Mercurio, P., O'Brien, J., Ralph, P. J., & Negri, A. P. (2015). A miniature bioassay for testing the acute phytotoxicity of photosystem II herbicides on seagrass. *PLOS ONE*, *10*(2), e0117541. https://doi.org/10.1371/journal.pone.0117541

Xu, Q. S., Hu, J. Z., Xie, K. B., Yang, H. Y., Du, K. H., & Shi, G. X. (2010). Accumulation and acute toxicity of silver in *Potamogeton crispus* L. *Journal of hazardous materials, 173*(1-3), 186-193. https://doi.org/10.1016/j.jhazmat.2009.08.067

Xu, Y., Ma, S., Huang, M., Peng, M., Bog, M., Sree, K. S., Appenroth, K.-J., & Zhang, J. (2015). Species distribution, genetic diversity and barcoding in the duckweed family (Lemnaceae). *Hydrobiologia*, *743*(1), 75–87. https://doi.org/10.1007/s10750-014-2014-2

Xu, Y., Yang, M., Cheng, F., Liu, S., & Liang, Y. (2020). Effects of LED photoperiods and light qualities on in vitro growth and chlorophyll fluorescence of *Cunninghamia lanceolata*. *BMC Plant Biology, 20*, 1-12 https://doi.org/10.1186/s12870-020-02480-7

Yahaya, N., Hamdan, N. H., Zabidi, A. R., Mohamad, A. M., Suhaimi, M. L. H., Johari, M. A. A. M., Yahya, H. N., & Yahya, H. (2022). Duckweed as a future food: evidence from metabolite profile, nutritional and microbial analyses. *Future Foods*, *5*, 100128. https://doi.org/10.1016/j.fufo.2022.100128

Yamaguchi, N. (2014). Chapter 12 Biodiversity conservation and sustainability friends or enemies?. In P. Sillitoe (Ed.), *Sustainable development: An appraisal from the Gulf region* (pp. 291-310). New York, Oxford: *Berghahn Books*. https://doi.org/10.1515/9781782383727-015

Yan, C., Qu, Z., Wang, J., Cao, L., & Han, Q. (2022). Microalgal bioremediation of heavy metal pollution in water: recent advances, challenges, and prospects. *Chemosphere*, *286*, 131870. https://doi.org/10.1016/j.chemosphere.2021.131870

Yang, J., Li, G., Xia, M., Chen, Y., Chen, Y., Kumar, S., Sun, Z., Li, X., Zhao, X., & Hou, H. (2022). Combined effects of temperature and nutrients on the toxicity of cadmium in duckweed (*Lemna aequinoctialis*). *Journal of Hazardous Materials*, *432*, 128646–128646. https://doi.org/10.1016/J.JHAZMAT.2022.128646

Yang, X., Xu, H., Shao, L., Li, T., Wang, Y., & Wang, R. (2018). Response of photosynthetic capacity of tomato leaves to different LED light wavelength. *Environmental and Experimental Botany, 150,* 161-171. https://doi.org/10.1016/j.envexpbot.2018.03.013

Yusuf, M., Fariduddin, Q., Hayat, S., & Ahmad, A. (2011). Nickel: an overview of uptake, essentiality and toxicity in plants. *Bulletin of Environmental Contamination and Toxicology*, *86*(1), 1–17. https://doi.org/10.1007/s00128-010-0171-1

Zavafer, A., Labeeuw, L., & Mancilla, C. (2020). Global trends of usage of chlorophyll fluorescence and projections for the next decade. *Plant Phenomics*, *2020*, 6293145. https://doi.org/10.34133/2020/6293145

Zhang, L. M., Jin, Y., Yao, S. M., Lei, N. F., Chen, J. S., Zhang, Q., & Yu, F. H. (2020). Growth and morphological responses of duckweed to clonal fragmentation, nutrient availability, and population density. *Frontiers in Plant Science*, *11*, 618–618. https://doi.org/10.3389/FPLS.2020.00618/BIBTEX

Zhang, T., Lu, Q., Su, C., Yang, Y., Hu, D., & Xu, Q. (2017). Mercury induced oxidative stress, DNA damage, and activation of antioxidative system and Hsp70 induction in duckweed (*Lemna minor*). *Ecotoxicology and Environmental Safety*, *143*, 46–56. https://doi.org/10.1016/J.ECOENV.2017.04.058

Zhang, Y., Hu, Y., Yang, B., Ma, F., Lu, P., Li, L., Wan, C., Rayner, S., & Chen, S. (2010). Duckweed (*Lemna minor*) as a model plant system for the study of human microbial pathogenesis. *PLOS ONE*, *5*(10), e13527–e13527. https://doi.org/10.1371/JOURNAL.PONE.0013527

Zhao, Z., Shi, H., Duan, D., Li, H., Lei, T., Wang, M., Zhao, H., & Zhao, Y. (2015). The influence of duckweed species diversity on ecophysiological tolerance to copper exposure. *Aquatic Toxicology*, *164*, 92–98. https://doi.org/10.1016/J.AQUATOX.2015.04.019

Zhong, Y., Li, Y., & Cheng, J. J. (2016). Effects of selenite on chlorophyll fluorescence, starch content and fatty acid in the duckweed *Landoltia punctata*. *Journal of Plant Research*, *129*(5), 997–1004. https://doi.org/10.1007/s10265-016-0848-6

Zhou, Y., Chen, G., Peterson, A., Zha, X., Cheng, J., Li, S., Cui, D., Zhu, H., Kishchenko, O., & Borisjuk, N. (2018). Biodiversity of duckweeds in eastern China and their potential for bioremediation of municipal and industrial wastewater. *Journal of Geoscience and Environment Protection*, *6*(3), Article 3. https://doi.org/10.4236/gep.2018.63010

Zhou, Y., Stepanenko, A., Kishchenko, O., Xu, J., & Borisjuk, N. (2023). Duckweeds for phytoremediation of polluted water. *Plants*, *12*(3), Article 3. https://doi.org/10.3390/plants12030589

Ziegler, P., Appenroth, K.-J., & Sree, K. S. (2023). Survival strategies of duckweeds, the world's smallest angiosperms. *Plants*, *12*(11), Article 11. https://doi.org/10.3390/plants12112215

Ziegler, P., Sree, K. S., & Appenroth, K.-J. (2016). Duckweeds for water remediation and toxicity testing. *Toxicological & Environmental Chemistry*, *98*(10), 1127–1154. https://doi.org/10.1080/02772248.2015.1094701

11. Appendix I

Supplementary figures

Figure S1. Measured and modelled responses of the assessed chlorophyll fluorescence induction endpoints to 72 h-long **Ni-treatments** of the *S. polyrhiza* UD0401 clone, as compared to their respective control data. Circles denote means (n = 4) of the repeated experiments (n = 3) at the applied concentrations. Thin black lines denote the best-fitting non-linear regression model for each ChlF endpoint with 95% confidence intervals (gray shaded areas).

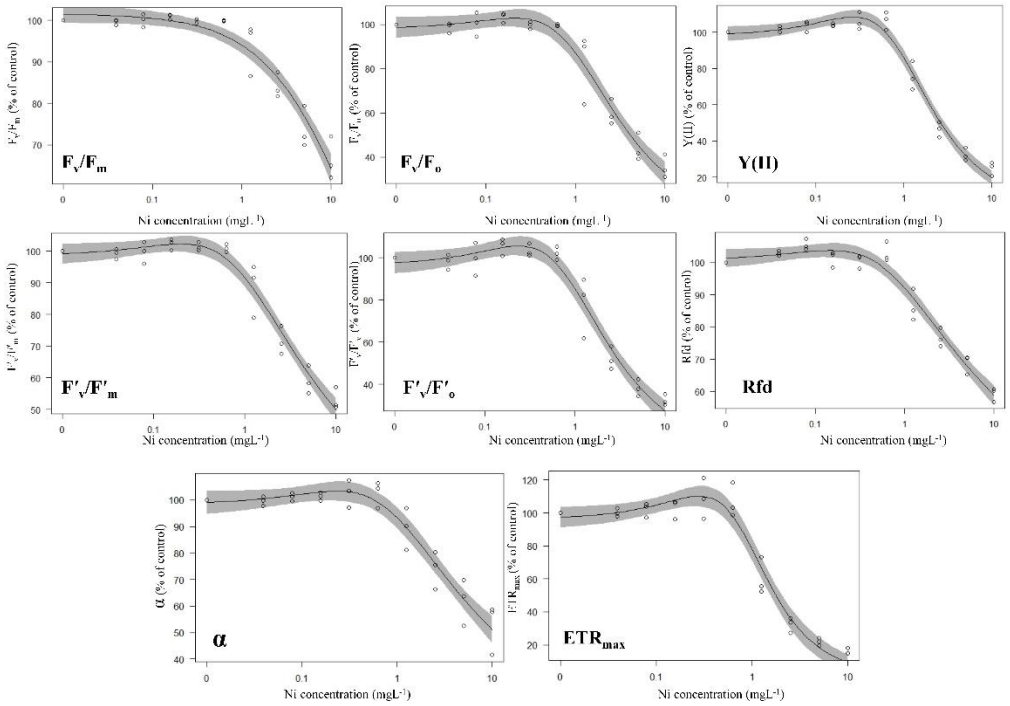

Figure S2. Measured and modelled responses of the assessed chlorophyll fluorescence induction endpoints to 72 h-long **Cr(VI)-treatments** of the *S. polyrhiza* UD0401 clone, as compared to their respective control data. Circles denote means (n = 4) of the repeated experiments (n = 3) at the applied concentrations. Thin black lines denote the best-fitting non-linear regression model for each ChlF endpoint with 95% confidence intervals (gray shaded areas).

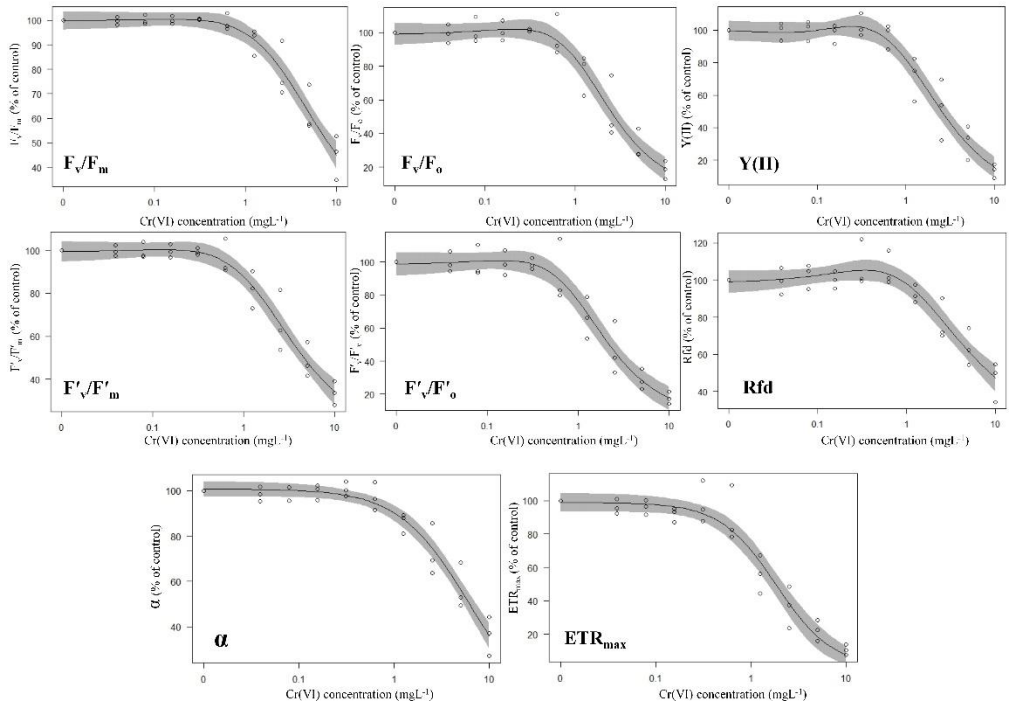

Figure S3. Measured and modelled responses of the assessed chlorophyll fluorescence induction endpoints to 72 h-long **NaCl-treatments** of the *S. polyrhiza* UD0401 clone, as compared to their respective control data. Circles denote means (n = 4) of the repeated experiments (n = 3) at the applied concentrations. Thin black lines denote the best-fitting non-linear regression model for each ChlF endpoint with 95% confidence intervals (gray shaded areas).

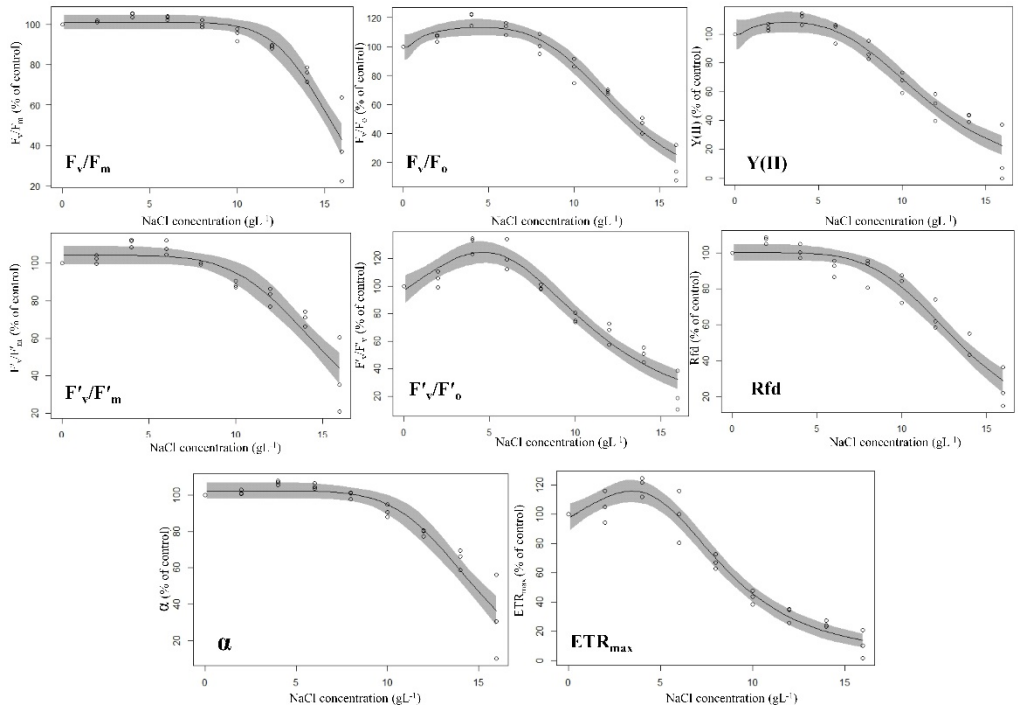

Figure S4. 3-parameter log-logistic concentration-response model fittings of F_v/F_o for the tested metals and metalloids. Circles denote individual measurements (n = 8), solid lines and shaded areas denote the fitted models and the corresponding standard errors of estimates, respectively.

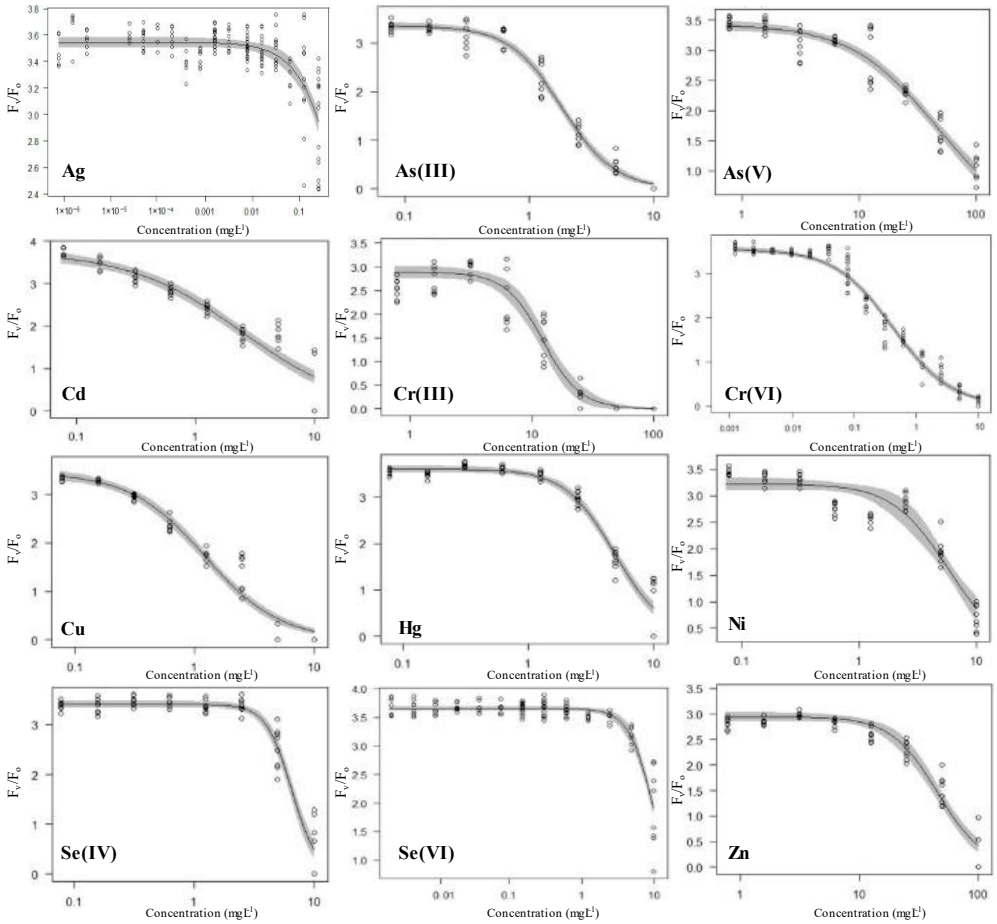

Figure S5. 3-parameter log-logistic concentration-response model fittings of **Y(II)** for the tested metals and metalloids. Circles denote individual measurements (n = 8), solid lines and shaded areas denote the fitted models and the corresponding standard errors of estimates, respectively.

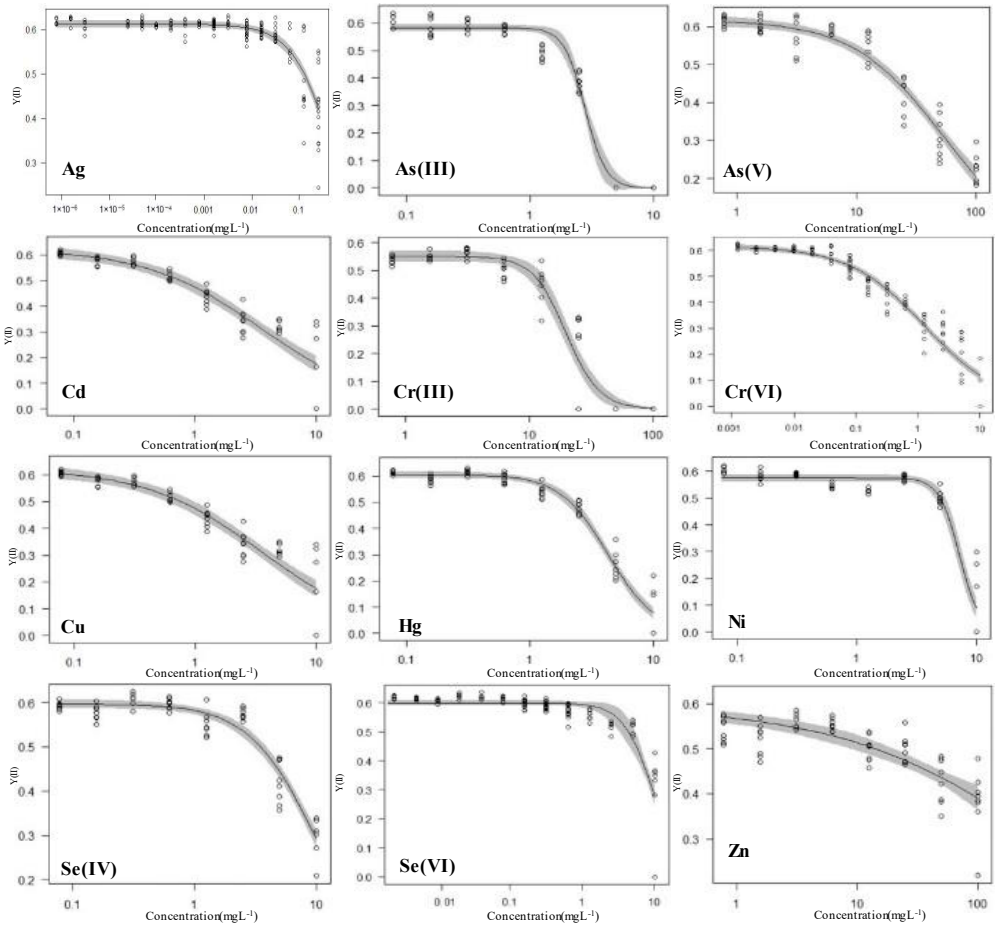

Figure S6. 3-parameter log-logistic concentration-response model fittings of **RGR_{area}** for the tested metals and metalloids. Circles denote individual measurements (n = 8), solid lines and shaded areas denote the fitted models and the corresponding standard errors of estimates, respectively.

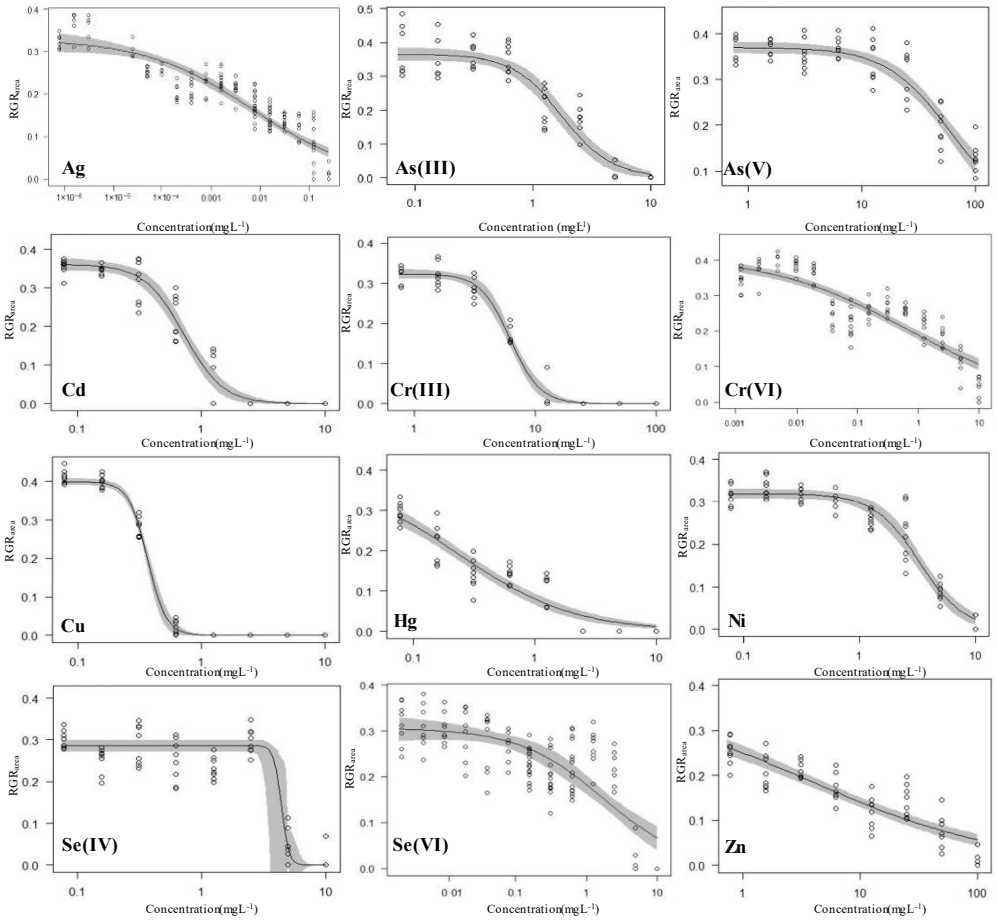

Figure S7. 3-parameter log-logistic concentration-response model fittings of **RGR_{frond}** for the tested metals and metalloids. Circles denote individual measurements (n = 8), solid lines and shaded areas denote the fitted models and the corresponding standard errors of estimates, respectively.

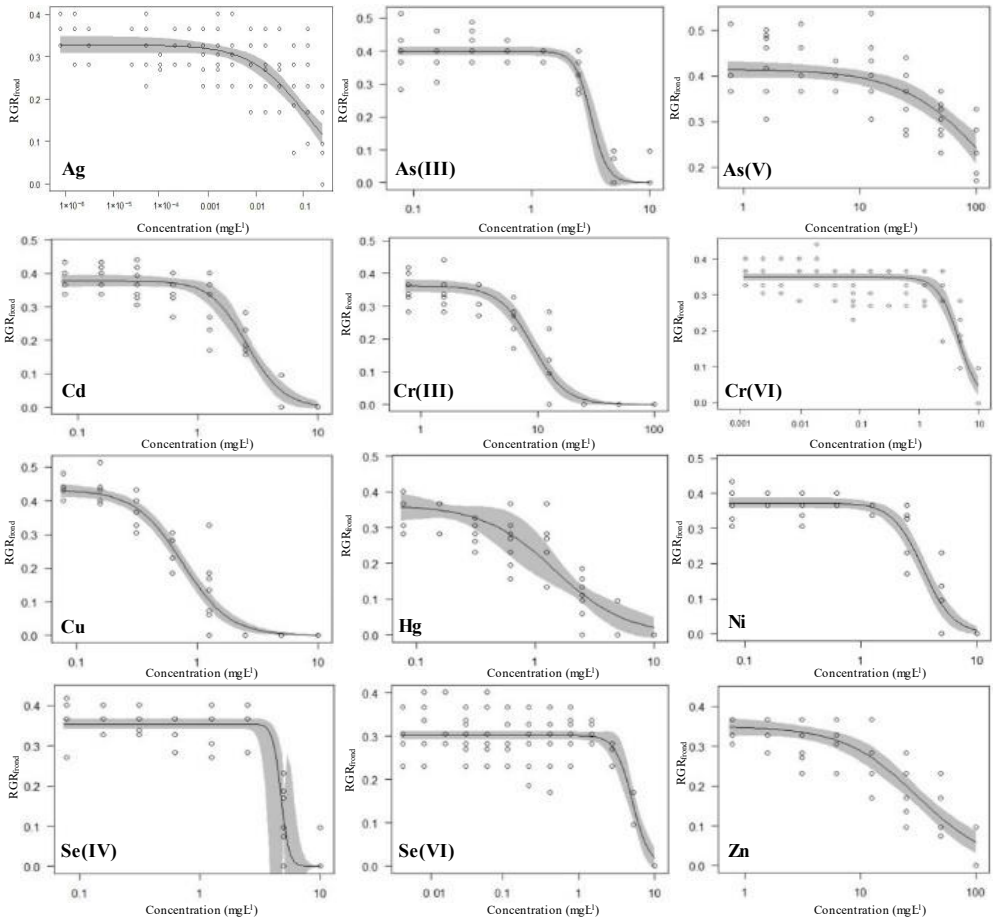

12. Appendix II

Supplementary Tables

Table S1. Summary statistics of the assessed chlorophyll fluorescence induction endpoints after 72 h-long **Ni-treatments** of the *S. polyrhiza* UD0401 clone. The table summarizes minimums (Min), maximums (Max), arithmetic means (Mean), standard deviations (SD) and coefficients of variation (CV) of pooled data, expressed as percentage of their respective control means, from 3 independent experiments with 4-4 parallel treatments at each applied Ni concentration (n = 12). Different upper cases indicate significantly ($p < 0.05$) different medians for different concentrations according to the Kruskal-Wallis test and post hoc Mann-Whitney pairwise comparisons.

Concentration (mg L^{-1})		**0**	**0.039**	**0.078**	**0.156**	**0.313**	**0.625**	**1.25**	**2.5**	**5**	**10**
Sample size (n)		**12**	**12**	**12**	**12**	**12**	**12**	**12**	**12**	**12**	**12**
F_v/F_m	**Min**	99.2	97.5	95.7	98.6	95.7	96	85.9	76.5	64.5	58
	Max	101.2	101.8	102.4	102	102.5	101.4	99.6	92.1	82.5	78.3
	Mean	100	99.6	100	100.9	99.9	99.9	93.8	84.1	73.7	66.4
	SD	0.6	1.1	1.9	1.2	1.8	1.5	5.6	5.1	5.5	5.6
	CV	0.6	1.1	1.9	1.1	1.8	1.5	5.9	6.1	7.5	8.4
	Median	100.2^{b}	99.5^{b}	100.9^{ab}	101.3^{a}	100.1^{ab}	100.2^{b}	96.5^{c}	84.6^{d}	73.6^{e}	66.4^{f}
F_v/F_o	**Min**	97.2	91.4	85.7	95	85.5	86.6	62.5	47	33.1	27.3
	Max	104.6	106.9	109.2	107.5	109.7	105.1	98.4	75.8	55.8	49.2
	Mean	100	98.6	100.2	103.3	99.7	99.6	82.1	59.9	43.9	35.5
	SD	2.3	4.1	6.8	4.3	6.3	5	14.4	9.3	6.9	5.9
	CV	2.3	4.2	6.8	4.1	6.4	5.1	17.6	15.6	15.8	16.6

	Median	100.4^{b}	98.1^{b}	103.1^{ab}	104.6^{a}	100.3^{ab}	100.6^{b}	88.3^{c}	60.1^{d}	43.1^{e}	35.2^{f}
Y(II)	**Min**	94.4	96.4	92.6	98.2	94.6	95.7	64.2	32.1	19.6	17.3
	Max	104.5	108.5	111.3	108.5	117.1	113.9	93.5	62.6	43	32.2
	Mean	100	101.8	103.6	103.9	105.8	106.5	75.6	46.4	32.5	24.9
	SD	3.1	3.2	5	3.9	5.3	5.4	10.4	9.5	7.5	4.7
	CV	3.1	3.1	4.9	3.7	5.1	5.1	13.8	20.5	23	19
	Median	99.3^{c}	101.6^{bc}	104.8^{ab}	104.0^{ab}	105.6^{ab}	106.4^{ab}	70.7^{d}	46.5^{e}	33.7^{f}	24.9^{g}
F'_v/F'_m	**Min**	96.6	93.4	93.1	96.6	92.5	94.7	77.1	60.2	49.4	46
	Max	103	104.7	106.5	105	107.1	104	101.3	84.3	67.4	62.5
	Mean	100	99.2	99.6	102.2	101.3	100.9	88.5	71.5	59.1	53.1
	SD	2.1	3.1	4	2.6	3.8	2.6	8.6	7.6	5.9	4.7
	CV	2	3.2	4.1	2.6	3.7	2.6	9.7	10.6	10	8.9
	Median	100.2^{b}	98.9^{b}	100.1^{ab}	102.6^{a}	101.8^{ab}	101.7^{ab}	89.1^{c}	72^{d}	59.2^{e}	52^{f}
F'_v/F'_o	**Min**	91.9	85.8	85.2	92.5	83.4	87.9	59.2	39.2	29.4	26.8
	Max	107.4	112	116.6	112.4	118.8	109.7	103	68.9	46.2	40.8
	Mean	100	98.2	99.5	105.4	103.5	102.1	78	52.2	38.2	32.5
	SD	4.9	7.3	9.3	6.3	9.1	6.1	15.3	9.4	5.6	4
	CV	4.9	7.5	9.3	6	8.8	6	19.6	18	14.6	12.4
	Median	100.3^{b}	97.2^{b}	100^{ab}	106.1^{a}	104.2^{ab}	104.1^{ab}	77.7^{c}	52.3^{d}	38.2^{e}	31.4^{f}
Rfd	**Min**	96.2	97.4	98.7	95.3	93	95.7	80.1	68.7	58	52.4
	Max	102.6	111.3	112.2	106.6	107.9	113.6	95.8	85.3	74.9	67.8
	Mean	100	102.8	105.5	101.2	100.5	102.9	86.4	76.7	68.8	59.3
	SD	1.9	3.9	4.7	3.4	3.7	4.9	4.8	4.6	4.5	4.2
	CV	1.9	3.8	4.5	3.4	3.7	4.8	5.5	6	6.5	7.2
	Median	100.4^{b}	102.5^{ab}	105.7^{a}	101.5^{ab}	101.1^{b}	102.6^{ab}	85.6^{c}	76.3^{d}	69.1^{e}	59.2^{f}

α	**Min**	98	96.7	97	98.9	91.7	93.1	77.9	56.9	45	38.3
	Max	101.6	102.9	105.9	106	110.7	107.2	97.8	87.3	72.4	66.1
	Mean	100	99.7	101.1	101.4	102.6	102.4	89.4	74	62	52.7
	SD	1.2	2.1	2.6	2	5	4.6	7.3	8.5	8.8	9
	CV	1.2	2.1	2.6	2	4.9	4.5	8.2	11.5	14.3	17
	Median	99.8^{b}	99.8^{b}	100.5^{ab}	101.0^{ab}	103.3^{a}	104.5^{ab}	89.3^{c}	72.2^{d}	62.5^{e}	55.2^{f}
ETR_{max}	**Min**	85.1	83.7	88.6	87.3	88.6	86.7	45	21.8	15.2	13.1
	Max	117.1	123.4	121.1	115.6	133.6	123.2	87.5	47.3	28.4	21.4
	Mean	100	100.1	102.1	102.9	108.6	106.8	60.4	32.4	21.9	17
	SD	9.9	10.7	9.5	9.3	12.4	11.7	15	8.1	4.4	2.6
	CV	9.9	10.7	9.3	9	11.4	10.9	24.9	24.9	20.2	15.3
	Median	98.2^{a}	99.5^{a}	102.1^{a}	103.3^{a}	107.7^{a}	105.7^{a}	53.5^{b}	31.4^{c}	21.9^{d}	17.6^{e}

Table S2. Summary statistics of the assessed chlorophyll fluorescence induction endpoints after 72 h-long **Cr(VI)-treatments** of the *S. polyrhiza* UD0401 clone. The table summarizes minimums (Min), maximums (Max), arithmetic means (Mean), standard deviations (SD) and coefficients of variation (CV) of pooled data, expressed as percentage of their respective control means, from 3 independent experiments with 4-4 parallel treatments at each applied Ni concentration (n = 12). Different upper cases indicate significantly ($p < 0.05$) different medians for different concentrations according to the Kruskal-Wallis test and post hoc Mann-Whitney pairwise comparisons.

Concentration (mg L^{-1})		**0**	**0.039**	**0.078**	**0.156**	**0.313**	**0.625**	**1.25**	**2.5**	**5**	**10**
Sample size (n)		**12**	**12**	**12**	**12**	**12**	**12**	**12**	**12**	**12**	**12**
F_v/F_m	**Min**	98.4	97.8	96.8	98.2	98.7	94.9	82.3	64.3	46.2	29.3
	Max	101.6	101.9	103.7	102.6	102.2	104	98	94.9	76.7	61.8
	Mean	100	99.8	100.1	100.1	100.4	99.1	91.6	78.8	62.8	46
	SD	1	1.5	2.1	1.5	1.2	3.1	5	10.1	10	9.5
	CV	1	1.5	2.1	1.5	1.2	3.1	5.5	12.8	15.9	20.7
	Median	100.1^{a}	100.1^{a}	99.9^{a}	99.7^{a}	100.3^{a}	98.4^{a}	92.9^{b}	75.1^{c}	61.2^{d}	47.5^{e}
F_v/F_o	**Min**	94.3	92.6	89.2	93.8	95.5	83.1	56.3	33.5	19.3	10.3
	Max	106	107.5	115.5	110.2	108.3	115.6	92.9	83.2	46.8	31.1
	Mean	100	99.4	100.7	100.7	101.5	97.2	76.2	53.3	32.8	19.6
	SD	3.6	5.3	8	5.6	4.4	11	11.7	16.7	9	6
	CV	3.6	5.4	8	5.6	4.4	11.3	15.3	31.3	27.4	30.8
	Median	100.3^{a}	100.1^{a}	99.4^{a}	98.7^{a}	101.1^{a}	94.3^{a}	78.0^{b}	45.6^{c}	30.5^{d}	19.4^{e}
Y(II)	**Min**	96.4	90.2	87	88.6	93.2	85	46.7	22.1	17.1	7.9
	Max	104.1	109.9	109.9	106.4	115.7	107.1	86.5	75.2	46.3	25.5
	Mean	100	99.6	100.2	98	102.5	96.8	71.3	51.9	31.6	14.5

	SD	2.4	5.9	6.8	5.7	6.9	7.5	12.7	17.1	10.8	5.3
	CV	2.4	6	6.8	5.9	6.8	7.7	17.8	33	34.1	36.3
	Median	99.8[a]	99.1[a]	101.0[a]	98.4[a]	100.8[a]	98.5[a]	75.9[b]	55.7[c]	33.7[d]	15.0[e]
F'_v/F'_m	**Min**	97	97.1	93	95.2	93.4	86.7	68	47.1	34.6	24.6
	Max	102.2	103.8	106.4	105.3	103.4	107.9	95.2	87.7	61.3	49.2
	Mean	100	99.7	99.5	99.5	99.4	96	81.8	66.1	48.5	35
	SD	1.7	2.5	4.5	3.2	2.5	7.4	8.1	12.8	9.3	7
	CV	1.7	2.5	4.5	3.2	2.5	7.7	10	19.3	19.1	20
	Median	100.5[a]	99.2[a]	99.9[a]	99.0[a]	99.5[a]	93.4[a]	81.6[b]	62.7[c]	49.0[d]	34.6[e]
F'_v/F'_o	**Min**	92.8	93.4	84.7	89.2	85.8	73.5	47.5	27.2	18.4	12.2
	Max	105.1	109.9	117.3	114.2	108.5	121.1	88.8	74.1	38.9	28.9
	Mean	100	99.6	99.4	99.2	98.6	92.3	66.2	46.4	28.6	18.6
	SD	4.1	6.1	10.6	7.7	5.6	16.9	12.2	14.6	7.2	4.8
	CV	4.1	6.1	10.7	7.7	5.7	18.3	18.4	31.4	25.3	25.6
	Median	101.2[a]	98.1[a]	99.8[a]	97.7[a]	98.8[a]	85.4[a]	65[b]	41.7[c]	28.9[d]	17.9[e]
Rfd	**Min**	92	89	93.5	93	96.4	94.9	80.6	66	51.5	29.6
	Max	106.7	113	113.5	109.6	130.4	119.9	102.8	92.2	76.4	70.1
	Mean	100	99.5	102.5	100.1	107.4	105.2	92.4	77.4	63.6	46.7
	SD	3.6	7.2	6.6	4.6	11.5	8.7	5.5	10	9.1	11.2
	CV	3.6	7.2	6.4	4.6	10.7	8.3	5.9	12.9	14.3	24
	Median	100.6[a]	98.3[a]	101.7[a]	100.5[a]	101.5[a]	101.3[a]	92.1[b]	74.3[c]	62.7[d]	47.8[e]
α	**Min**	96.9	94.7	93.1	95	96.7	90	79.6	55.8	40.9	24.5
	Max	103.2	104.8	106.4	105.5	106.6	105.8	94.8	89	70	54.1
	Mean	100	98.5	99.6	99.6	100.6	97.3	86.1	72.9	56.9	37.7
	SD	1.7	3.3	3.6	3.1	3.4	5.9	4.6	10.6	10.6	9.3

	CV	1.7	3.3	3.7	3.1	3.4	6.1	5.3	14.5	18.7	24.6
	Median	99.7[a]	98.0[a]	100.3[a]	100.8[a]	100.1[a]	95.4[a]	86.5[b]	70.3[c]	55.2[d]	38.6[e]
ETR_{max}	**Min**	85.1	81.1	82	79.3	76.8	70.8	38.5	19.5	14	7.1
	Max	117.1	110	112.2	102.9	121.4	121.9	70.4	52.1	31.2	18.1
	Mean	100	96.2	96.2	91.8	98.2	90.1	55.9	36.6	22.4	11.2
	SD	9.2	10.3	10.2	6.7	15.4	16.3	10.6	11.3	6.8	3.4
	CV	9.2	10.7	10.6	7.3	15.7	18.1	19	30.9	30.2	30.6
	Median	98.9[a]	96.9[ab]	93.8[ab]	91.4[b]	96.4[ab]	87.0[ab]	57.0[c]	38.6[d]	23.1[e]	11.1[f]

Table S3. Summary statistics of the assessed chlorophyll fluorescence induction endpoints after 72 h-long **NaCl-treatments** of the *S. polyrhiza* UD0401 clone. The table summarizes minimums (Min), maximums (Max), arithmetic means (Mean), standard deviations (SD) and coefficients of variation (CV) of pooled data, expressed as percentage of their respective control means, from 3 independent experiments with 4-4 parallel treatments at each applied Ni concentration (n = 12). Different upper cases indicate significantly ($p < 0.05$) different medians for different concentrations according to the Kruskal-Wallis test and post hoc Mann-Whitney pairwise comparisons.

Concentration (g L^{-1})		**0**	**2**	**4**	**6**	**8**	**10**	**12**	**14**	**16**
Sample size (n)		**12**	**12**	**12**	**12**	**12**	**12**	**12**	**12**	**12**
F_v/F_m	**Min**	98.4	100	102.3	100.2	97	88.6	86	68.5	13.8
	Max	101.2	104	106.3	104.9	102.8	99.4	93	86.2	68.2
	Mean	100	101.5	104.6	103.1	100.3	94.9	89	75.3	41
	SD	0.8	1.1	1	1.4	2	3.3	2.7	5.9	19.1
	CV	0.8	1.1	1	1.4	2	3.4	3	7.8	46.7
	Median	100.0^{d}	101.4^{c}	104.9^{a}	103.7^{b}	100.3^{cd}	95.9^{e}	88.6^{f}	73.7^{g}	37.5^{h}
F_v/F_o	**Min**	94.3	100	109.1	100.7	89.9	67.4	62.6	36.7	4.3
	Max	104.6	116.7	127.1	121.1	111.3	97.7	77.9	62.5	36.4
	Mean	100	106	119.6	112.8	101.3	84.1	68.9	45.9	17.8
	SD	3.1	4.5	4.7	6.1	7.6	9.1	5.9	8.4	11.4
	CV	3.1	4.3	3.9	5.4	7.5	10.8	8.5	18.2	63.8
	Median	99.9^{d}	105.1^{c}	120.5^{a}	114.7^{b}	101.0^{cd}	86.1^{e}	68.3^{f}	43.4^{g}	13.9^{h}
Y(II)	**Min**	94.4	98.3	104.6	83.9	81.6	54.5	35.2	26.5	0
	Max	104.5	112.2	115.5	112	100.1	77.5	62.4	52.9	40.5
	Mean	100	104.7	111	101.6	87.8	66.7	50.1	42.1	14.6

	SD	3	4.2	3.6	7.8	6.1	7.3	9	7.9	18.5
	CV	3	4	3.3	7.7	7	10.9	18	18.7	126.2
	Median	99.8^{c}	104.7^{b}	112.4^{a}	102.3^{bc}	85.9^{d}	67.8^{e}	50.9^{f}	42.0^{g}	0.0^{h}
F'_v/F'_m	**Min**	96.6	96.9	107	102.4	95.9	82.2	70.7	58.3	12.9
	Max	103	107.7	113.8	114.1	104.2	94.3	88.4	82.8	64.4
	Mean	100	102	110.7	108	99.7	88.6	82.2	70.4	38.9
	SD	2.2	3	2.2	3.7	2.4	3.3	5.6	7.5	18.3
	CV	2.2	3	2	3.4	2.4	3.7	6.8	10.6	47.1
	Median	100.6^{bc}	102.1^{b}	110.8^{a}	108.2^{a}	99.6^{c}	88.1^{d}	82^{e}	68.4^{f}	35.8^{g}
F'_v/F'_o	**Min**	91.9	93	119.3	106.1	90.8	65.6	49.3	36	5.9
	Max	107.4	120.5	140.5	142	110.2	87.5	76.4	66	42.2
	Mean	100	105.2	130.4	121.9	99.2	76.4	66	50.3	22.5
	SD	5.2	7.7	6.6	11.3	5.6	6	8.7	9.4	13.1
	CV	5.2	7.3	5.1	9.2	5.6	7.9	13.2	18.7	58.5
	Median	101.3^{bc}	104.9^{b}	129.8^{a}	122.0^{a}	98.7^{c}	74.9^{d}	65.4^{e}	46.9^{f}	18.8^{g}
Rfd	**Min**	96.2	97.9	94.5	82	77.3	67.5	49.4	39.6	12.1
	Max	102.1	111.6	110.6	99.3	98.8	89.7	75.7	62.3	42.9
	Mean	100	106.9	100.8	91.6	90.1	81.4	64.9	47.3	24.6
	SD	1.7	3.3	4.5	6	7.6	7.5	8.3	6.8	10
	CV	1.7	3.1	4.5	6.5	8.4	9.3	12.7	14.4	40.6
	Median	100.6^{b}	107.8^{a}	99.6^{b}	90.4^{c}	92.9^{c}	83.8^{d}	62.3^{e}	45.3^{f}	22.2^{g}
α	**Min**	98	98.3	104.1	101.3	96	86.1	73.4	57	0
	Max	101.6	106.1	108.8	108.8	105.2	98.3	84.7	78	60
	Mean	100	101.5	106.7	104.8	100	91	79.4	64.8	32.3
	SD	1.3	2.3	1.3	2.3	2.6	3.7	3	7.2	21

	CV	1.3	2.3	1.2	2.2	2.6	4.1	3.8	11.1	65
	Median	99.7^{c}	101.3^{c}	106.8^{a}	105.1^{b}	99.9^{c}	90.8^{d}	79^{e}	63.2^{f}	30.8^{g}
ETR_{max}	**Min**	85.1	87.8	101.2	60.6	58.9	35	23.1	17.5	0
	Max	117.1	127.4	129.1	138.3	84.2	56.6	38.8	33.7	23.9
	Mean	100	105.1	119.4	98.7	67.4	43.3	31.9	25	11
	SD	10.1	13.1	7.4	20.2	6.4	5.6	5.6	4.9	9
	CV	10.1	12.5	6.2	20.4	9.4	13	17.5	19.5	81.7
	Median	98.9^{b}	103.3^{b}	120.8^{a}	98.5^{b}	67.2^{c}	42.6^{d}	31.8^{e}	23.9^{f}	10.1^{g}

Table S4. The results of the 3-parameter log-logistic model fittings (DF - degrees of freedom, RSS - residual sum of squares, F-value, p-value and Pseudo R^2), and the calculated 20% (EC_{20}) and 50% effective concentrations (EC_{50}) for frond number- (RGR_{frond}) and frond area-based relative growth rates (RGR_{area}), dark-adapted-(F_v/F_o) and light-adapted- photochemical efficiency (Y(II)) as estimates ± standard errors of estimates.

Toxicant	Endpoint	DF	RSS	F-value	p-value	Pseudo R^2	EC_{20} (mg L^{-1}±SE)	EC_{50} (mg L^{-1}±SE)
Ag	**RGR_{frond}**	169	0.69	2.62	<0.005	0.76	0.016±0.003	0.11±0.02
	RGR_{area}	169	0.26	14.94	<0.001	0.92	0.0001±0.00006	0.005±0.001
	F_v/F_o	169	5.27	1.18	0.300	0.71	0.31±0.03*	1.27±0.43*
	Y(II)	169	0.23	0.31	0.990	0.85	0.14±0.01*	0.55±0.07*
As(III)	**RGR_{frond}**	69	0.15	0.68	0.670	0.96	2.59±0.12	3.21±0.17
	RGR_{area}	69	0.19	2.94	0.010	0.94	0.90±0.12	1.77±0.15
	F_v/F_o	69	2.85	1.22	0.310	0.99	0.93±0.05	1.84±0.06
	Y(II)	69	0.11	25.55	<0.001	0.99	2.14±0.10	2.80±0.06
As(V)	**RGR_{frond}**	69	0.20	0.40	0.880	0.73	41.43±8.07	132.18±23.91*
	RGR_{area}	69	0.11	0.95	0.460	0.91	24.75±3.02	60.70±4.41
	F_v/F_o	69	4.50	1.08	0.380	0.93	14.41±1.62	47.15±2.68
	Y(II)	69	0.10	2.55	0.030	0.96	16.10±1.61	54.33±3.01
Cd	**RGR_{frond}**	69	0.17	2.97	0.010	0.95	1.59±0.22	2.58±0.17
	RGR_{area}	69	1.02	0.82	0.560	0.97	0.44±0.04	0.73±0.04
	F_v/F_o	69	8.12	11.05	<0.001	0.96	0.54±0.11	2.45±0.25
	Y(II)	69	0.25	2.47	0.030	0.93	0.78±0.17	3.59±0.38

Cr(III)	**RGR_{frond}**	69	0.17	0.66	0.680	0.96	5.68±0.61	9.02±0.60
	RGR_{area}	69	0.05	1.05	0.400	0.98	4.21±0.31	6.22±0.23
	F_v/F_o	69	8.72	6.01	<0.001	0.96	7.52±0.80	12.35±0.74
	Y(II)	69	0.24	1.34	0.250	0.97	12.92±1.11	19.92±0.99
Cr(VI)	**RGR_{frond}**	132	0.32	4.60	<0.001	0.87	2.69±0.36	4.69±0.32
	RGR_{area}	132	0.34	22.01	<0.001	0.89	0.02±0.002	0.66±0.15
	F_v/F_o	132	6.98	10.01	<0.001	0.98	0.09±0.008	0.42±0.02
	Y(II)	132	0.27	6.87	<0.001	0.97	0.18±0.03	1.28±0.1
Cu	**RGR_{frond}**	69	0.14	1.18	0.330	0.97	0.40±0.04	0.75±0.04
	RGR_{area}	69	0.03	1.75	0.120	0.99	0.29±0.01	0.37±0.01
	F_v/F_o	69	4.36	22.54	<0.001	0.98	0.45±0.05	1.23±0.08
	Y(II)	69	0.21	11.42	<0.001	0.97	0.90±0.10	1.86±0.11
Hg	**RGR_{frond}**	69	0.26	9.24	<0.001	0.92	0.56±0.33	1.47±0.38
	RGR_{area}	69	0.10	9.31	<0.001	0.96	0.05±0.01	0.24±0.03
	F_v/F_o	69	3.72	1.58	0.170	0.97	2.60±0.14	4.87±0.17
	Y(II)	69	0.11	2.05	0.070	0.98	2.32±0.15	4.30±0.15
Ni	**RGR_{frond}**	69	0.17	0.21	0.970	0.94	2.27±0.20	3.44±0.20
	RGR_{area}	69	0.08	2.43	0.030	0.96	1.77±0.20	3.28±0.20
	F_v/F_o	69	6.36	28.93	<0.001	0.94	2.73±0.47	5.81±0.35
	Y(II)	69	0.16	2.80	0.010	0.95	5.51±0.26	7.21±0.25
Se(IV)	**RGR_{frond}**	69	0.16	1.00	0.430	0.93	4.27±1.68	4.73±0.64
	RGR_{area}	69	1.36	15.4	<0.001	0.90	4.01±1.87	4.41±1.18

	F_v/F_o	69	4.20	0.31	0.930	0.96	4.62±0.17	6.48±0.19
	Y(II)	69	0.06	6.56	<0.001	0.95	4.10±0.25	9.73±0.42
Se(VI)	**RGR_{frond}**	131	0.34	2.16	0.020	0.84	3.26±0.47	4.78±0.35
	RGR_{area}	131	0.48	12.18	<0.001	0.80	0.26±0.15	1.73±0.42
	F_v/F_o	131	5.06	0.46	0.920	0.91	5.96±0.32	10.39±0.34*
	Y(II)	131	0.29	3.24	<0.001	0.87	4.83±0.59	9.40±0.47
Zn	**RGR_{frond}**	69	0.21	1.76	0.120	0.89	11.28±2.93	31.23±3.90
	RGR_{area}	69	0.10	7.37	<0.001	0.93	0.27±0.10	3.88±0.78
	F_v/F_o	69	4.78	13.25	<0.001	0.96	24.42±2.41	45.31±2.28
	Y(II)	69	0.12	4.46	<0.001	0.84	24.85±9.53	350.56±128.85*

*Extrapolated values from the model fittings when the calculated effective concentrations were out of the applied concentration range.

13. Appendix III

Steinberg medium preparation and composition

Step 1. Preparation of stock solutions: Firstly, five stock solutions were prepared using the following chemicals in their corresponding concentrations (columns 1–4).

Stock No.	Source Chemical	Stock Concentration (g L^{-1})	Stock Concentration (mol L^{-1})	Medium Concentration (mg L^{-1})
1.	KNO_3	17.50	3.46×10^{-3}	350.00
	KH_2PO_4	4.50	0.66×10^{-3}	90.00
	K_2HPO_4	0.63	0.072×10^{-3}	12.60
2.	$MgSO_4 \times 7H_2O$	5.00	0.41×10^{-3}	100.00
3.	$Ca(NO_3)_2 \times 4H_2O$	14.75	1.25×10^{-3}	295.00
4.	H_3BO_3	0.12	1.94×10^{-6}	0.12
	$ZnSO_4 \times 7H_2O$	0.18	0.63×10^{-6}	0.18
	$Na_2MoO_4 \times 2H_2O$	0.044	0.18×10^{-6}	0.044
	$MnCl_2 \times 4H_2O$	0.18	0.91×10^{-6}	0.18
5.	$FeCl_3 \times 6H_2O$	1.50	2.81×10^{-6}	1.50
	Na_2EDTA	0.76	4.03×10^{-6}	0.76

The prepared stocks were stored in the fridge, however we always used freshly prepared stock No. 5 due to EDTA precipitation.

Step 2. Preparation of Steinberg medium: It was preferred to prepare medium in batches. To prepare 1 L of Steinberg medium, 20–20 ml of stocks No. 1–3 and 1–1 ml of stocks No. 4–5 were diluted using ultrapure distilled water to the final volume. The pH of the prepared Steinberg medium was measured to be at ~6.0.